Shun Hing Institute of Advanced Engineering
信興高等工程研究所

Report and Research Highlights
2017 - 2018

July 2018

香 港 中 文 大 學
The Chinese University of Hong Kong

Printed in August 2018, this report contains information known as at July 2018.

Every effort has been made to ensure that the information contained in this report is correct at the time of printing. Shun Hing Institute of Advanced Engineering (SHIAE) – CUHK, reserves the right to make appropriate changes to the materials presented in this report without prior notice.

For further information, please visit our website: http://www.shiae.cuhk.edu.hk

Contents

Introduction of SHIAE

Mission of SHIAE

The MISSION of the Institute is to spearhead, conduct, promote and co-ordinate research in advanced engineering. There is no end to the list of areas to be explored and the plan is to give priority to research topics that are both exciting and innovative. The Institute also aspires to transferring its research results to industry for practical application and to put across to the community at large the role of engineering as a driving force for human development through educational activities.

As a pioneering institute exploring the forefront of the engineering science, The Shun Hing Institute of Advanced Engineering will

- spearhead state-of-the-art advanced engineering research
- create and sustain synergy with world-class researchers
- develop with and transfer to industries cutting edge technologies
- promote appreciation of engineering in society through educational programmes

The Shun Hing Education and Charity Fund was founded the late by Dr. William Mong Man Wai with the aim of enhancing educational opportunities for the younger generations. The Fund has already sponsored numerous educational and research programmes in Hong Kong, the Mainland, and overseas educational institutions. Himself an engineer and a firm believer in advancing the quality of life through the development of science and technology, Dr. Mong had been there to support the establishment and growth of this Institute from the beginning.

Centre of Excellence at CUHK

The Chinese University of Hong Kong is an internationally renowned institution of higher learning devoted to quality teaching and both academic and applied research. The University has established 29 research institutes and a number of research centres with a view to pursuing up-front research endeavours with focused goals and objectives. The Shun Hing Institute of Advanced Engineering plays a crucial part in the research infrastructure of the Chinese University which is committed to exciting research programmes in advanced engineering areas. The Institute is now in its second decade of development, and we are particularly pleased to have received continual staunch support and guidance from Mr. David Mong Tak Yeung, Chairman and CEO of the Shun Hing Group and the Shun Hing Education and Charity Fund.

As a strategic centre of excellence at The Chinese University of Hong Kong, the Institute supports greater regional and international research collaborations, and strives to attract talent from the world over to achieve greater internationalization, a vision strongly advocated by every member of the University.

Commitment of the Faculty of Engineering

The Faculty of Engineering was founded in 1991 and was built upon existing strengths with added talent from all over the world. The Faculty has been able to attract some of the best minds. Many received their training in leading universities in North America, Great Britain and Australia. Most of them have extensive experience in industry and many are leaders in their fields. This team of top-notch talent is gathered to nurture local talent through educational programmes, and break new frontiers in research through innovative and exciting research endeavours.

The positioning of The Shun Hing Institute of Advanced Engineering in the William M.W. Mong Engineering Building is deliberate as a key nucleating point to integrate research endeavours in the Engineering Faculty and its neighbours. Our members join hands with their counterparts from the Faculties of Science and Medicine in many interesting research collaborations. It is the ambitious goal of the Faculty of Engineering that the Institute should become a lighthouse for the local technology landscape to herald the migration towards high value-added technology and an information economy.

The mission of the Institute is to spearhead, conduct, promote and co-ordinate research in advanced engineering. There is no end to the list of areas to be explored and the plan is to give priority to research topics that are both exciting and innovative. The Institute also aspires to transferring its research results to industry for practical application and to put across to the community at large the role of engineering as a driving force for human development through educational activities.

Building on Strength and The Way Ahead

Many of the Institute's research projects are built upon areas in which the Faculty has already achieved outstanding performance. These are areas that have great potential for further technological advancement and in line with industrial development in Hong Kong. The Institute provides a vibrant R&D environment to spur new discoveries and speed up their translation into applications. Since 2012, we have expanded our scope to cover new frontiers in Renewable Energy striving to answer tomorrow's energy challenges. Last year, we further expand the research scope in Multimedia Technologies to include Artificial Intelligence, Big Data Analytics and Deep Learning as well.

Technology Transfer

Synergy with industry is the ultimate goal of research and development in Hong Kong. External experts have been brought in to the Institute to lead research projects that could benefit the industrial sector.

The technology transfer arm of the Faculty of Engineering plays an important role in the traffic between the Institute and industry. The Institute houses an array of top-notch research and development activities encompassing contract research, spin-off companies, and consultancies.

Contribution to Society

The Institute has been making contributions to the progress of Hong Kong through a wide range of educational activities like training courses, seminars, symposiums which disseminate the latest technologies to promote appreciation of engineering in society and arouse interest of the younger generations in engineering.

Organization of SHIAE

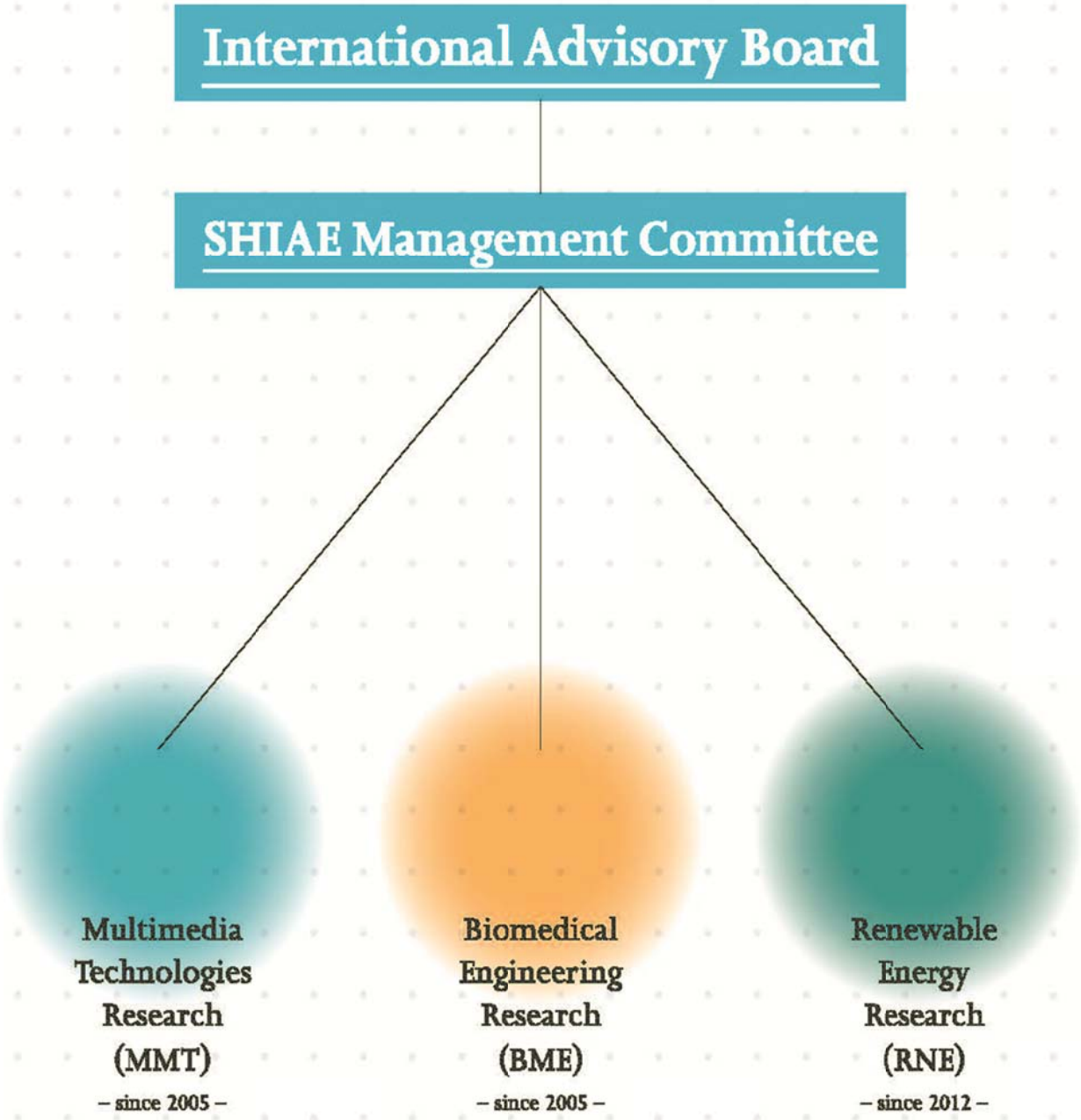

We also provide support and sponsorship to the Faculty of Engineering in organizing prestigious academic conferences in Hong Kong so as to raise our international profile.

Composition of International Advisory Board

(with effect from August 1, 2016)

Chairman:

Dr. David T.Y. MONG 蒙德揚先生

Chairman & Group CEO
Shun Hing Electronic Holdings Limited
Hong Kong

Members:

Professor Victor ZUE

Delta Electronics Professor of Electrical Engineering and Computer Science
Massachusetts Institute of Technology
U.S.A

Dr. Harry SHUM 沈向洋博士

Executive Vice President, Technology and Research
Microsoft Corporation
U.S.A.

Professor Yongmin KIM

Affiliate Professor
University of Washington
U.S.A.

Professor C.C. Jay KUO

Professor of Electrical Engineering and Computer Science
University of Southern California
U.S.A.

Professor Paul, Kit-lai YU

Provost, Revelle College, Jacobs School of Engineering
University of California, San Diego
U.S.A.

Professor Tai Fai FOK 霍泰輝教授

Pro-Vice-Chancellor
The Chinese University of Hong Kong
Hong Kong

Professor Wing-shing WONG 黃永成教授

Choh-Ming Li Professor of Information Engineering
The Chinese University of Hong Kong
Hong Kong

Professor Ching Ping WONG 汪正平教授

Dean of Engineering
The Chinese University of Hong Kong
Hong Kong

Professor Pak Chung CHING 程伯中教授

Director of Shun Hing Institute of Advanced Engineering
Choh-Ming Li Professor of Electronic Engineering
The Chinese University of Hong Kong
Hong Kong

Composition of Management Committee

(with effect from June 15, 2018)

Chairman:

Professor Pak Chung CHING *(ex-officio)*
Director of SHIAE, and Choh-Ming Li Professor of Electronic Engineering

Members:

Professor Ching Ping WONG *(ex-officio)*
Dean of Faculty of Engineering

Mr. Terrence CHAN
Managing Director of Shun Hing Electronic Holdings, Limited
Hong Kong

Professor Jack C.Y. CHENG
Department of Orthopaedics and Traumatology

Professor Jianwei HUANG
Department of Information Engineering

Professor Tan LEE
Department of Electronic Engineering

Professor Wei-Hsin LIAO
Department of Mechanical and Automation Engineering

Professor Dennis Y.M. LO
Department of Chemical Pathology
(until June 14, 2018)

Professor Raymond Kai-yu TONG
Department of Biomedical Engineering

Member and Secretary:

Professor John C.S. LUI
Choh-Ming Li Professor of Computer Science and Engineering

Shun Hing Visiting Scholars/ Fellows

The Institute has launched a Shun Hing Distinguished Scholar Program with an aim to attract distinguished scholars to pursue research collaboration with our faculty and to strengthen our research profile. The following scholars visited to work either on a short term or on a longer term engagement with the Institute between 2017 and 2018.

Shun Hing Fellows and Research Associate:
(in alphabetical order)

Dr. ABBASNEJAD Ghasem 2016 - 2017
National University of Singapore, Singapore

Dr. LEE Chinghuan 2016 - 2018
National Chung Kung Univesrity, Taiwan

Mr. LEUNG Wing Cheong 2017 - 2018
Hong Kong Polytechnic University, Hong Kong

Dr. LI Qiang 2017 - 2018
School of Communication and Information Engineering, China

Dr. Wang Jianjian 2018 - 2019
Tsinghua University, China

Financial Status of SHIAE

		As at 30 June 2018 HK$
INCOME		
Start Up Seed Fund		44,500,000
New Funding pledged in Dec 2017		10,000,000
Interest and investment income		7,142,755
Sub-total:		61,642,755
EXPENDITURE		
Research funding granted since 2005-2018	(1)	43,611,200
Committed Research Budget in 2019	(2)	1,515,000
Unspent remaining fund from all completed projects		-3,191,127
Committed staff cost		212,370
Operating cost		4,945,557
Sub-total:		47,093,000
BALANCE as at 30 June 2018		**14,549,755**

Note (1) Annualized Research Funding to each research areas granted since 2005

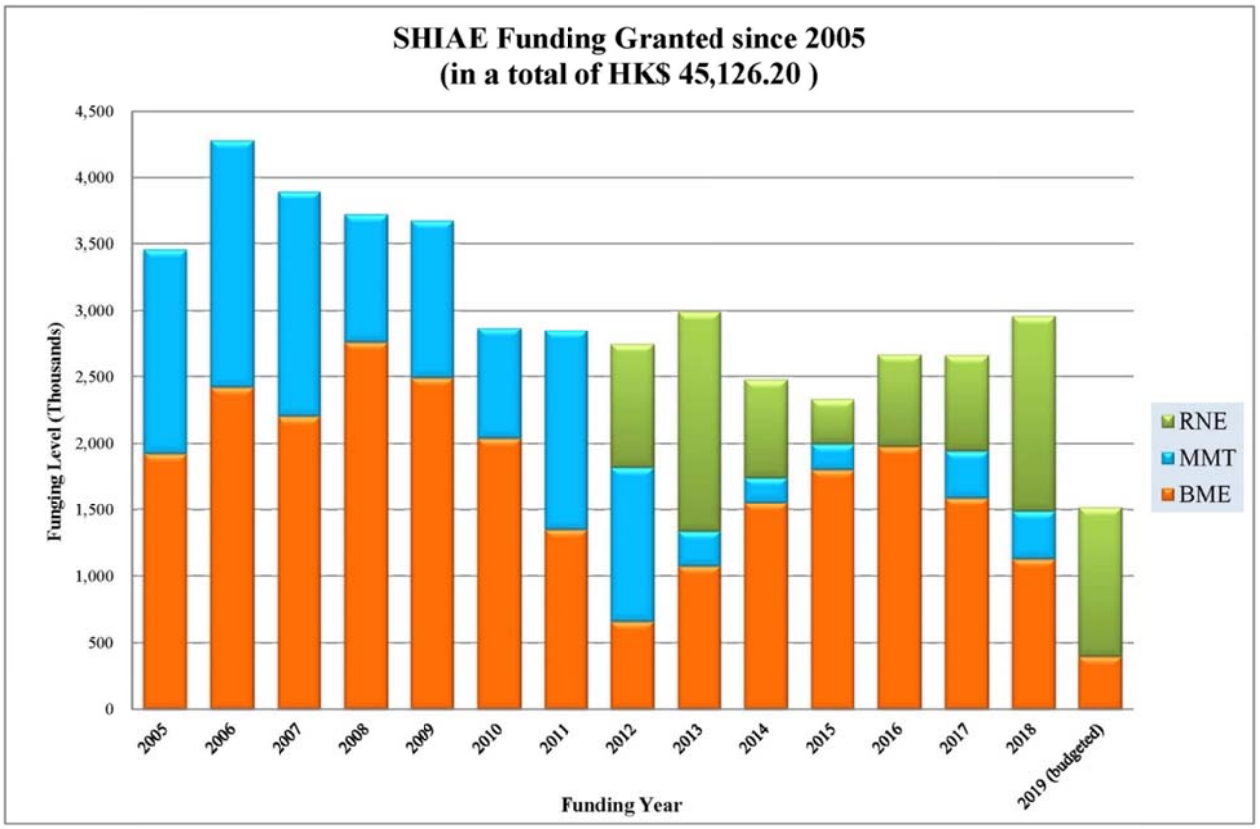

This figure shows the distribution of the SHIAE funding granted to each track of research projects, namely Biomedical Engineering (BME), Multimedia Technology (MMT) and Renewable Energy (RNE) annually.

Note (2) Detail funding level on each batch of projects (in HK$ '000)

Funding Year / No. of projects	2019 (committed)	2018	2017	2016	2015	2005 - 2014
Year 2005 / 6 Projects	-	-	-	-	-	6,108
Year 2006 / 5 Projects	-	-	-	-	-	3,175
Year 2007 / 7 Projects	-	-	-	-	-	4,146
Year 2008 / 4 Projects	-	-	-	-	-	3,976
Year 2009 / 5 Projects	-	-	-	-	-	3,306
Year 2010 / 5 Projects	-	-	-	-	-	2,789.2
Year 2011 / 4 Projects	-	-	-	-	-	2,476
Year 2012 / 5 Projects	-	-	-	-	-	1,520
Year 2013 / 4 Projects	-	-	-	-	-	2,948
Year 2014 / 3 Projects	-	-	-	-	1,002	1,002
Year 2015 / 4 Projects	-	-	-	1,328	1,328	-
Year 2016 / 4 Projects		-	1,213	1,340	-	-
Year 2017 / 4 Projects		1,447	1,447	-	-	
Year 2018 / 4 Projects	1,515	1,515	-	-	-	
WOSP2007		-	-	-	-	25
	1,515	2,660	2,668	2,330	2,330	32,991.20
Accumulated Total:	**HK$45,126.20**					

This table shows the detail amount of SHIAE funding granted to each batch of research projects. The subtotal amount of **1.515 million** budgeted for 2019 is committed to support research projects in July 2019.

Research - *Outstanding Research Highlights*

Academic Publications

So far **52 projects** have been successfully completed and **415 articles** arising from the results of these research projects have been published in international conference proceedings and journals. The other **12 on-going projects** are also progressing well with encouraging results produced. All publications generated by each individual projects are kept in the archive of SHIAE office. The chart below shows the number of academic publications produced each year.

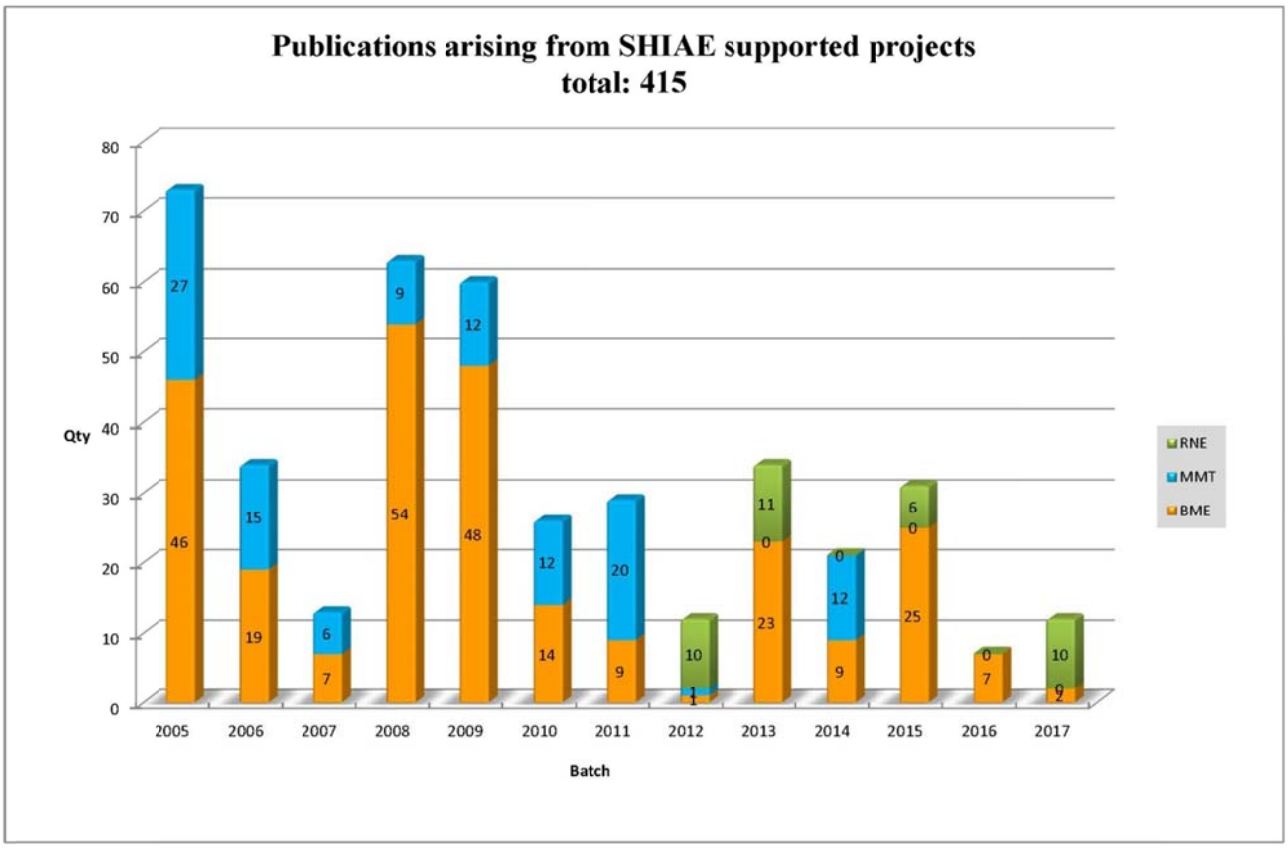

The list of publications can also be downloaded from the webpage of SHIAE at www.shiae.cuhk.edu.hk/research.htm

Renewable Energy Track

Research Reports In Renewable Energy

Newly Funded Projects (2018-2020)	* Development of a Novel CoolingTower with Free Daytime RadiativeCooling for Reducing EnergyConsumption in Buildings
	* Megahertz Current Sensor for Megahertz Renewable Energy Converter
	* Development of High-Performance Triboelectric Nanogenerators for Renewable Blue Energy Harvesting
Continuing Projects (2017-2019)	* Tunable spindle using self-excited vibration for high efficiency renewable electric generators
(2016-2018)	* Robust NiMo–yttria stabilized zirconia (NiMo–YSZ) anode materials for solid oxide fuel cells
Completed Projects (2015-2017)	* Experimental and modeling study of biodiesel combustion

The following reports are enclosed in “Research Highlights” printed in November 2017.

Completed Projects (2013-2015)	* Earth-Abundant Metal/Metal Oxide Nanostructures for Rechargeable Li-Air Batteries: Catalyst Design and Mechanistic Investigation
	* Graphene-based asymmetric supercapacitors with high energy density for clean energy storage systems

The following reports are enclosed in “Research Highlights” printed in July 2015.

Completed Projects (2012)	* Vibration Energy Harvesting Utilizing Multifunctional Phononic Meta-Materials and Structures
Completed Projects (2012)	* Understanding Electron and Phonon Transport in Boron Carbide Nanowires for Thermoelectric Energy Conversion
	* Ternary Hybrid Polymer/Nanocrystal Bulk Heterojunction Solar Cells with Cascade Energy-Level Alignmen

(Funded Year)

DEVELOPMENT OF A NOVEL COOLINGTOWER WITH FREE DAYTIME RADIATIVECOOLING FOR REDUCING ENERGYCONSUMPTION IN BUILDINGS

Principal Investigator: Professor CHEN Chun
Department of Mechanical & Automation Engineering
CUHK

Project Start Date: 1 July 2018

ABSTRACT

The air-conditioning systems in buildings consume about 30% of the total electricity in Hong Kong. In a typical air-conditioning system, the conventional cooling tower drags the outdoor air to cool the cooling water for rejecting heat to the atmosphere. To reduce the energy consumption, this project proposes to develop a novel cooling tower with free daytime radiative cooling. A basin coated with a film of radiative cooling metamaterial will be implemented into the cooling tower. The film can reflect the solar irradiance and draw the heat from the water through the infrared transparency window of the atmosphere to the cold sink of outer space. The radiative cooling is free and renewable because the cold sink of outer space can be effectively regarded as a cooling reservoir. Consequently, the cooling water temperature will decrease without consuming additional energy, so that the coefficient of performance (COP) of chillers will increase. The design of the proposed cooling tower will be supported by computational fluid dynamics (CFD) simulations. A prototype will be fabricated and the energy efficiency will be measured. The proposed project will offer a novel cooling tower that can utilize renewable cooling and reduce the energy consumption in buildings.

INNOVATION AND PRACTICAL SIGNIFICANCE:

Conventional cooling towers drag the outdoor air to cool the cooling water for rejecting heat to the atmosphere. Lower cooling water temperature results in a higher COP of chillers. Therefore, it is worthwhile to enhance the heat rejection in cooling towers without consuming additional energy. The innovation of this work is to develop a cooling tower with free daytime radiative cooling. The proposed cooling tower utilizes free and renewable cooling to lower the cooling water temperature. Consequently, the COP of chillers is expected to increase by 10 to 20%. A prototype will be fabricated and tested in this project. With the collaboration with the heating, ventilation, and air-conditioning (HVAC) industry, we will actively see further development of the prototype and potential technology transfer. If successful, the novel cooling towers can be potentially used in commercial and residential buildings to reduce the energy consumption and the associated carbon dioxide emissions.

PROJECT OBJECTIVES:

1. ***To propose a novel cooling tower with free daytime radiative cooling.*** Improving the design of cooling towers can increase the energy efficiency of the air-conditioning systems. This study will propose a novel cooling tower with free daytime radiative cooling. The proposed cooling tower will utilize renewable cooling, thus, it can be potentially applied in buildings to reduce the energy consumption.

2. ***To develop a numerical model for predicting the energy efficiency of the cooling tower.*** To support the design, a model is needed to accurately predict the energy efficiency of the cooling tower with radiative cooling. This study will develop a multi-phase numerical model on the basis of computational fluid dynamics (CFD). The developed CFD model can be used in the future for supporting the design of cooling tower with free daytime radiative cooling.

3. ***To optimize the system parameters using the validated numerical model.*** The system parameters, including fan speed, water velocity, infrared emissivity, etc., can influence the energy efficiency of the proposed cooling tower. This study will optimize the system parameters using the validated CFD model by testing various combinations. The optimized system parameters can be used in the future as a design guideline of cooling tower with radiative cooling.

4. ***To fabricate a prototype and conduct experiments to validate the design.*** It is important to experimentally validate that the proposed cooling tower can achieve the desirable energy efficiency. This study will fabricate a prototype and conduct experiments to validate the design. The experimental data can be used in the future to support the design of cooling tower with radiative cooling.

5. ***To estimate the energy saving from using the proposed cooling tower.*** Only if the energy saving can cover the initial capital investment within a reasonable payback period, will the building owner decide to adopt the cooling tower with free daytime radiative cooling. Thus, this study will estimate the energy saving from using the proposed cooling tower. The estimation method can be applied in the future to support the decision making of whether or not to invest in the proposed cooling towers.

MEGAHERTZ CURRENT SENSOR FOR MEGAHERTZ RENEWABLE ENERGY CONVERTER

Principal Investigator: Professor LOH Poh Chiang Andrew
Department of Electronic Engineering
CUHK

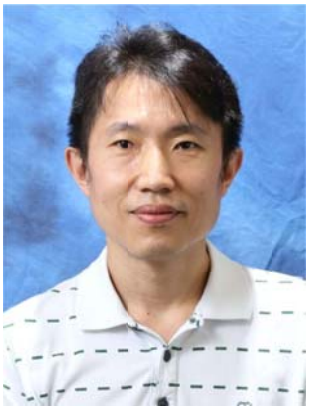

Project Start Date: 1 July 2018

ABSTRACT

Power converter is an essential interface for tying a renewable source (e.g. solar and wind) to the power system. It usually consists of three main components: microprocessor, power semiconductor devices and sensors. If the microprocessor is viewed as the "brain" of a power converter, the sensors and power devices will be its "sense organs" and "limbs". Recently, technological progress has pushed the operational speed of the "brain" to the gigahertz range, while the development of wide bandgap (WBG) devices has allowed the "limbs" to reach the megahertz range with high efficiency and power density (power per unit volume). These are significant achievements motivated largely by the booming renewable energy industry. The next trend of rapid development anticipated is related to the "sense organs" or mostly current sensors, which presently, are still confined below hundreds of kilohertz. The megahertz responses of the "limbs" are therefore not sensed properly, and may hence affect the control, protection and monitoring of a power converter. These are nontrivial issues, judging from the amount of power generated by a typical renewable source. There is thus an intense need to develop an advanced current sensing technique that can sense from DC to a few megahertz with a high noise immunity and a low manufacturing cost. Presently, no existing commercial sensors can meet the target, which is why it will be the next trend of rapid development.

INNOVATION AND PRACTICAL SIGNIFICANCE:

The developed current sensor will have a frequency bandwidth up to 10 megahertz. It is thus around 40 times wider than that of a commonly used Hall current sensor. Such wide bandwidth permits the realization of fast control and reliable protection in the newest generation of power converters built using WBG devices. The resulting converters can be sized for renewable energy generation or miniaturized for routinely used laptop adapter, EV charger and phone charger to name only a few. There will be a revolutionary reduction of size and weight, enabled by the high-frequency operation of WBG devices. In addition, the developed sensor is of great commercial competitiveness due to its small size and low cost, made possible by its integration into an inexpensive printed circuit board. This merit will promote the coming era of WBG devices with extremely high efficiency, but has its commercialization hindered many years due to its high price. Moreover, the substantial market volume and the all-important cost factor have led to the development of a wide range of alternative current sensing methods. The market demand for isolated current sensors will, in fact, hit 100 million in 2020. This is roughly equivalent to the amount of iPhones produced in 2012 [1]. Therefore, the developed current sensor is revolutionary, yet with great potential and competitiveness to be converted into a commercial product.

PROJECT OBJECTIVES and LONG-TERM IMPACT:

Recent effort in renewable energy generation field has been devoted to improving the performance of the power converters, especially in terms of efficiency and power density [2]. To realize these goals, WBG device has been recognized as the most promising candidate. However, there are multiple barriers to the population of power converters built by WBG devices [3]. Some of the well-known barriers include cost and reliability. Another one that gets less press but affects both manufacturers as well as end users is high-performance current sensing techniques [4]. Therefore, to address the barrier, the overall objective of this project is to develop an ultrafast and nonintrusive current sensor with compact size and low cost for next generation power converters. The specific research objectives corresponding to the challenges of this project are listed as follows:

1. **Ultrafast** current sensor**:** *the developed current sensor has a frequency bandwidth up to 10 MHz, which can well meet the requirement of fast protection in next generation power converters*. WBG device can switch at extremely high frequency (up to megahertz), which is the key to realization of high-efficiency and high power-density renewable energy generation. However, in terms of the short-circuit protection of WBG devices, switching current measurement becomes a significant challenge, which is unachievable for the widely used Hall current sensors that have a bandwidth limited to 250 kHz. *For power converters, lack of a reliable protection is as if driving without a seat belt, which may cause the breakdown of the power converter system under abnormal working conditions*. In comparison, the developed current sensor, with a frequency bandwidth up to 10 MHz, can well meet the requirement of protection for next generation power converters and will contribute a lot to the population of WBG devices.

2. **Nonintrusive** current sensor**:** *the developed current sensor has a very low insertion inductance less than 1nH*. High-speed WBG power devices are highly sensitive to parasitic inductances. *If too many parasitics are around a WBG device, its performance can be reduced to that of a mere silicon device, or worse: this scenario can result in circuit instability and application malfunction*. Therefore, low-level insertion parasitics, especially inductance down to nH range, has to be considered in the design of a current sensor for next generation power converters.

3. **Compact** current sensor**:** *the developed current sensor is extremely compact to enable the high power density of a power converter*. High power density of power converters is demanded in order to enable a good utilization of the energy resources and a low operating cost, which has roughly doubled every 10 years since 1970. *However, today's bulky current sensor is a major barrier for a continuation of this trend. Recent photovoltaic inverter (from Google little box challenge) has achieved 2kW power rating with its volume as two iPhone5s, while the industrial applied current sensor for PV inverters is as large as an Apple watch which is unsuitable for high power density application*. For the power density increase to follow the past trend of doubling each decade, the research focus must shift from the classical range of power semiconductors, topologies, and control to the new areas of compact current sensors.

DEVELOPMENT OF HIGH-PERFORMANCE TRIBOELECTRIC NANOGENERATORS FOR RENEWABLE BLUE ENERGY HARVESTING

Principal Investigator: Professor ZI Yunlong
Department of Mechanical & Automation Engineering
CUHK

Project Start Date: 1 July 2018

ABSTRACT

Electricity is the world's fastest growing form of end-use energy consumption. Between 2015 and 2040, world net electricity generation will increase by 45%. Non-renewable fossil fuels still account for >60% of electricity generation. However, 70% of the Earth's surface is covered by ocean, which represents a huge untapped clean and renewable energy source. Estimated to provide power of over 75 TW, ocean energy could satisfy energy demands around the world. To effectively harvest this "blue energy" especially the low-frequency mechanical energy generated by ocean waves, three-dimensional networks of triboelectric nanogenerators (TENG) have been proposed. To test this concept, however, TENG units first need to be refined to optimize their output performance. To date, factors that limit the performance include the challenge that achievable charge density is limited by the phenomenon of air breakdown; additionally, the parasitic capacitances brought by the conductive seawater may suppress the performance of TENG. We propose experimental and theoretical studies that will focus on mitigating these limiting factors by developing novel structural and material designs, greatly enhancing the output performance of TENG. The proposed research will lay the cornerstone for further technologic advancement in large-scale harvesting of kinetic water energy using TENG units.

INNOVATION AND PRACTICAL SIGNIFICANCE:

***Innovation**: The innovation of the proposed research lies in the development of high-performance TENGs for blue energy harvesting. Traditional water energy harvesting uses electromagnetic generators (EMG), which are usually huge, heavy, expensive, and technically difficult for construction in deep water. Further, studies have demonstrated that EMG are extremely inefficient in harvesting the low-frequency mechanical energy that is generated by ocean waves. TENG possess several advantages over EMG technology as they are lightweight and able to float, cost-effective and easy to produce, and efficient in harvesting low-frequency energy. Our research will focus on maximizing TENG output through addressing two crucial fundamental issues: the air-breakdown effect inside TENG and the parasitic capacitances brought by seawater, which have never been systematically studied before. For the first time, we propose to develop TENGs with novel designs to address these issues. It is expected that the output performance of TENG could increase 10-100 times through our proposed research.*

***Practical significance**: Considering the challenges of energy security and environmental protection, developing renewable energy sources is of critical importance for Hong Kong. With Hong Kong's extensive coastline and water area percentage of 59.8%, Hong Kong is strategically placed to take advantage of a convenient, clean and renewable power source. Especially for areas with complex*

coastlines that are not suitable for water shipping, electrical generation is the best option to utilize them. Additionally, the ocean currents and tropical storms that are common in Hong Kong, provide an abundant amount of mechanical energy that could potentially be converted to electrical energy. Lastly, developing the blue energy harvesting technology to replace the fossil fuels will also decrease the emissions of pollutants and greenhouse gases, which is critical for environmental protection. Therefore, developing blue energy harvesting through TENG is beneficial to Honk Kong on many levels including the mediating the energy crisis, promoting environmental protection, and advancing both economic and social development in Hong Kong.

PROJECT OBJECTIVES:

1. To simulate and experimentally demonstrate a TENG design that will minimize the air-breakdown effect using controlled high pressure and inert gas environments.

2. To simulate and experimentally develop optimized structural/material designs to minimize the influences of the parasitic capacitances brought by the conductive seawater.

3. To determine the optimized designs and produce a TENG that provides maximal available output, and to compare with other technologies used in blue energy harvesting.

Long-term impact:

The proposed research will advance TENG technology *via* two avenues: a) by promoting fundamental studies on improving TENG output for use in practical applications; b) by addressing the energy and environmental issues in Hong Kong and facilitate related economic and industrial developments. The crucial fundamental and technological challenges that will be solved include: the mitigation of the electrostatic discharging induced by the air-breakdown effect in TENGs; the optimization of the TENG design to prevent the impacts of the parasitic capacitances brought by the seawater; and the related mechanism and understandings of TENG to reach its maximal output energy in these conditions. This research will also be helpful in addressing issues of social development, including developing affordable renewable energy sources, promoting environmental protection, and lessening our contribution to global warming. Our ultimate goal is to develop TENG as a high-output, robust, and low-cost blue energy harvesting technology, which will set foundation for the next-generation renewable energy technology, to achieve the long-term positive impact on the environment and world energy consumption.

WORK IN PROGRESS

TUNABLE SPINDLE USING SELF-EXCITED VIBRATION FOR HIGH EFFICIENCY RENEWABLE ELECTRIC GENERATORS

Principal Investigator: Professor Ping GUO
Department of Mechanical & Automation Engineering
CUHK

Research Team Members:
Han Gao, Research assistant [1]
Jianjian Wang, Postdoc fellow [1]
Jing Huang, PhD student [1]
Ru Yang, PhD student [1]

[1] Dept. of Mechanical and Automation Engineering, CUHK

Reporting Period: 01 July 2017 – 31 May 2018

INNOVATION AND PRACTICAL SIGNIFICANCE:

This project proposes a novel spindle design for renewable electric generators, which utilizes high frequency vibration for improved tribological performance, higher energy efficiency, and reduced wear. The proposed design is supported by three major innovations: **(1)** vibration-induced friction reduction; **(2)** self-excited vibration without any extra power supply; and **(3)** a tunable spindle structure for a wide operation range. This project, if successful, will significantly improve the performance of traditional renewable electric generators in terms of efficiency and lifetime, which have play an ever increasing role in the era of clean energy.

ABSTRACT

Considering the world population growth, diminishing of fossil fuel sources, and environmental pollution, the use of renewable resources, such as hydroelectric, nuclear, and wind energy, has been emerging as an important form of clean energy. The core functional part in these renewal energy technologies is an electric generator. One critical issue determining the efficiency and reliability of renewable electric generators lies in the interaction between the spindle shaft and bearing surfaces. The friction coefficient largely influences the power generation efficiency while the contact condition determines the wear rate of the shaft and bearings. This project proposes a novel spindle design for renewable electric generators, which utilizes high frequency vibration for improved tribological performance, higher energy efficiency, and reduced wear. The proposed design is supported by three major innovations: (1) vibration-induced friction reduction; (2) self-excited vibration without any extra power supply; and (3) a tunable spindle structure for a wide operation range. The proposed design has a high potential for commercialization due to its much improved performance without major increase in cost and design complexity. This project, if successful, will not only help the development of fundamental research but also the application of renewable electric generators.

1. OBJECTIVES AND SIGNIFICANCE

This project proposes a novel spindle design for renewable electric generators, which utilizes high frequency vibration for improved tribological performance, higher energy efficiency, and reduced

wear. The proposed design is supported by three major innovations: (1) vibration-induced friction reduction; (2) self-excited vibration without any extra power supply; and (3) a tunable spindle structure for a wide operation range. This project, if successful, will significantly improve the performance of traditional renewable electric generators in terms of efficiency and lifetime, which have play an ever increasing role in the era of clean energy.

2. RESEARCH METHODOLOGY

This research project will be carried out to accomplish a prolonged bearing lifetime for the rotating-spindle-type electric generators together with a higher energy efficiency. There are three main research tasks in this project:

1. Propose a low friction bearing technology by the principle of vibration-induced friction reduction to prolong the lifetime of high-load bearings and increase the power efficiency in rotating-spindle-type electric generators.
2. Establish a self-tunable vibration generating device without extra electric power supply or piezoelectric elements, which reduces the extra cost for vibration system and simplifies the overall structure.
3. Realize a self-excited vibration spindle system accommodated with position-adjustable-bearings, which is capable of changing the resonant frequency of the spindle. Therefore an optimized vibration-induced friction reduction effect will be accessible when the self-excited vibration frequency is in accordance with the resonant one.

3. RESULTS ACHIEVED SO FAR

3.1. Research Progress

We have developed a non-contact journal bearing with bi-directional driving capability utilizing the coupled resonant mode. It combines the functions of an axis positioner, non-contact journal bearing, and rotary motor. The shaft levitation is achieved by creating a stable air film using near-field acoustic force; while the non-contact rotation is realized by controlling the pressure distribution within the air film using coupled resonant mode. The mechanism of non-contact rotation can be explained by the schematics shown in Fig. 1. Unlike previous designs utilizing a traveling wave and viscous shear force, the rotational driving force is mainly contributed by the tangential component of the levitation pressure. During the compression stage of the air film, due to the slope angle of the bearing upper surface, the net reaction force from the air produces a circumferential force acting in the counter clockwise direction of the shaft. During the release stage, both the bearing surface slope angle and the pressure force change the direction, so the net reaction force still produces a counter clockwise torque on the shaft. For both the compression and expansion stages, the reaction force applied on the shaft has a circumferential component in the same direction.

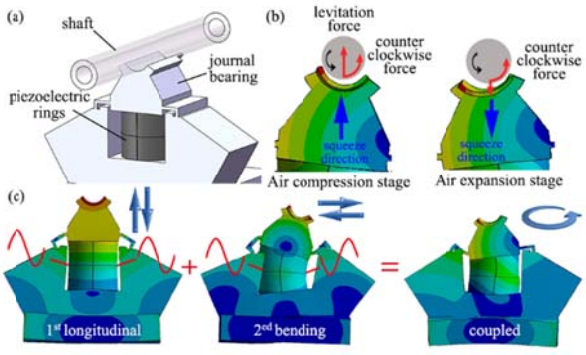

Figure 1. (a) Design of a single driving unit; (b) operation principle for shaft levitation and rotation; and (c) coupled mode shapes.

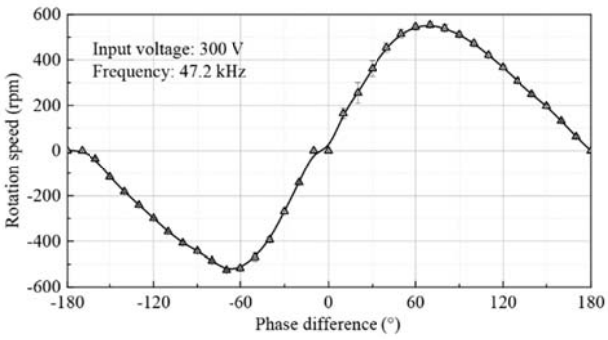

Figure 2. The relationship between rotation speed and phase angle.

The non-contact shaft rotation can be achieved and controlled by exciting the structure at a frequency between the two modes and adjusting the input phase angle or input voltage amplitude. The bearing was excited at 47.2 kHz with a voltage amplitude of 300 V, while the phase angle was adjusted from -180° to +180°. The relationship between the rotation direction as well as speed and the input phase angle is plotted in Fig. 2. The bearing demonstrated identical performance when rotated in the clockwise and counter clockwise directions. The rotation speed reached a peak value of ±555 rpm at a phase angle of 70°. The bearing could be switched to a pure levitation state by setting the phase angle to 0° or 180°.

Based on the design principle proposed in this project, an advanced functional prototype with six driving units was fabricated for two-dimensional radial position control. The 3D model and functional prototype are shown in Fig. 3. The main body of a U-shaped bearing frame was fabricated from a single aluminum alloy workpiece using electrical discharge machining (EDM) to ensure the coaxiality between the two sets of driving units. On each side, three identical driving units are placed 120° apart. Each driving unit functions similarly as the single unit described in the previous sections. The overall operating frequency of this design would be higher than that in a single unit due to the increased stiffness from the unibody design.

In additional to the levitation and rotation control, the radial position control capability is demonstrated. The driving units were grouped by their angular position and controlled by the signals #1 – #3, as shown in Fig. 3. In the vertical direction, the shaft position could be controlled in a range of 18.3 μm, when the signals #1 and #2 were simultaneously varied from 100 V to 350 V. The minimal stable increment could reach 200 nm when the voltage increment was 5 V, as shown in Fig. 4(a). In the lateral direction, the radial position could be controlled in a range of 2.1 μm, when we adjusted the amplitudes of signals #1 and #2 in the opposite direction. The minimal stable increment could also reach 200 nm when the voltage increment was 10 V, as shown in Fig. 4(b). Finally, the radial runout was measured at a rotation speed of 512 rpm, when the driving frequency was 64.9 kHz with a 75° phase shift angle. The total indicator runout was within 6 μm as indicated in Fig. 4(c), which is a combination from the shaft form inaccuracy and spindle runout.

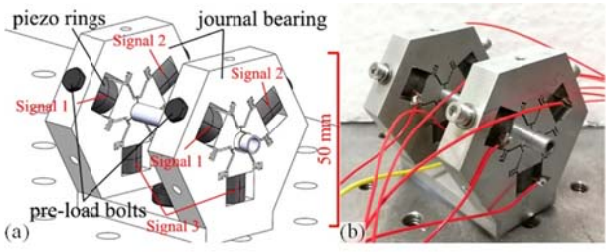

Figure 3. Design of the active non-contact journal bearing with six driving units: (a) 3D model and (b) functional prototype.

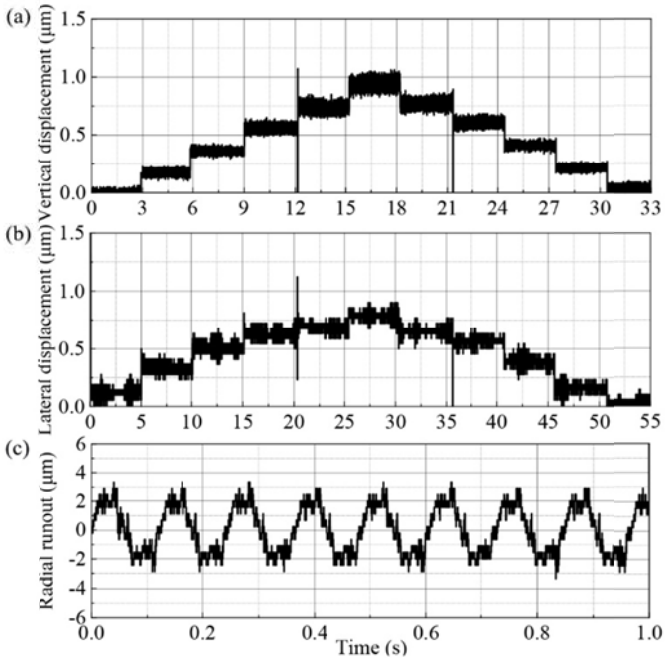

Figure 4. Active axis position control in the (a) vertical and (b) lateral directions; and (c) shaft runout during rotation.

3.2. Commercialization Efforts

1. Press Conference
We have made a press conference at CUHK on Oct 9, 2017 about our research outputs, which was reported by a number of local media, including Sing Tao Daily, Ming Pao, Oriental Daily News, Hong Kong Economic Journal, Apple Daily, Wen Wei Po, Ta Kung Pao, Metro Daily, Headling Daily, Sky Post, Hong Kong Commercial Daily, Sing Pao, South China Morning Post, etc. One of the press released photo is attached for reference (shown in Fig. 5).

2. Exhibition at InnoCarnival 2017
We have demoed our work, levitating actuator using near-field acoustic, at the Inno Carnival at the science park during Oct 21 – 29. It attracted some attention from different investors. The highlight includes the presentation of our project to Secretary for Innovation and Technology of Hong Kong, as shown in the attached figure (Fig. 6).

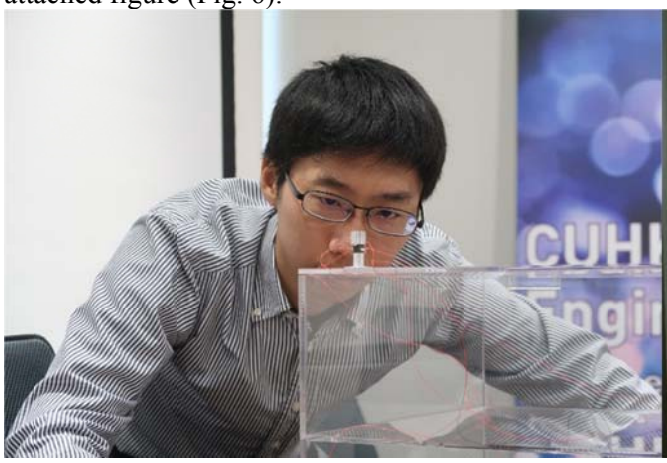

Figure 5. Press conference photo

Figure 6. Presentation at InnoCarnival 2017

3. Hasbro Presentation

We have presented our research results at the Tech Summit of Hasbro, Hong Kong on October 18. Hasbro is an American-based multinational toy and board game company (which makes the board game, Monopoly). The company showed some interest in our technology.

4. Academic Presentation

We have also presented our work in various academic settings and invited presentations, including Northwestern University (Jan 29, 2018, USA), Technical University of Denmark (May 22, 2018, Denmark), and KTH Royal Institute of Technology in Stockholm (May 25, 2018, Sweden).

4. PUBLICATION AND AWARDS

J[1] J. Wang, P. Feng, J. Zhang, and P. Guo, "Experimental study on vibration stability in rotary ultrasonic machining of ceramic matrix composites: Cutting force variation at hole entrance," *Ceramics International*, 2018.
J[2] P. Guo and H. Gao, "An active non-contact journal bearing with bi-directional driving capability utilizing coupled resonant mode," *CIRP Annals Manufacturing Technology*, 2018.
C[3] S. Gao and P. Guo, "Modeling and tool trajectory monitoring of an ultrasonic elliptical vibration tool," *International Symposium on Flexible Automation*, Kanazawa, Japan, 15-19 July, 2018.
C[4] R. Yang, J. Huang and P. Guo, "Frequency dependence of levitation force in near-field acoustic levitation," *International Symposium on Flexible Automation*, Kanazawa, Japan, 15-19 July, 2018.
*C[5] J. Wang, Y. Yang, and P. Guo, "Effects of vibration trajectory on ductile-to-brittle transition in vibration cutting of single c*rystal silicon using a non-resonant tool," CIRP Conference on Surface Integrity, Tianjin, 11-13 July, China

WORK IN PROGRESS

ROBUST NICKEL-MOLYBDENUM–YTTRIA STABILIZED ZIRCONIA (NIMO–YSZ) ANODE MATERIALS FOR SOLID OXIDE FUEL CELLS

Principal Investigator: Professor Yongsheng CHEN
Department of Mechanical & Automation Engineering
CUHK

Research Team Members:
Dr. Chinghuan Lee (postdoctoral fellow)[(1)],
Mr. Jiazheng Ren (graduate student)[(1)]

[(1)] Dept. of Mechanical and Automation Engineering, CUHK

Reporting Period: 01 August 2016 – 30 April 2017

ABSTRACT

This proposal aims to develop new anode materials to improve durability of the state-of-the-art solid oxide fuel cells (SOFCs). SOFCs are electrochemical devices that convert chemical energy of a fuel (commonly hydrogen, more importantly, fuels derived from *renewable* sources, such as biomass and municipal wastes) and oxidant directly into electrical energy. They are energy efficient and environmentally benign, and their large scale applications in electricity production may address the environmental, climate change, and water concerns that we are facing today.

There are major technical barriers that have to be overcome before SOFCs can be commercialized and widely used for power generation. Among them is anode degradation. For the state-of-the-art Ni–YSZ anodes, carbon deposition (or coking) on and sulfur poisoning of the anode are responsible for the performance loss due to the presence of impurities in carbonaceous fuels, a price that comes with the SOFC's fuel flexibility. These problems are usually dealt with separately. We will design new NiMo-YSZ anode materials to mitigate carbon deposition and sulfur poisoning simultaneously with the PI having several years' experience in studying these phenomena in steam reforming reactions. If successful, this project will promote the final commercialization of SOFC technology for power generation.

1. OBJECTIVES AND SIGNIFICANCE

Solid oxide fuel cells (SOFC) are electrochemical devices that convert chemical energy of a fuel (commonly hydrogen) and oxidant directly into electrical energy. They are much more energy efficient and environmentally benign than conventional electric power generation processes. Their large scale applications in electricity production may one day replace the current heat engine based electric power generation and address the environmental, climate change, and water concerns that face us today.

Major parts of a SOFC include anode, cathode, and electrolyte. Anode and cathode are the places where H_2 oxidation and O_2 reduction take place while electrolyte provides a separation for the gases and a tunnel for ions (O^{2-} or H^+). Materials-wise, state of the art electrolyte, anode and cathode are yttria-stabilized zirconia (YSZ), Ni–YSZ and lanthanum strontium manganite-YSZ (LSM-YSZ) composite, respectively. Compared to other fuel cell types, one advantage of SOFCs is its fuel-flexibility. They can operate not only on hydrogen, but also on hydrocarbon fuels from various sources, for example, natural gas (CH_4) and fuels derived from *renewable* sources, such as biomass and municipal wastes. This flexibility is due to the SOFC operation conditions, which dictate that SOFC is also a steam reformer and the anode serves as a *catalyst* (i.e., a functional material that promotes a chemical reaction). Inside a SOFC, hydrocarbons react with steam to produce hydrogen and carbon monoxide (termed "steam reforming").

There are major technical barriers to be overcome before SOFCs can be commercialized and widely used for power generation. Among them is anode degradation. For Ni–YSZ anodes, degradation may fall in three categories: (1) material transport mechanism; (2) deactivation and passivation mechanism, and (3) thermo- mechanical mechanism. Deactivation and passivation mechanism is responsible for the performance loss due to the presence of impurities in carbonaceous fuels, a price that comes with SOFC's fuel flexibility. It involves carbon deposition and sulfur poisoning. This proposal aims to tackle the anode degradation by carbon deposition and sulfur poisoning, and if successful, will greatly promote the commercialization of the SCFC technology.

The project objectives include the following: (1) find the optimal composition of NiMo-YZS anode materials for minimal degradation; (2) determine the proper formation of NiMo; (3) determine the optimal H_2S content and other reaction conditions for minimal coking and sulfur poisoning; (4) perform multiple characterization techniques to determine the degradation mechanism in NiMo-YSZ anode materials.

2. RESEARCH METHODOLOGY

We will develop nickel-molybdenum–yttria stabilized zirconia (NiMo–YSZ) anode materials. In our design, Ni and Mo will be metal nano-particles, either in separate phases or in alloy form. The Mo oxide layers on Mo surface are active for aromatization reaction (producing benzene from CH_4 or CO and H_2). The proposed research includes two tasks: (1) catalyst synthesis and steam reforming and (2) anode deactivation mechanisms. In other words, we will design bifunctional NiMo-YSZ catalyst, test them under reaction conditions relevant to real SOFC operation conditions, and use materials characterization techniques to study their deactivation mechanism. A catalyst testing system has been installed in Room 112 of the William M.W. Mong Engineering Building. The system is configured to carry out multiple reactions including steam reforming as shown in Figure 1. Different gases can be delivered to the system at prescribed flow rates controlled by a computer. More importantly, a controlled evaporation and mixing (CEM) device is installed to ensure stable steam delivery to the system. Gas analysis is carried out simultaneously by online IR spectrometer and gas chromatography (GC).

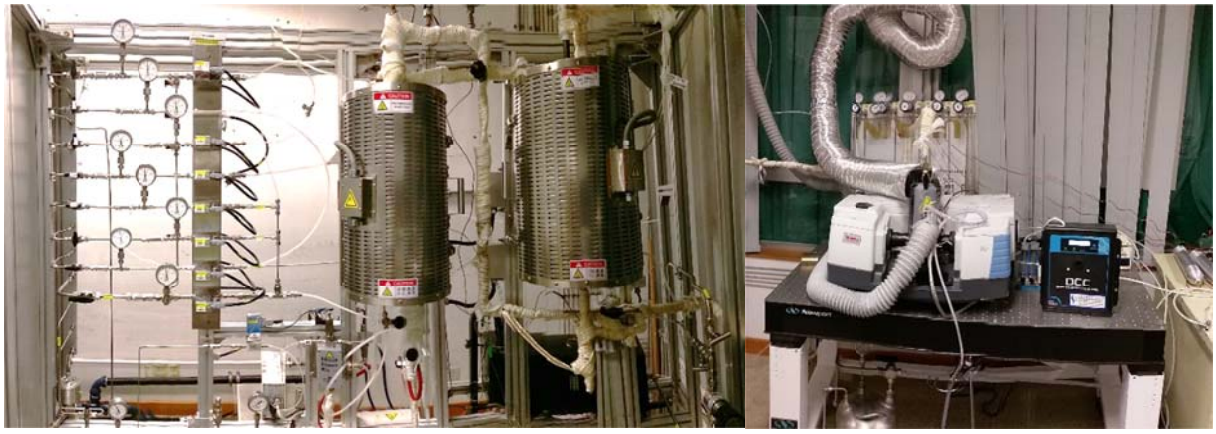

Figure 1 The catalyst testing system. Left: reactor, gas manifold and steam generator; right: IR spectrometer with 2-m gas cell for gas detection and quantification.

Among a few other things, one promising development in this project is to establish a catalyst evaluation method that has the potential to revolutionize the way how scientists and engineers test steam reforming catalysts. It is well known that carbon deposition and sulfur poisoning are two major catalyst deactivation mechanisms in steam reforming. Our previous work has shown that a major contribution of sulfur poisoning is enhanced carbon deposition. However, due to technical difficulty, carbon deposition kinetics has never been measured experimentally. Moreover, the typical method for gas analysis is GC, which has two disadvantages: 1) low time resolution as GC usually samples every 20 minutes or so; and 2)

complexity in experimental setup and data analysis. Because GC columns usually cannot endure too much moisture, so the gas effluent from the reactor needs to pass through a cold trap to remove steam before being analyzed by a GC, this is a loss of important information as steam is a major reactant. Another problem is that GC measures only concentrations of different gases, however, to determine catalyst conversion and selectivity, gas flow rates leaving the reactor are needed. This is a challenge for GC-based analysis. In this project, we use a IR spectrometer to measure the concentrations of polar gases present in the effluent. By taking advantage of the intrinsic relationship between flow rates and concentrations and the general mass balance, we are developing a method to measure the flow rates of major reactants and products including H_2O and H_2 as well as carbon deposition rate. The data sampling rate is 12 sec/point. Thus, this new method is going to make a breakthrough in steam reforming catalyst evaluation, a manuscript on this topic is in preparation.

Experimental parameters are chosen to reflect real reaction conditions relevant to SOFC operation. The steam-to-carbon ratios in the feed will be between 1~2.5 and the temperature is set at 800 ^oC; Some N_2 is co-fed to dilute the reactants achieving high conversion rate of CH_4. Three NiO catalysts will be prepared by oxidation of commercially available Ni nano-powders with average sizes of 20, 40 and 50 nm. The oxidized temperatures of Ni will be 600~1000 ^oC for pre-sintering and forming solid solutions with YSZ. Two nanosized Molybdenum sources have been ordered. They are 1) metal Mo with a particle size of 40 nm and 2) MoO_3 with a particle size of 13-80 nm. The raw materials will be mechanically mixed by planetary ball milling technique. The atomic ratios of Ni/Mo will be fixed among the different sources. The powder mixtures for catalyst tests will be prepared in the Ni/Mo atomic ratios of 160, 20, 10, 3, and so forth. A gas mixture of 10 ppm H_2S balanced by CH_4 will be used to conduct sulfur poisoning tests. Various materials characterization techniques will be used to study anode deactivation mechanism.

3. RESULTS ACHIEVED SO FAR

a. Modeling of SMR reactions:

The total inlet molar flow rate: $F_i = F_{i,CH4} + F_{i,H2O} + F_{N2}$, (1)

where $F_{i,CH4}$, $F_{i,H2O}$ and F_{N2} stand for the inlet flow rates of CH_4, H_2O and N_2, respectively. It is well recognized that there are four major chemical reactions under the reaction conditions: SMR, water gas shift reaction (WGS), methane decomposition (MD) and Boudouard reaction (BR).

The chemical reaction rates of SMR, RWGS, MD and BR are defined as the molar consumption rates of CH_4, CO, CH_4 and the molar generation rate of CO_2, respectively. Based on the stoichiometry of the four chemical reactions, the total molar flow rate of the effluents is:

$$F_o = F_i + 2F_{SMR} + F_{MD} - F_{BR}, \quad (2)$$

where F_{DRM}, F_{MD} and F_{BR} stand for the chemical reaction rates of SMR, MD and BR, respectively. Based on the stoichiometric relationships, after the reactions, the molar flow rates of CH_4, H_2O, CO_2, and CO in the effluents are:

$$F_{o,CH4} = F_{i,CH4} - F_{SMR} - F_{MD} \quad (3)$$

$$F_{o,H2O} = F_{i,H2O} - F_{SMR} - F_{WGS} \quad (4)$$

$$F_{o,CO2} = F_{WGS} + F_{BR} \quad (5)$$

$$F_{o,CO} = F_{SMR} - F_{WGS} - 2F_{BR}, \quad (6)$$

where $F_{o,CH4}$, $F_{o,H2O}$, $F_{o,CO2}$ and $F_{o,CO}$ are the outlet molar flow rates of CH_4, H_2O, CO_2 and CO, and F_{WGS}, the chemical reaction rate of WGS. After reactions, the molar concentrations of CH_4, CO_2, CO, and H_2O in the outlet were analyzed by FTIR. Basically, the concentrations of these components can be expressed:

$$C_{CH4} = (F_{o,CH4}) / F_o \quad (7)$$

$$C_{H2O} = (F_{o,H2O}) / F_o \quad (8)$$

$$C_{CO2} = (F_{o,CO2}) / F_o \quad (9)$$

$$C_{CO} = (F_{o,CO}) / F_o \quad (10)$$

Substituting Equations 1 - 6 for these related factors in Equations (7), (8), (9) and (10), the four equations above form a linear nonhomogeneous equation set in which F_{SRM}, F_{WGS}, F_{MD} and F_{BR} are the unknowns:

$$(2C_{CH4} + 1) * F_{SRM} + (C_{CH4} + 1) * F_{MD} - C_{CH4} * F_{BR} = (1 - C_{CH4}) F_{i,CH4} - C_{CH4} * (F_{i,H2O} + F_{N2})$$

$$(2C_{H2O} + 1) * F_{SRM} + F_{WGS} + C_{H2O} * F_{MD} - C_{H2O} * F_{BR} = (1 - C_{H2O}) * F_{i,H2O} - C_{H2O} * (F_{i,CH4} + F_{i,N2})$$

$$2C_{CO2} * F_{SRM} - F_{WGS} + C_{CO2} * F_{MD} - (C_{CO2} + 1) * F_{BR} = -(F_{i,CH4} + F_{i,H2O} + F_{i,N2})$$

$$(2C_{CO}-1) * F_{SRM} + F_{WGS} + C_{CO} * F_{MD} + (2- C_{CO}) * F_{BR} = -(F_{i,CH4} + F_{i,CO2} + F_{i,N2}) * C_{CO}$$

Solving these equations, the important flow rates related to the reaction are obtained in terms of concentrations measureable by IR. For example, the production rate of H_2, which is $3* F_{SMR} + F_{WGS} + 2* F_{MD}$, and the carbon formation rate, $F_{MD} + F_{BR}$, can be expressed in C_{CH4}, C_{H2O}, C_{CO2}, and C_{CO}.

b. Initial experimental test of the SMR modelling: A 10% Ni supported on γ-Al_2O_3 (Ni/Al_2O_3) was prepared by impregnation method and is used as a reference. During 10 hours of reaction under different steam carbon ratio, the concentrations of the major reactants and productions, CH_4, H_2O, CO, and CO_2 were measured by IR and are shown in **Fig. 2**. There are three stages in the process as detailed in the caption.

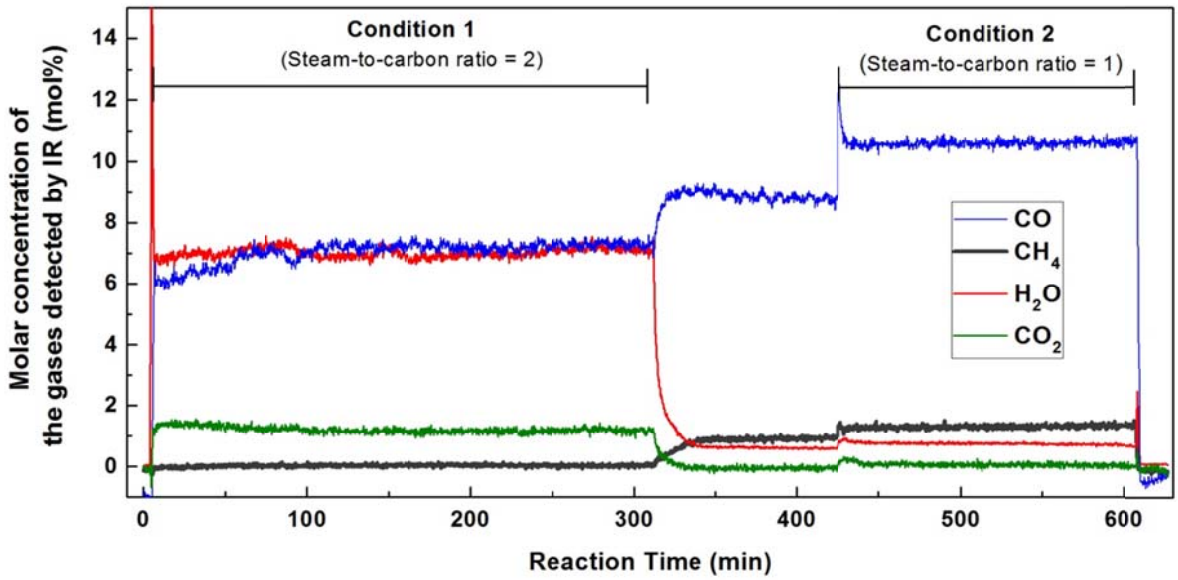

Figure 2 Molar concentrations of the important effluent gases as a function of reaction time during SMR operations measured by IR spectrometer. Note that between 0 – 430 minutes, the effluent is diluted by extra N_2 gas.

By applying the method developed previously, the H_2 and CO production rates are determined as shown in Fig. 3. Both production rates are stable during the test. Changes are observed when the steam to carbon ratio (S/C ratio) changes from 2 to 1 resulting in lower H_2 and a little bit higher CO production rates. Also shown in Fig. 3 are the CH_4 and H_2O conversion rates. At 2:1 S/C ratio, CH_4 is completely converted while at 1:1 S/C ratio the CH_4 conversion rate is lower at about 90%. Contrary to the featureless profiles of the conversion rates and H_2 and CO production rates, the carbon deposition rate is really dynamic. It is believed that some of the features are artifacts due to current experimental errors which can be significantly minimized upon optimization; nevertheless, it may mark the start of a new era

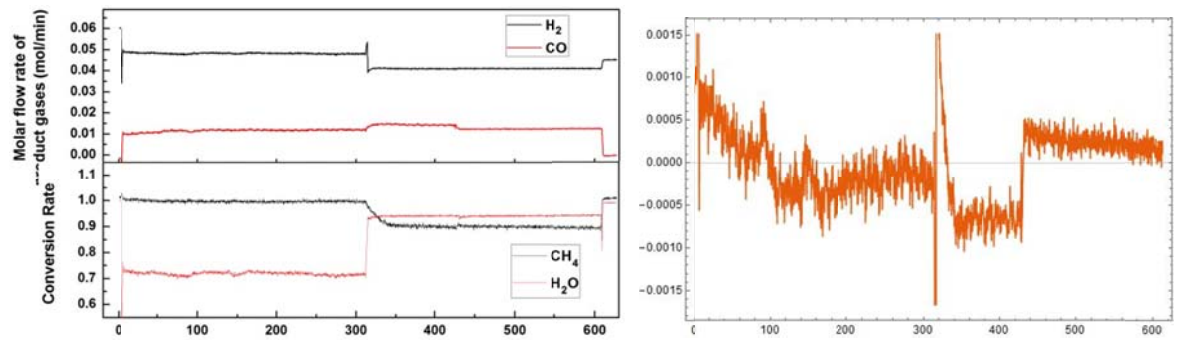

when we can experimentally observed carbon deposition kinetics in real time.

Figure 3 Catalytic performance of a 10%Ni/Al_2O_3 catalyst in the steam reforming reactions shown in Fig. 2. Left top: H_2 and CO production rates; left bottom: CH_4 and H_2O conversion rates; and right: carbon deposition rate.

4. PUBLICATION AND AWARDS

The postdoctoral researcher, Dr. Chinghuan Lee, applied for Research Fellowship Scheme 2016-17 based on this SHIAE project and received about HK$190,000 additional funding from the Faculty of Engineering and Office of Research and Knowledge Transfer. This frees up some of the Staff costs; hopefully we can reallocate some of the funds for general expenses. So far, we have not published journal papers from the research, but we are confident that 2~3 manuscripts will be submitted in the following months.

COMPLETED

EXPERIMENTAL AND MODELING STUDY OF BIODIESEL COMBUSTION

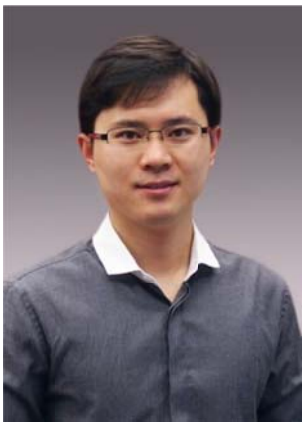

Principal Investigator: Professor Wei REN
Department of Mechanical & Automation Engineering
CUHK

Co-Investigator (if any): Enoch Dames[(2)]
Research Team Members: Zhili Li(1), Zhen Wang(1), Qiang Wang(1), Hongbo Ning(1), Liuhao Ma(1), Junjun Wu(1)

[(1)] Dept. of Mechanical and Automation Engineering, CUHK
[(2)] Department of Chemical Engineering, MIT, USA

Reporting Period: 01 July 2015 – 31 July 2017

ABSTRACT

Liquid fossil fuels such as gasoline, diesel, and kerosene are the most popular choices for transportation. However, the burning of fossil fuels has led to serious environmental issues of air pollution and global warming. Biofuels offer an attractive alternative to fossil fuels and can contribute significantly to sustainable development in terms of economic and environmental concerns. Biodiesel, with its numerous desirable fuel properties, is among the best candidates to replace diesel fuel in engine systems. Considerable effort is currently being devoted to the development of quantitatively predictive mechanisms for biodiesel combustion, which are required by the design of new engines and fuel blends. However, the detailed biodiesel combustion chemistry is still far from completion. This research aims to enlarge the experimental shock tube database of biodiesel surrogate and component combustion measurements. In order to accomplish this, a novel aerosol shock tube technique is designed to allow measurements of the very-low-vapor-pressure biofuels. Ignition delay times, species time-histories, and elementary reaction rate constants will be measured to understand the fundamental chemical kinetics of biodiesel surrogates. The proposed study will result in new and valuable information to improve the existing understanding of biodiesel combustion.

1. OBJECTIVES AND SIGNIFICANCE

1). *To develop and test the new method of laser diagnostics and shock tube for studying combustion chemical kinetics of biofuels with very low vapor pressure*. The necessity of gas-phase fuel loading in shock tubes is the most important limitation of conventional gas-phase shock tubes used for combustion research. However, the large fatty acid methyl esters (FAMEs) composing biodiesel have so low vapor pressures (sub-Torr) that obtaining sufficient gas-phase fuel molecules in a shock tube is virtually impossible. We propose a novel design of Laval nozzle to be used in the CUHK shock tube to generate uniform fuel aerosol, making it suitable to study biodiesel combustion. This new design can be extended for studying chemical kinetics of all types of biofuels and even those of nanoparticle-laden combustion in the future.

2). *To investigate the influence of alkyl chain length and C=C bond on the combustion kinetics of methyl esters.* Most of the previous biodiesel combustion research focused on the short-chain methyl esters containing <5 carbon atoms. Moreover, FAMEs in biodiesel are mostly unsaturated containing C=C double bonds, while considerably less work has been reported on unsaturated methyl esters. We will systematically investigate the chemical kinetics of methyl esters with varied alkyl chain lengths and the existence of C=C bond in the molecular structure.

3). *To measure the ignition delay times, species time-histories, and elementary reaction rate constants during the oxidation of methyl oleate.* The biodiesel blends are usually composed of five FAMEs with methyl oleate (MO, $C_{19}H_{36}O_2$) the largest constituent. The kinetic properties of MO is not yet well-understood, and especially no experimental data for MO currently exist in the literature. With the advanced aerosol shock tube/laser diagnostics technique, our research can provide such valuable shock

tube data for the validation of reduced/detailed kinetic mechanisms for biodiesel fuels.

4). *To understand and interpret the experimental data of methyl oleate pyrolysis and oxidation by detailed kinetic modeling*. Detailed kinetic modeling using state-of-the-art quantum chemistry techniques will be performed to interpret the measured species time-history data during the pyrolysis and oxidation of methyl oleate. Meanwhile, individual reaction rate, the core parameter in the chemical kinetic model controlling the reaction pathways, can be directly measured by carefully selecting the reactive mixtures. Such reaction rates can be directly incorporated into kinetic mechanisms, yielding immediate improvements. These results assist further understanding of the mechanisms in terms of improving biofuel combustion efficiency and reducing emissions.

2. RESEARCH METHODOLOGY

We divide the work into the following three tasks to achieve the goal of this research project.

Task 1: to develop the advanced shock tube/laser diagnostics for the low-vapor-pressure biofuel combustion.

The next generation of shock tube is under-construction and will be installed in the Laser Diagnostics and Combustion Laboratory at CUHK. A novel design of Laval nozzle used in this shock tube makes it suitable to study fuels with very low-vapor-pressure (sub-Torr) such as the real biodiesel. In the current work, the fuel aerosol/gas mixtures being studied undergo two subsequent shock heatings and compressions. First the incident shock (500-800 K) can evaporate any distillate liquid fuel. A visible laser at 665 nm will be used to check the complete vaporization of all fuel droplets before the arrival of the reflected shock wave by monitoring the droplet-induced laser extinction. Then the reflected shock will bring the purely gas-phase mixtures to combustion-relevant temperatures (1000-2000 K) where the chemistry can be observed. The large inner dimension of our shock tube (ID: 12 cm) ensures negligible non-ideal effects caused by the boundary layer.

Fuel chemistry and chemical kinetics are then studied in the shock tube with the aid of advanced laser diagnostics and pressure sensors. Laser-absorption diagnostics are widely used for shock tube chemical kinetics studies, due to their species-specific and non-intrusive properties with fast time response (microsecond). Commercial quantum cascade lasers (QCLs) at the wavelengths of 4.3 μm, and 4.6 μm, and 5.2 μm will be used for the sensitive detection of CO, CO_2 and NO. Interband cascade lasers (ICLs) at 2.5 μm and 3.6 μm will be implemented for H_2O and CH_2O diagnostics. These absorption sensors will be integrated with the shock tube via five optical windows to achieve simultaneous multi-species detection.

Task 2: to fully understand the combustion chemical kinetics of biodiesel surrogates.

Chemical kinetic mechanisms are developed and validated using a combination of complex computer-aided computations and experimental data obtained under carefully controlled conditions. These mechanisms are built to understand the precise reaction pathways undertaken during fuel oxidation that transforms fuel into CO_2 and H_2O while producing heat. We start the biodiesel study with its surrogates processing relatively small molecular size for the validation of previous mechanisms. We expect several elementary reaction rate constants controlling the surrogate consumption pathways, such as the initial unimolecular decomposition and hydrogen atom abstraction reactions, to be measured using the shock tube/laser absorption technique.

Task 3: to perform experimental and modeling study of the chemical kinetics of biodiesel component.

Methyl oleate ($C_{19}H_{36}O_2$), the major component of the current biodiesel in use, is selected in this work for the fundamental study of its combustion kinetics. First, ignition delay time will be measured during the oxidation of MO at varied temperatures, pressures, and equivalence ratio. Ignition delay time is defined as the time between the arrival of the reflected shock wave (marked by the 50%-rise point of the pressure) at the observation port and the extrapolation of the maximum slope of the emission signal (here OH* emission) to the baseline. We will extend these measurements to lower and higher pressures to cover wider experimental conditions (1-40 atm) using our advanced shock tube facility. All these data will test the ability of a mechanism to simulate the overall combustion reaction of fuel and oxygen combining to form products and release heat. Second, the mole fractions of individual molecules (fuel, products, or intermediates) can be

measured throughout the reaction process using the species-specific laser-absorption diagnostics as developed in Task 1. Such time-histories primarily test the subset of the mechanism that includes reactions relating to the measured species. These measurements enable us to follow the time sequence of events occurring in a complex combustion system, from initial fuel breakdown, the formation of intermediates, radical build-up, and finally to the formation of the combustion products. Detailed kinetic modeling will be performed to interpret the measured species time-history data.

3. RESULTS ACHIEVED

1). Developed the advanced shock tube and laser diagnostics for time-resolved species detection.

We have developed a novel shock tube suitable to study fuels with very low-vapor-pressure (sub-Torr) such as the real biodiesel. The details can be found in Fig. 1. Compared to Stanford's method of aerosol generation using a supersonic nebulizer, our method can generate more uniform fuel aerosol with known fuel concentration and equivalence ratio. The fuel aerosol/gas mixtures being studied undergo two subsequent shock heatings and compressions.

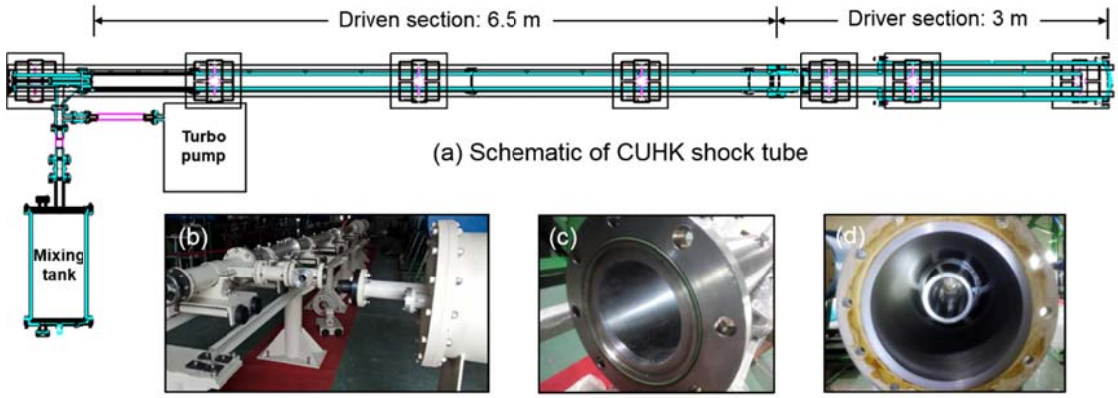

Fig. 1. (a) The stainless-steel, 10-m long shock tube recently built for high-temperature chemical kinetics study. (b) The polished driven section with six pairs of optical windows. (c) The driver section with an insert to achieve uniform shock conditions.

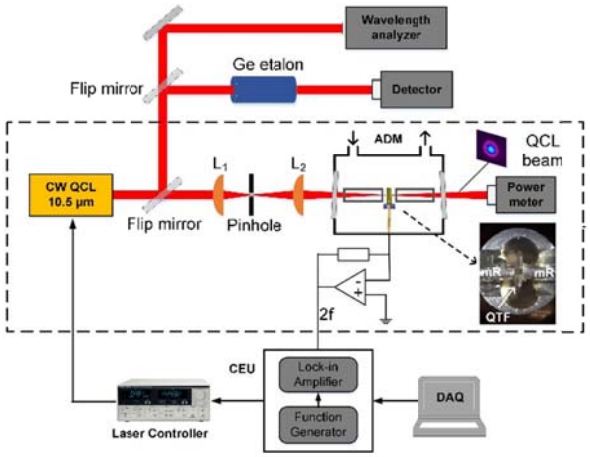

Fig. 2. Schematic and photo of the QEPAS sensor setup for C_2H_4 detection. L_1, L_2: plano-convex lens; ADM, acoustic detection module; QTF, quartz tuning fork; mR, micro-resonator; CEU, control electronics unit; DAQ, data acquisition.

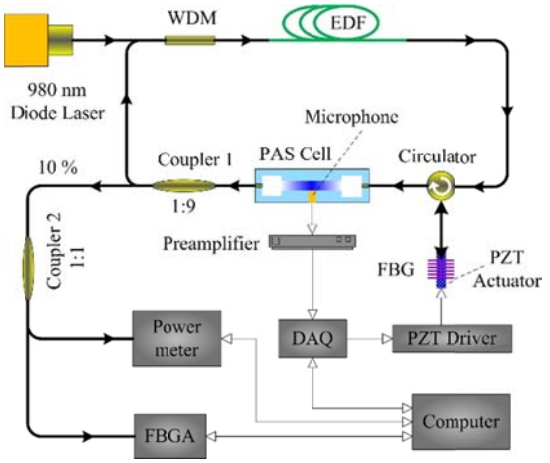

Fig. 3. Configuration of the FLI-PAS gas detection system. WDM, wavelength division multiplex; EDF, erbium doped fiber; FBG, fiber Bragg grating; PZT, piezoelectric transducer; DAQ, data acquisition card; FBGA, FBG interrogation analyzer.

Time-resolved laser diagnostics are required to monitor the species concentration time-histories during the pyrolysis or combustion of biofuels. We developed several different types of optical sensors for the sensitive detection of C_2H_4 using a quantum cascade laser near 10.5 μm, and C_2H_2 using a custom-designed fiber laser near 1.5 μm. These optical sensors achieve a detection sensitivity on ppm level that can be later applied in the combustion diagnostics during biodiesel combustion. Figure 2 and Figure 3 depict the basic experimental setup for C_2H_4 and C_2H_2, respectively. Parts of the results were published in *Optics Express* [J1] and the *Journal of Lightwave Technology* [J2].

2). Improved the understanding of the combustion chemical kinetics of methyl butanoate.

We performed shock tube study of the thermal decomposition of methyl butanoate (MB) using recently developed tunable diode laser absorption diagnostics. This paper extends the previous work by Farooq et al. of MB pyrolysis by taking advantage of new advancements in laser absorption sensors. Shock tube experimental conditions covered a temperature range of 1259–1521 K and pressure of ~1.5 atm. A much lower reactant concentration of 0.2% was used instead of 2–3% by Farooq et al. to eliminate large uncertainties in absorption cross-sections during the endothermic pyrolysis process. In the current study, new discoveries of CO_2 and CO yields were observed during MB pyrolysis. Reaction pathway and sensitivity analyses were performed according to the current CO_2/CO measurements and detailed kinetic modeling. These results were reported in the *10th Asia-Pacific Conference on Combustion* [C1] and *The 1st National Combustion Chemistry Meeting* [C2].

3). Comprehensive understanding of the reaction kinetics of methyl propanoate.

We theoretically and experimentally studied the high-temperature reaction kinetics of two important biodiesel surrogates, methyl propanoate (MP) decomposition and ethyl formate (EF) hydrogen-abstraction. In MP decomposition, the unimolecular decomposition kinetics of MP including the direct C−O/C−C bond fissions and molecular reaction channels, were studied by using high-level *ab initio* calculations and Rice-Ramsperger-Kassel-Marcus/master equation (RRKM/ME) theory. The phenomenological rate constants were determined using the RRKM/ME theory over a temperature range of 1000−2000 K and a pressure range of 0.01 atm to the high-pressure limit. At 1 atm, the branching ratios show that the dissociation reactions MP ↔ $\bullet CH_2C(=O)OCH_3 + CH_3$, MP ↔ $CH_3OC\bullet(=O) + C_2H_5$ and MP ↔ $CH_3CH_2C(=O)O\bullet + CH_3$ dominate MP pyrolysis over the temperature range of 1000−1500 K. Our calculated rate constants were adopted in a detailed kinetic model to reproduce the laser-absorption measured CO and CO_2 concentration time-histories during the pyrolysis of 0.2% MP/Ar in a shock tube from 1292−1551 K and at 1.6 atm. The updated mechanism accurately predicted the early-time CO and CO_2 formation over the entire temperature range. In particular, our mechanism well reproduced the CO_2 time-histories from the early-time formation to the final plateau level. Figure 4 presents comparisons of the measured and simulated concentration time-histories of CO and CO_2 at 1369 and 1551 K and at 1.6 atm during the pyrolysis of 0.2% MP/Ar. These results were reported in the journal of *Combustion and Flame [J3]*.

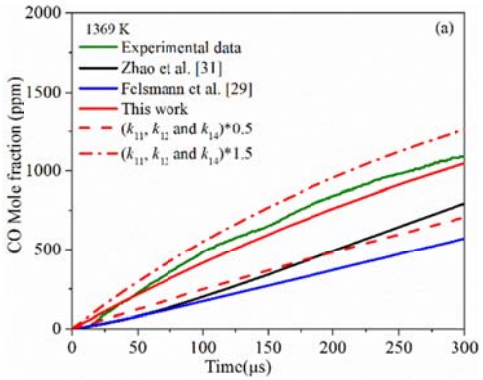

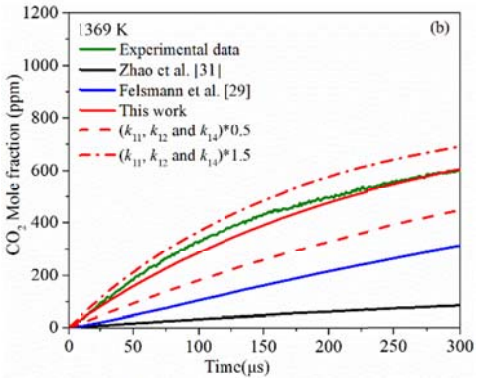

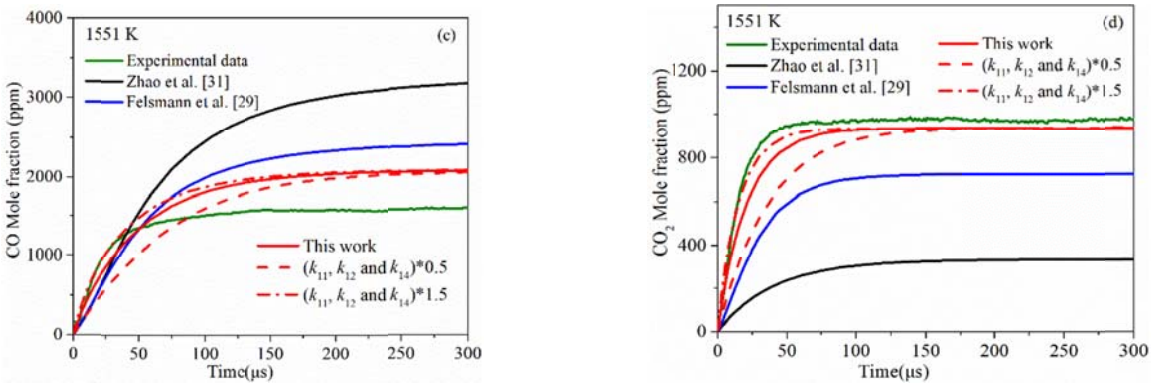

Fig. 4. Comparisons of the measured (olive line) and simulated concentration time-histories of CO and CO_2 at 1369 and 1551 K and at 1.6 atm during the pyrolysis of 0.2% MP/Ar.

4). Chemical kinetics of large methyl esters and biodiesel component.

We also performed experimental and modeling study of the large methyl ester and biodiesel component. We collaborated with Stanford University to measure the ignition delay time of methyl oleate. All these data were used to test the ability of the mechanism to simulate the overall combustion reaction of fuel and oxygen combining to form products and release heat. We also performed detailed kinetic modeling to interpret the measured species time-history data. Since the rate constant of Fuel+OH→Product affects the combustion behavior significantly, we performed quantum chemistry calculation of this rate constant. Particularly the energies of this reaction were obtained using the ONIOM method at the theory level of CCSD(T)/CBS(D-T):M06-2x/6-311++G(d,p). The preliminary results are in good comparison with previous estimations. All these experimental data and theoretical results will result in another high-impact journal paper.

4. PUBLICATION AND AWARDS

J[1] Z. Wang, Z. Li, and W. Ren, "Quartz-enhanced photoacoustic detection of ethylene using a 10.5 μm quantum cascade laser," *Optics Express*, OSA Publishing, USA, 24 (pp. 4143-4154), 2016.

J[2] Q. Wang, Z. Wang, and W. Ren, "Theoretical and experimental investigation of fiber-ring laser intracavity photoacoustic spectroscopy (FLI-PAS) for acetylene detection", *Journal of Lightwave Technology*, DOI: 10.1109/JLT.2017.2748137 (2017).

J[3] H. Ning, J. Wu, L. Ma, W. Ren*, D. F. Davidson, and R. K. Hanson, "Chemical kinetic modeling and shock tube study of methyl propanoate decomposition", *Combustion and Flame*, ELSEVIER, 184 (pp. 30-40), 2017.

C[1] W. Ren, D. F. Davidson and R. K. Hanson, "Methyl butanoate thermal decomposition: an improved shock tube study," *the 10th Asia-Pacific Conference on Combustion*, the Combustion Institute, Beijing, China, 2015.

C[2] W. Ren, "Experimental and modeling study of methyl butanoate in a shock tube," *the 1st National Combustion Chemistry Meeting*, Chinese Chemistry Society, Chengdu, China, 2015.

C[3] L. Ma, H. Ning, J. Wu, and W. Ren, "Exploration of temperature/H_2O nonuniformity in a premixed laminar flame using tunable laser absorption spectroscopy", *the 2016 International Conference in Aerospace for Young Scientists*, Beijing, China, 2016. (**Best paper award**)

Biomedical Engineering Track

Research Reports In Biomedical Engineering

Newly Funded Projects (2018-2020)	* Development of Highly SensitiveQuantitative Phase Microscopy forLabel-free Imaging of NeuronalNetwork Activities
Continuing Projects (2017-2019)	* Development of a Novel Robotic Manipulator for Confined Space Surgery
	* Development of an Inertial Microfluidics Based Approach for the Isolation of Mitochondria from Biological Samples
(2016-2018)	* An MRI-guided Robotic System for Breast Biopsy
	* Intention-driven Shoulder Rehabilitation for Targeted Meuro-muscular Training using an Exo-musculoskeletal Robot
	* Engineering Antimicrobial Surfaces Based on Micro-topography Using a Novel Ultrasonic Machining Method
Completed Projects (2015-2017)	* Development of a Novel flexible Surgical Robot with Haptic Sensation
	* Development of Injectable Supramolecular Hydrogels for Regenerative Medicine

	* Developing Optomechanical Devices based on Layered Nanomaterials for Single-Biomolecule Mass Spectrometry

The following reports are enclosed in "Research Highlights" printed in August 2017

Completed Projects	
(2014-2016)	* Development of High-speed Laser Scanning Microscope for In Vivo Deep Brain Imaging
	* Mechanism for the Transcytosis of Targeted Nanoparticles Across the Blood-brain barrier
(2013-2015)	* Development of the Next Generation Neurosurgical Assistant System Based on Functional Brain Mapping
	* Biomimetic scaffold for stem cell based cartilage regeneration and drug delivery

The following reports are enclosed in "Research Highlights" printed in June 2015

Completed Projects	
(2012)	* Dielectrophoresis Nano-separator for Precision Manufacturing of Polymeric Nanoparticles for Tumor-Targeted Drug Delivery

The following reports are enclosed in "Research Highlights" printed in June 2014

Completed Projects	
(2011)	* Viewing Biomolecules at the Right Site by Plasmonic Tweezers and Surface Enhanced Raman Scattering

The following reports are enclosed in "Research Highlights" printed in 2013

Completed Projects	
(2010)	* An inexpensive functional finger prosthesis with rebounded type progressive hinge lock
	* Diffusion Tensor MRI Predictors of Cognitive Impairment in Confluent White Matter Lesion
	* Lanthanide-impregnated molecularly imprinted polymer microspheres as antibody mimics on an optofluidic platform for the detection of disease biomarkers
(2009)	* Terahertz probe for in vivo imaging
	* Signal Processing Strategies on Cochlear Implant Devices for Effective Speech Perception of Tonal Languages
	* Development of A Robotic Endoscope Holder for Nasal Surgery

The following reports are enclosed in "General Report and Research Highlights 2009-2011" printed in October 2011.

Completed Projects	
(2008)	* Development of highly sensitive and large throughput surface enhanced Raman scattering (SERS) substrates for molecular diagnosis
Completed Projects	
(2008)	* Research on Language and Brain Waves
	* Development of an Efficient Locomotion Mechanism for Wireless Active Capsule Endoscope
(2007)	* Bio-electromagnetic Modeling and Experiment Setup for Medical Electronics RF Safety Assessment
	* Medical Applications of Terahertz Imaging
	* Hybrid Assistive Knee Braces with Smart Actuators
(2006)	* RF Radiation Effect and Efficiency of Wireless Medical Devices on Human Body
	* Photonic biosensor micro-arrays for screening of common cancers

The following reports are enclosed in "Research Highlights 2005-2007" printed in January 2008.

Completed Projects	
(2005)	* Cochlear Implants
	* Virtual Anatomy and Dexterous Simulators for Minimal Access Cardiothoracic and Neuro-endoscopic Surgeries
	* Systematic Synthesis of Nano-informatics Chips by Nano-Robotics Manipulation

(Funded Year)

DEVELOPMENT OF HIGHLY SENSITIVE QUANTITATIVE PHASE MICROSCOPY FOR LABEL-FREE IMAGING OF NEURONAL NETWORK ACTIVITIES

Principal Investigator: Professor Renjie ZHOU
Department of Biomedical Engineering, CUHK

Project Start Date: 1 July 2017

ABSTRACT

With the median life expectancy in Hong Kong and many developed countries rapidly increasing, aging related neurological disorders, such as stroke, Alzheimer's disease, and dementia, are of great social and economic relevance. The challenge in neuroscience lies in the ability to monitor neuronal network activities to study mechanisms of increasingly complex behaviors under normal and disease conditions. These demands of neuroscience can only be met by developing novel neural imaging technologies at single neuron levels. Neuronal network activities are characterized by electrical impulses called the action potentials. Fluorescence-based imaging techniques using bright voltage-sensitive dyes can directly map the action potential signals, but they suffer from photobleaching of the fluorescent proteins, preventing them for long-term neuronal network functional studies. Therefore, the development of a label-free optical imaging technique (i.e., without using fluorescent tags) is critical in solving this issue. During this project, we propose to develop a highly sensitive interference microscopic technique for imaging the action potential signals in neuronal networks. To demonstrate the feasibility of this imaging technique, we plan to first achieve the mapping of action potentials of cultured neurons, derived from induced pluripotent stem cells. After that, we plan to map the neuronal network activities of multicellular organisms, e.g., Caenorhabditis elegans. As the world's first neural imaging system of this type, we envision that it will enable many important discoveries in neuroscience.

INNOVATION AND PRACTICAL SIGNIFICANCE:

The development of optical recording techniques for mapping action potentials is important as it offers many key advantageous over the traditional electrophysiology techniques (e.g., patch clamping), such as:

a. *Noninvasiveness without physical contacts,*
b. *Spatial and temporal resolvability,*
c. *High-throughput measurement capability.*

However, label-free optical imaging techniques (i.e., without using fluorescent tags), that do not suffer from photobleaching and slow kinetics of fluorescent proteins, still have not been developed for long term and high speed recording of action potential signals on excitable mammalian cells. Among possible label-free techniques, interferometric microscopy, particularly the quantitative phase microscopy (QPM), is promising in satisfying the sensitivity and speed requirements needed for imaging action potentials. The PI, Prof. Renjie Zhou who is an expert on QPM, has recently

implemented MEMS-based mirrors and highly sensitive cameras into QPM systems. He recently co-developed a theory for understanding the phase noise limit in such systems, which has led to achieve 10-4 temporal sensitivity with 10 ms temporal resolution in a QPM system. In order to image neuronal action potentials as proposed in this project, we need to further achieve 10-5 temporal sensitivity and 1 ms temporal resolution. Therefore, we will develop a QPM system that integrates the following technical innovations:

a. A high stable interferometric microscopy design,

b. A better usage of the dynamic range of a high well-depth camera,

c. Capability of operating in the reflection-mode QPM system to inheritably provide 10x better sensitivity.

Our system will enable us to image, for the first time, the electrical activities of cultured neurons, such as those from induced pluripotent stem cells, without fluorescence labeling. This work will promote strong collaborations with the School of Biomedical Sciences at CUHK through the Co-I Prof. Vincent Cheung who is a neurobiologist. By mapping the neural network activities of multicellular organisms, e.g., Caenorhabditis elegans, it will establish our technique as an important neural imaging tool for revealing functional maps of complex nervous systems in the future.

PROJECT OBJECTIVES:

1. Develop a high sensitivity and high speed transmission-mode interferometric microscopy system

The temporal sensitivity of interferometric microscopy systems have been always limited to 10^{-3}, i.e., 1 milliradiance in phase, which has prevent this microscopy technique for many important biomedical imaging applications that involve subtle dynamical morphology changes of a few nanometers, e.g., neuron action potential signal across axonal plasma membrane at the voltage-gated ion channels. Specifically, to resolve neuron action potential signals requires 10^{-5} temporal sensitivity, 1 ms temporal resolution, and 0.5 μm spatial resolution. Developing an interferometric microscopy system with the above performance will greatly benefit neurobiology and neuropathology research.

2. Apply the developed interferometric microscopy system for optical electrophysiology of mammalian neurons

Highly efficient voltage probes have been recently developed to optically record action potentials, but there are still major limitations in those incoherent optical recording techniques, mostly due to the photobleaching and the slow kinetics of fluorescence proteins, thus limiting the recording period and the resolvability of very closely spaced voltage spikes. Our interferometric microscopy platform that will be developed and applied to record action potential signals is fast and noninvasive, and it does not suffer from photobleaching. Using our system to examine a single mammalian neuron's action potential signals will help us validate our technique. If successful, this will enable us to extend our microscopy system for mapping the whole neural network of multicellular organisms, e.g., *C. elegans*, and to reveal the correlation between the organism's behaviors and its neural signal distribution due to environmental stimulations over an extended period of time.

3. Extend to a reflection-mode interferometric microscopy system for potential in-vivo neural imaging applications

The transmission-mode interferometric microscopy system is suitable for imaging cultured neurons in the dish or brain slices ex vivo. However, in order to be ultimately used it for in-vivo optical electrophysiology, a reflection-mode interferometric microscopy system is needed. If developed, this system will open new avenues for in-vivo electrophysiology that will enable groundbreaking discoveries in neuroscience.

WORK IN PROGRESS

DEVELOPMENT OF A NOVEL ROBOTIC MANIPULATOR FOR CONFINED SPACE SURGERY

Principal Investigator: Professor AU, Kwok Wai Samuel
Department of Mechanical & Automation Engineering, CUHK

Co-Investigator (if any): Prof. Philip Chiu[(2)]

Research Team Members:
Yuanpei Choi, PhD Student, Research Assistant [(1)]
H. Y. Yip, MPhil Student, Research Assistant [(1)]
Vincent Hui, Research Associate [(1)]

[(1)]Dept. of Mechanical and Automation Engineering, CUHK
[(2)]Dept. of Surgery, CUHK

Reporting Period: 1 July 2017 – 31 May 2018

INNOVATION AND PRACTICAL SIGNIFICANCE:

Although substantial progress has been made, existing flexible instruments still lack synergy among the core surgical enablers including the instrument accessibility, size, and surgical functionalities. The success of this project will provide a new mechanical and control framework for the development of robotic instrument that is capable of overcoming these limitations. This innovative robotic system enables surgeons to provide more accurate, effective, and less invasive procedure even for the complex cases such as skull base surgery, which are currently difficult to treat even with the state-of-the-art robotically assisted surgery. The proposed technology can also allow more patients suitable for and can benefit from MIS in these anatomical regions, ultimately, improving the quality of life of patients

ABSTRACT

Minimally Invasive Surgery (MIS) has been widely adopted in many surgical specialties. Still, for some hardly accessible anatomical regions, only limited options of MIS can be offered by physicians. Accessing these regions often require surgical tools passing through tortuous natural orifices. Yet, existing surgical instruments are predominantly straight and rigid with limited surgical capabilities.

Inspired by nature, a robot with dexterous flexible structure will allow us to address the aforementioned clinical challenges. Here, we focus on the development of the hardware design and intelligent kinematic-based control algorithms for dexterous flexible manipulator. These enabling technologies will be integrated together to set out a robotic platform for accessing and navigating tortuous, narrow spaces in the human that is not possible before. The platform should be versatile for the use in many minimally invasive procedures demanding for flexible access to confined anatomical areas, such as sinuses, base of skull, esophagus, bronchi, ureter, kidney, urinary bladder. To demonstrate the clinical efficacy and general practicality, we will perform the mock surgical procedures with the platform on phantom. The success of the development can offer significant benefits to the patients and open up a great opportunity for future technology transfer and commercialization.

1. OBJECTIVES AND SIGNIFICANCE

Robotic Minimally Invasive Surgery (MIS) has been widely adopted in many surgical specialties [1][2]. In 2016 alone, over 750,000 surgical procedures were performed world-wide using the da Vinci Surgical Robotic System [3]. Nevertheless, existing surgical robotic platforms are bulky in size, while their instruments are predominantly straight and rigid with a large diameter (dia.~8mm). These system limitations prevent the physicians to provide less invasive diagnostics and treatment to patients who have diseases in the hardly accessible anatomical regions (e.g. paranasal sinuses, base of skull, larynx, bronchi, and etc.) [4-7]. For example, in endonasal sinuses and skull base surgery (Fig. 1), physicians normally use straight and rigid tools to reach the target site through the nostril. Due to the limitations of the instrument dexterity, only a small fraction of patients (below 20%) are suitable for this surgery [4-7]. Patients with this disease opt to receive more invasive treatment that requires creation of surgical accesses through the patients' forehead or cheek such as lateral rhinotomy. These large, traumatic openings can create serious complications including double vision, retention of mucus that can lead to infectious complications, brain swelling, seizures and cheek disfigurement.

Inspired by nature, we know that dexterous flexible robot will be the technological pathway to address this fundamental clinical and robotic problem. There is a need to have a tiny flexible robotic manipulator that can navigate through the tortuous natural orifices and also offer superior dexterity and surgical capabilities to perform surgical tasks in a confined space. To achieve this goal, we focus on the development of the hardware design and intelligent kinematic-based control algorithms for dexterous flexible manipulator. These enabling technologies will be integrated together to set out a robotic platform for accessing and navigating tortuous, narrow spaces that are not accessible using existing methods. The platform should be versatile for the use in many minimally invasive procedures demanding for flexible access to confined anatomical areas, such as sinuses, base of skull, esophagus, bronchi, ureter, kidney, urinary bladder.

This success of the project will enable surgeons to provide more accurate, effective, and less invasive procedure even for the complex cases in the anatomical regions, which are currently difficult to treat even with the state-of-the-art robotically assisted surgery. The proposed technology can allow more patients suitable for and can benefit from MIS in these regions, ultimately, improving the quality of life of patients.

1. D. B. Camarillo, T. M. Krummel, and J. K. Salisbury, "Robotic technology in surgery: past, present, and future," The American Journal of Surgery, 188, pp. 2S-15S, 2004.
2. G. D. Hager et al., "Surgical and interventional robotics: Part III [Tutorial]," IEEE Robotics and Automation Magazine, vol. 15, issue 4, pp. 84-93, 2008.
3. Intuitive Surgical Annual Report 2016 (http://www.annualreports.com/HostedData/AnnualReports/PDF/NASDAQ_ISRG_2016.pdf)
4. P. Castelnuovo, I. Dallan, P. Battaglia, and M. Bignami, "Endoscopic endonasal skull base surgery: Past, present and future," Eur. Arch. Otorhinolaryngol., vol. 267, no. 5, pp. 649–663, 2010.
5. L. M. Cavallo, F. Esposito, and P. Cappabianca, "Surgical limits in transnasal approach to opticocarotid region and planum sphenoidale: An anatomic cadaveric study," World Neurosurg., vol. 73, no. 4, pp. 301–303, 2010.
6. J. Burgner et al. "A telerobotic system for transnasal surgery," IEEE Trans. Mechatron., vol. 19, no. 3, pp. 996–1006, Jun. 2014.

7. J. S. Chneider, J. Burgner, J. R. Webster, and P. T. Russell, “Robotic surgery for the sinuses and skull base: What are the possibilities and what are the obstacles?,” Curr. Opin. Otolaryngol. Head Neck Surg., vol. 21, no. 1, pp. 11–16, 2013.

2. RESEARCH METHODOLOGY

The proposed project consists of four main aims:

a. **Aim 1: Modeling of flexible instrument with coupled tendon drive.** In this phase, we will establish a framework of mechanics-based modeling for coupled tendon driven flexible instruments.
   i. ***Task 1.1: Develop Kinematics Models*** We will derive and explore different kinematics model for tendon-driven flexible instruments and investigate pros/cons and practicality for these models
   ii. ***Task 1.2: Analyze the effect of cable friction and compliance.*** We will extend the proposed models to consider the frictional and compliance effect in the cable transmission. We will analyze the corresponding performance degradation and hope to use that information for the design of feedback compensation in the future development.
   iii. ***Task 1.3: Simulation and experimental validation*** We will conduct simulation and experiments to validate our proposed models. We will characterize the instrument and identify the necessary model parameters experimentally.

b. **Aim 2: Design and fabricate complex hybrid-flexible robotic instrument** This aim is to investigate and fabricate different flexible instrument designs. During the design process, the PI and the Co-PI, Dr. Philip Chiu will establish a set of relevant design requirements. The PI will also seek the expert knowledge from collaborator, Dr. Zheng Li for instrument design and fabrication.

c. **Aim 3: Design a closed-loop controller for instrument control**, **based on the fusion of the measurement of the distal sensors, proximal motor encoder, and cable tension**. In this aim, we will develop a control framework that allows us to achieve high performance servo control as well as stable interaction with environment based on the fusion of sensing measurement.

d. **Aim 4. Evaluate the clinical efficacy of the proposed system** This aim is to evaluate the overall instrument system performance. We will integrate the proposed manipulator-instrument system with the da Vinci Research kit (dVRK) robot and setup the software to support the tele-operated instrument control. Co-PI, Dr. Philip Chiu and other physicians will be invited to evaluate the clinical efficacy of the system on a human phantom.
   i. ***Task 4.1: Construct an experimental actuation unit for flexible instrument prototypes.*** We will build and develop a computer-controlled actuation unit for testing the flexible instrument. The system will be capable of handling coupled tendon drive and supporting high bandwidth, output torque experiment and testing.
   ii. ***Task 4.2 Develop a proof-of-concept surgical robot system, integrating with the dVRK robot*** We will integrate the flexible manipulator system to our dVRK robot to offer tele-operated control for clinical evaluation.

3. RESULTS ACHIEVED SO FAR

- For Aim 1: We has been performed and various kinematics models have been developed and verified in both simulations and hardware of our initial flexible instrument. We also developed a novel friction model to explain the performance degradation in the tendon driven flexible instrument and initial experiments were performed to verify the results.
- For Aim 2: We has designed and constructed initial hybrid flexible instrument prototypes for investigation. More design iterations will be required to further improve the instrument performance.
- For Aim 3: Initial closed-loop kinematics control study of flexible instrument was performed. Significant performance was observed. More advanced closed-loop controller will be designed in the next phase of development.
- For Aim 4: We have constructed the experimental actuation unit for flexible instrument prototypes. We also integrated with a basic flexible instrument with dVRK and the corresponding kinematics model was implemented into the same software framework. Basic tele-operated control for the initial flexible instrument was performed.

4. PUBLICATION AND AWARDS

[1] X. Y. Chu, T. Y. Chung, and K. W. Samuel Au., "A Systematic Modelling Approach for Motor-Cable-Joint Kinematics of Coupled Tendon-Driven Surgical Instrument," Hamlyn Symposium on Medical Robotics, June 2018 (Accepted)
[2] K. LU, H. B. Lin, C. W. Vincent Hui, and K. W. Samuel Au "A Case Study of Gravity Compensation for da Vinci Robotic Manipulator: A Practical Perspective," ICRA18 workshop on Supervised Autonomy in Surgical Robotics, May 2018.
[3] K. C. Lau, Yuanpei Cai, Y. Yam, and K. W. Samuel Au, "Comparison Study of Geometric Representation for Continuum Manipulator," ICRA18 workshop on Supervised Autonomy in Surgical Robotics, May 2018.

WORK IN PROGRESS

DEVELOPMENT OF AN INERTIAL MICROFLUIDICS BASED APPROACH FOR THE ISOLATION OF MITOCHONDRIA FROM BIOLOGICAL SAMPLES

Principal Investigator: Professor Megan Yi-Ping HO
Department of Biomedical Engineering, CUHK

Research Team Members:
Shirui Zhao, Research Associate as Shun Hing Fellow[(1)]
Md. Habibur Rahman, PhD Student[(1)]
Qinru Xiao, MSc Student[(1)]
Tinna Stevnsner, Associate Professor[(2)]
An-Chi Wei, Assistant Professor[(3)]
Chen Chang, Master Student[(1)]

[(1)]Department of Biomedical Engineering, CUHK
[(2)]Department of Molecular Biology and Genetics, Aarhus University of Hong Kong, Denmark
[(3)]Graduate Institute of Biomedical Electronics and Bioinformatics, National Taiwan University, Taiwan

Reporting Period: 1 July 2017 – 31 May 2018

INNOVATION AND PRACTICAL SIGNIFICANCE:

Defective mitochondria have been linked to several important human diseases, that urgently calls for the fundamental understanding of the disease mechanisms. To this end, presented here is a previously unavailable strategy enabling a fast and cheap isolation of mitochondria from samples of clinically relevant sizes. The proposed technology is revolutionary, yet highly transformable to a commercial product for routine clinical investigations and biological studies. Therefore, the developed platform will have a broad appeal to the pharmaceutical and clinical sectors targeting mitochondrial diseases. Table 1 summarizes the practical cost and expected performance for the isolation of mitochondria using the inertial based approach compared with other commercially available kits.

Table 1. Comparison between the Inertial Based Isolation of Mitochondria and the Commercially Available Kits.

	Inertial Based	Thermofisher	Abcam	Qiagen
Assay Time (Post-Lysis)	10 min	40 min	>30 min	>45 min
Required Cells	100	2×10^7	4×10^7	5×10^6
Bench Top Availability	Yes	Yes	Yes	Yes
Purity	High	High	High	High
Required Reagent Exchange	No	Yes	Yes	Yes
Price Per Isolation (HKD)	20	45	97	296

ABSTRACT

This project aims to develop a novel approach to rapidly isolate mitochondria from samples of clinically relevant sizes. While currently available methods are mostly laborious and not suitable for small-scale analyses in the clinics, the proposed approach is able to handle 200 microliters of sample and process the isolation within 30 minutes. Aside from the possibility for small-scale analysis, the proposed approach offers many distinct features, including the simple procedures, undemanding equipment request, minimal damages to the isolated mitochondria, and continuous batch processing. Possibilities to analyse mitochondria from a limited amount of clinically relevant patient samples are expected to expand our knowledge towards the basic biological mechanisms of mitochondrial function, and to elucidate how mitochondria are involved in the development of diseases such as cancers, premature aging syndromes, diabetes and neurodegenerative disorders. For instance, it becomes practical to obtain mitochondria from the patient samples, and to elucidate how defective mitochondria link to the mitochondria-associated diseases. Furthermore, the isolation principle may be tailored for an array of subcellular fractions, rendering more efficient identifications and characterizations of intracellular organelles of interest and, consequently, advancing the study of biology and medicine continuously.

1. OBJECTIVES AND SIGNIFICANCE

1.1. Objectives

- To optimize and fabricate the inertial microfluidic chip for the isolation of mitochondria
- To demonstrate effective recovery of mitochondria using purified mitochondria as a model
- To develop a series of protocols for the characterization of isolated mitochondria
- To revise the design chip for a rapid isolation of functional mitochondria from crude human cell lysates of a clinically relevant sample size

2. RESEARCH METHODOLOGY

2.1. Task 1: Optimization of the Microfluidic Chip Using Purified Mitochondria

We have designed and fabricated the chip capable of separating polystyrene particles of 1.9 μm and 7.32 μm (Figure 1a). The inertial lift and so-called Dean drag forces collectively render particles of different sizes to migrate differently along the channel width. More specifically, mitochondria of smaller sizes compared to other cytosolic fractions (i.e. nuclei and cell debris) migrate to the outer half of the channel, whereas the larger cellular organelles move to the inner half of the channel. The size-dependent equilibrium position is determined by the inertial forces of the particulates and the Dean vortices generated by the spiral channel geometry. Prior to the start of this project, we have optimized that the design to direct up to 90% of mouse liver mitochondria (provided by Aarhus University) into the targeted outlet. Due to the heterogeneous nature of mitochondria, the microfluidics design (channel geometry) and the operating flow rates have been optimized empirically as shown in Figure 1b.

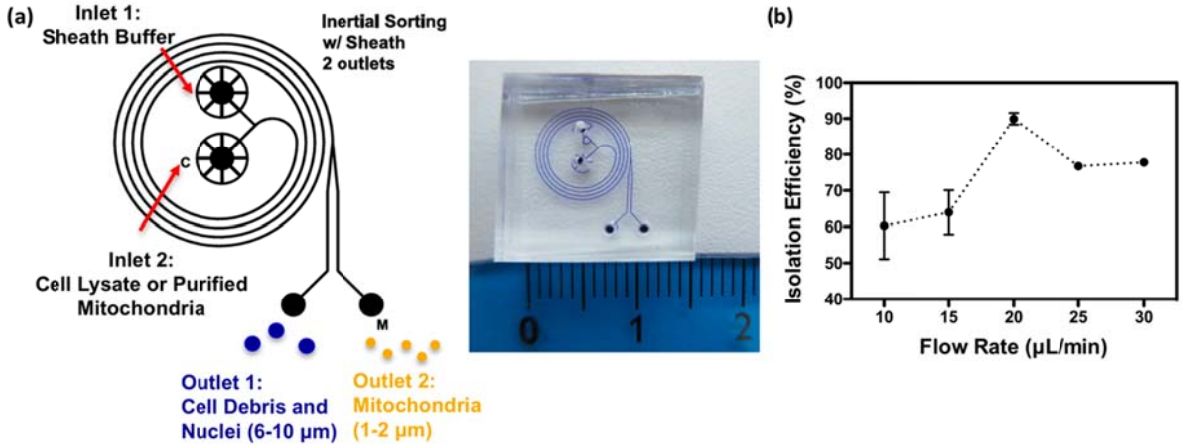

Figure 1. (a) Schematic showing the design of the chip. (b) Optimization of flow rates using purified mitochondria.

2.2. Task 2: Characterization of the Isolation Performance

As a parallel effort of Task 1, we have established relevant characterization techniques to evaluate (1) the isolation efficiency, (2) the isolation purity and (3) the mitochondrial functionality.

(1) The isolation efficiency: As a fast method to quantify the amount of retrieved functional mitochondria isolated by the microfluidic chip, the active mitochondria are stained with a commercially available fluorescent dye, MitoTracker™ Red FM. This red-fluorescent dye accumulates in mitochondria with a membrane potential - a hallmark for functional mitochondria. We have established the protocols by measuring the total fluorescence intensity (ex. by a fluorimeter).

(2) Isolation purity: Western blotting analysis will be performed to check the purity of the isolated mitochondria. The Ku86 protein will be used as the marker for the nuclei, while Tom20 will be used to identify the mitochondrial specific protein. The isolation purity will be determined by comparing the fractions of the two proteins from samples retrieved from the two outlets.

(3) The mitochondrial functionality: To further validate whether the retrieved mitochondria retain their biological functionality, mitochondrial generated reactive oxygen species (ROS) from unsorted and sorted mitochondria will be measured by a fluorescently labelled probe 2',7'-dihydrodichlorofluorescein (DCFH) which emits an intense green fluorescence upon deacylation and subsequent oxidation. ROS, as a typical product of cellular metabolism, are mainly generated by mitochondria. Therefore, the measured fluorescence intensity of DCFH may serve as an indication of the mitochondrial functionality after isolation.

2.3. Task 3: Optimization of the Chip Design for Crude Biological Samples

Due to its large diversity, isolation of mitochondria presents a tangible challenge when it comes to separating this organelle from other cellular components. The subsequent task is to optimize and validate the chip design for handling biological crude sample. Human embryonic kidney cells (HEK293) are used as a model cell line. Crude cell lysate will be prepared following standard protocols. Briefly, the cells will be homogenized by lysing the cell membranes in a hypotonic buffer followed by mechanical disruption with a Dounce glass homogenizer. Samples from the two individual outlets are collected without further post-processing and then analysed by the characterization techniques developed in Task 2. Based on the MitoTracker™ Red FM staining, current isolation efficiency is around 75% from crude cell lysates. Further investigation will be conducted using other cell lines of high metabolic requirements, such as mouse muscle cells (C2C12).

3. RESULTS ACHIEVED SO FAR

3.1. Isolation of mitochondria from crude cell lysates

Through pre-processing, namely cell lysis by Dounce homogenization, current chip design is able to isolate 75% of functional mitochondria with 200 microliters of crude cell lysates in 20 minutes (Figure 2a). In the second year, this project will focus on the characterization of isolated mitochondria by validating the isolation purity and further investigation of the functionality of isolated mitochondria as discussed in Task 2.

As observed in Figure 2b, the isolation efficiency decreases as the cell concentration increases. This is not surprising because the excessive cellular contents may affect the flow profile, rendering less optimal sorting (i.e. 3540 cells/μL). Therefore, further emphasis will also be placed on improving the isolation yield (i.e. the total amount of isolated mitochondria) by enabling the processing of higher concentration of samples.

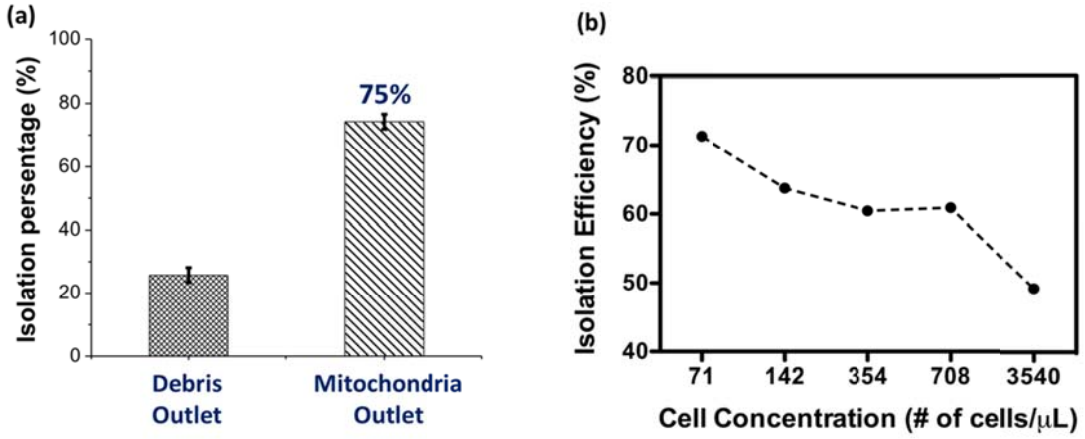

Figure 2. (a) Mitochondrial isolation efficiency of the current design. (b) Negative correlation of the cell concentration and isolation efficiency.

3.2. Optimization from the perspective of cell pre-processing

Dounce homogenization has been the most widely used method for breaking up the cell membrane, however, the level of shear is largely determined by the clearance between the pestle and the mortar, as well as the number of strokes and grinding speed. The poor reproducibility due to the operational variation poses a significant challenge for the continuous optimization of our device's isolation efficiency. To fundamentally resolve the limitation, we have moved forward and designed a microfluidic device to extract mitochondria directly on-chip. Preliminary results have shown promise in processing small amount of sample with high retrieval efficiency (Manuscript in Preparation). We plan to integrate both the extraction and isolation modules on-chip as an all-in-one processing strategy for mitochondrial extraction. Furthermore, similar strategy is also expected to adopt for the isolation of other subcellular organelles, such as autophagosomes.

3.3. Future Perspectives

Preliminary data obtained under the support of this project has served as the foundation of the following submitted grant proposals:

- RGC General Research Fund (GRF): "On-Chip Extraction and Isolation of Mitochondria and the Subsequent Characterization of Mitochondrial Subtypes" (Ref. no.: 14201518), PI: Megan Yi-Ping Ho (Result pending)
- Columbus Program, Ministry of Science and Technology (MOST), Taiwan: "Integrative Platform of Mitochondrial Toxicity Screening" (Ref. no.: 107WFA0110185), PI: An-Chi Wei, Co-I: Megan Yi-Ping Ho (Funded)

4. PUBLICATION AND AWARDS

C[1] C. Chang, Y. P. Ho and A. C. Wei, "Computational Modeling of Mitochondrial Metabolism and Dynamics in Ageing, " *The 1st International Mitochondria Meeting for Young Scientists*, Kyoto, Japan, 2018.

Note: Chen Chang has been awarded a Young Investigator Scholarships by the YongMito Program: http://www.fbs.osaka-u.ac.jp/YoungMito2018/YoungMito2018/Scholarships_%26_Awards.html

WORK IN PROGRESS

AN MRI-GUIDED ROBOTIC SYSTEM FOR BREAST BIOPSY

Principal Investigator: Professor David Navarro-Alarcon/ Professor Yun-Hui LIU
Department of Mechanical and Automation Engineering, CUHK

Co-Investigator (if any):
Yun-hui Liu[(1)], Defeng Wang[(2)], Hayley Louise Chung[(3)], Terrance Chan[(4)]

Research Team Members:
Satwinder Saini[(1)], Man Kiu Chow[(1)], Henry Ng[(1)], Tianxue Zhang[(1)]

[(1)]Dept. of Mechanical and Automation Engineering, CUHK
[(2)]Dept. of Imaging and Interventional Radiology, CUHK
[(3)]Time Medical Systems Ltd.,
[(4)]North District Hospital

Reporting Period: 1 July 2016 – 30 April 2017

ABSTRACT

Breast cancer is the most common cause of cancer mortality in wo men in the world. To determine whether a growth of breast tissue is cancerous or not, a biopsy is conducted to extract and analyse sample cells from the suspicious area. In this research project we aim to develop a new robotic system which can accurately insert the biopsy needle into the target lesion. The trajectory of the robot is guided with real-time visual feedback from a magnetic resonance imaging (MRI) scanner. To operate the robot inside the scanning room, the mechanical structure of the robot is fabricated with non-magnetic materials such as aluminium and nylon, and a combination of pneumatic and piezoelectric actuators are used to drive the motion of the mechanism. Compared to the traditional manual biopsy, the proposed robot has the potential to considerably improve the accuracy, shorten the overall procedure's time, and reduce the trauma inflicted to the tissues.

1. OBJECTIVES AND SIGNIFICANCE

Objective: In China, 187,000 breast cancer cases were diagnosed in 2012, accounting for nearly 12% of the whole world new cases. To improve the disease's survival rate, it is important to accurately detect cancerous growths in early stages by performing a breast biopsy. This procedure is usually conducted in a minimally-invasive manner by a radiologist that inserts a biopsy needle into the tissues and guides it with some imaging modality such as MRI. Our aim in this project is to develop a robot which can insert the biopsy needle into the tissues; our main idea is to develop a system that can be guided with real-time images from the MRI scanner.

Significance: In traditional MRI-guided biopsy, the radiologist first scans the patient to gets a diagnosis image, which he/she uses to estimate the lesion's position and then to insert the needle. A second scan is performed to corroborate the location, which if deviated from the target, further adjustments/scans are performed; this results in a repetitive and time consuming process. To cope with this problem, we propose to build a robot to automate the needle insertion. The novelty of this robot is its capability to operate within the scanner's bore. This innovative feature will allow radiologists to considerably reduce the procedure's time and cost. We hope that this university-industry collaboration will also greatly improve the chances for commercialisation of the obtained research outputs.

2. RESEARCH METHODOLOGY

2.1 Design Requirements

There are several design requirements that must be taken into consideration when developing this type of system, these include: (1) satisfying the scanner's dimensional constraints, (2) selecting non-magnetic materials and actuators, (3) adapting electronics to avoid visual artifacts. In our model we consider the dimensions of a Time Medical PICA scanner. Fig. 1 shows the proposed set-up, which requires the robot to have a vertical height smaller than 220 mm, and a width smaller than 400mm. The required linear motion range to perform a biopsy is [x, y, z] = [130, 90, 50] mm.

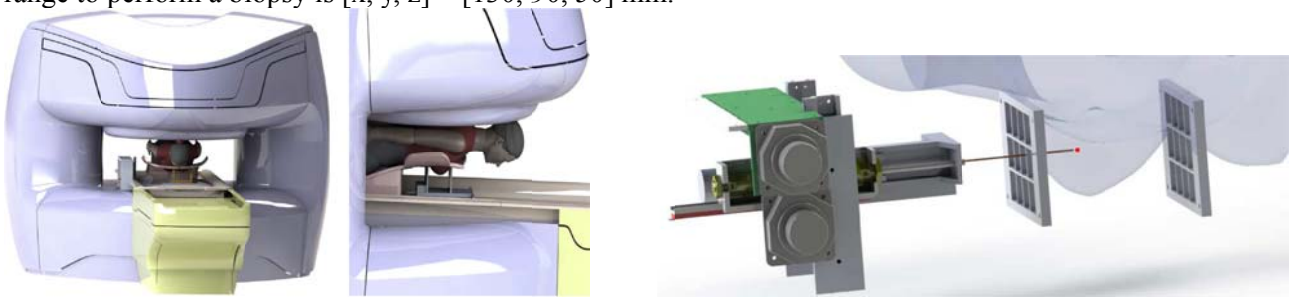

Fig. 1. (left) Conceptual MRI-guided biopsy set-up. (right) Needle insertion using the grid method

2.2 Proposed Mechanical Structure

To fulfil the above given design requirements, we propose to develop a robot consisting of three active linear joints for needle positioning and insertion motions. This 3-DOF design in intended to replicate the linear motions of a manual biopsy using the grid method. Fig. 2 conceptually depicts the details of proposed 3-DOF mechanism. To achieve stable motion, non-magnetic slides (made of aluminium, silicon nitride, graphite) are used on each active axis. An aluminium power screw with a nylon nut is used in the x-axis to transmit motion from actuator to the joint. Two parallel slides provide stable support to the biopsy gun from both sides; this vertical axis uses a brass rack and pinion to transmit the motion from the actuator to the joint.

The first two DOF of this system serve to align the needle's axis with the target lesion; these joints are driven by piezo-electric motors. To measure the robot's configuration, position sensors are embedded in all three joints. The mechanism that drives the needle is actuated by a double-acting pneumatic cylinder. The insertion mechanism is attached to the parallel slides of the vertical axis to provides support to the biopsy gun from both sides. The axis' slide has a linear travel range of 75 mm, which is used for providing smooth pushing/pulling motions to the piston rod. To perform the task, the cylinder must generate a pushing force of at least 3 N (a recent clinical study reports that a maximum force of 2.3 N is required to penetrate breast tissues). The pneumatic cylinder under consideration has piston areas of $A_1 = 67.5\times10^{-6}$ m^2 and $A_2 = 59.5\times10^{-6}$ m^2 and maximum chamber pressure of $p_1 = 340000$ pa. By setting an opposing pressure of $p_2 = 100000$ pa, we calculate that the cylinder has a maximum pushing force of $f = A_1 p_1 - A_2 p_2 = 17$ N, which is sufficient to penetrate the tissues with the needle.

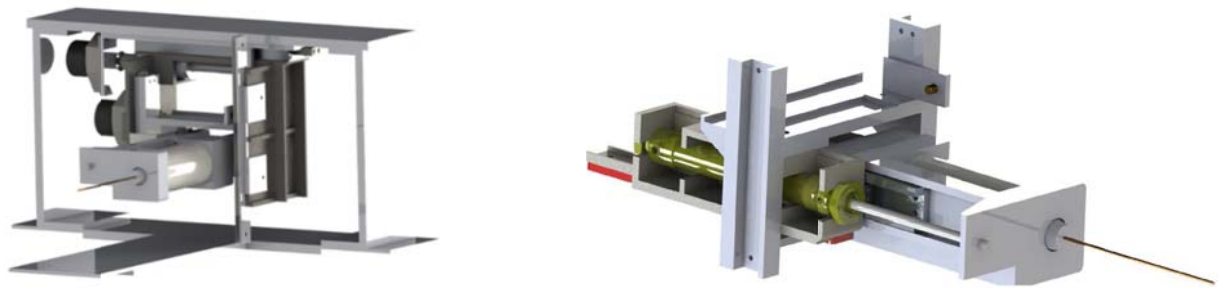

Fig. 2 (left) Conceptual model of the 3-DOF robot. (right) Details of the insertion mechanism

2.3 Motion Control System

The control system is composed of three servo modules: a stage positioning controller, a pneumatic regulator, and a needle insertion controller. The piezo-motors that drive the x-y joints are used for initial needle positioning; these motors come with its own motion controller, current amplifier, and a feedback sensor. A

pair of pressure regulated valves are used for driving the motion of the cylinder. To accurately regulate the cylinder's chamber pressure, two pressure sensors are installed in close proximity to the ports. A position sensor measures the linear displacements along the needle's insertion joint. In our system, we use pneumatic actuation to drive the needle as it presents the best performance for continuous MRI.

2.4 Adaptive Controller Design

The pneumatic valves used in our system can control the pressure being output to the cylinder; this pressure is directly proportional to the reference voltage. To drive the pneumatic cylinder, long tubing lines (of around 6 meters in our set-up) must be passed into the room through the panel's wave guides. Due to the long tubing length, the pressure commanded by the valves may differ from that inside the cylinder's chambers, here denoted by p. This situation can be fairly modelled by the following first-order system:

$$\delta p/\delta t = -H(p - d - u)$$

where d models the steady-state deviation from the control reference u; the parameter $H > 0$ determines the response of the chamber. To control the chamber's pressure, we propose the following adaptive regulator:

$$u = p_d - \hat{d};\ \delta\hat{d}/\delta t = kH(p - p_d)$$

for p_d as the desired pressure, $\hat{d}$ as the adaptive state, and k as a feedback gain. The above controller can asymptotically regulate the chamber's pressure. By computing the time derivative of the Lyapunov function

$$V = \left(|p - p_d|^2 + \left|\hat{d} - d\right|^2/k\right)/2$$

we can show that $\delta V/\delta t = -H|p - p_d|^2$, which clearly proves the stability. To command the pushing forces, we use the force-pressure relation $f = A_1 p_1 - A_2 p_2$, which allows us to solve p_{di} from a desired force f_d. The chamber pressures for forward and backward motions are, respectively, computed as follows:

$$p_{d1} = (f_d + A_2)/A_1; p_{d2} = -(f_d + A_1)/A_2$$

3. RESULTS ACHIEVED SO FAR

3.1 The Fabricated Prototype

Fig. 3 shows the developed robotic prototype, which has an overall dimension of 400×220×260 mm. As we can see in this figure, the structure of the robot is mostly 3D printed. The rigidity of the mechanism is secured by reinforcing the x-platform with an aluminium plate (Al 7075), and by transmitting the x-y motions with an aluminium power screw and a brass rack and pinion. This figure clearly depicts the individual motions of the robot joints. This figure shows a simulated biopsy set-up, where we can see that the fabricated prototype is compact enough to perform lateral insertions inside the open bore scanner considered in our model

Fig. 3 (left) The fabricated robot prototype. (right) A simulated lateral insertion with a breast coil model

3.2 Closed-Loop Robot Performance

The performance of the pressure regulator is evaluated by commanding a target trajectory of pd1 = sin(t/2)/2 + 2, while applying external disturbances to feedback pressure (these were introduced by manually pushing the cylinder's rod, thus altering the chamber's pressure). Fig. 4 (left) depicts the pressure tracking results, where D1 and D2 denote disturbances. We can see that our adaptive method can adaptively control the chamber's pressure while recovering from perturbations. We also tested the performance of the pneumatic positioning controller. For that we command the system to regulate the position of the needle with incremental steps of 25 mm. Fig. 4 (right) depicts the performance of our pneumatic-based needle positioning controller.

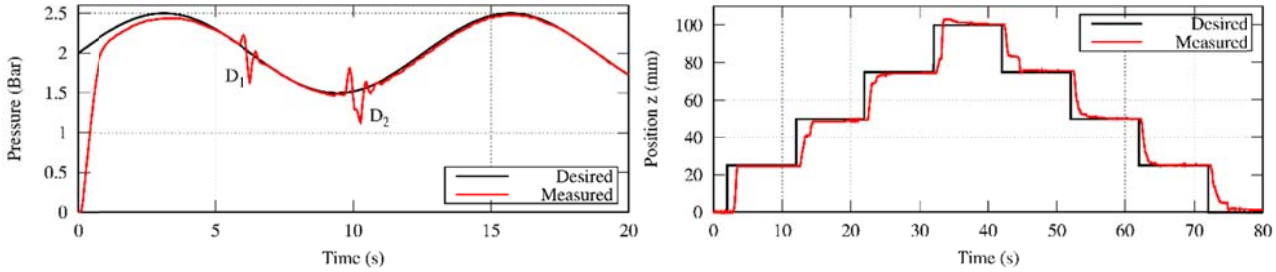

Fig. 4 (left) Trajectory tracking of the pressure controller. (right) Position regulation of the biopsy needle

3.3 MRI-Based Experiments

We experimentally evaluate the robot's performance and MR compatibility using a 0.2 T Time Medical Mona scanner, an MR head coil, and a silicon breast phantom tissue (see Fig. 5). For that, we first test the insertion performance into a breast phantom. Fig. 6 (left) shows the insertion distance estimated with the MRI scans; the system was required to insert the needle with 5 mm increments. Our results show an accuracy of ± 0.4 mm. Finally, we experimentally evaluate the signal-to-noise ratio (SNR) induced by the mechanism when located inside the scanner. We compare the SNR that is computed by imaging the phantom with and without the robot. Fig. 5 shows the obtained results.

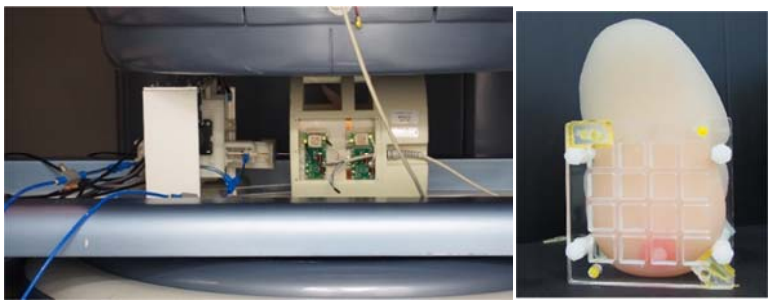
Fig. 5 The scanner, head coil, and phantom tissue used for the MRI experiments

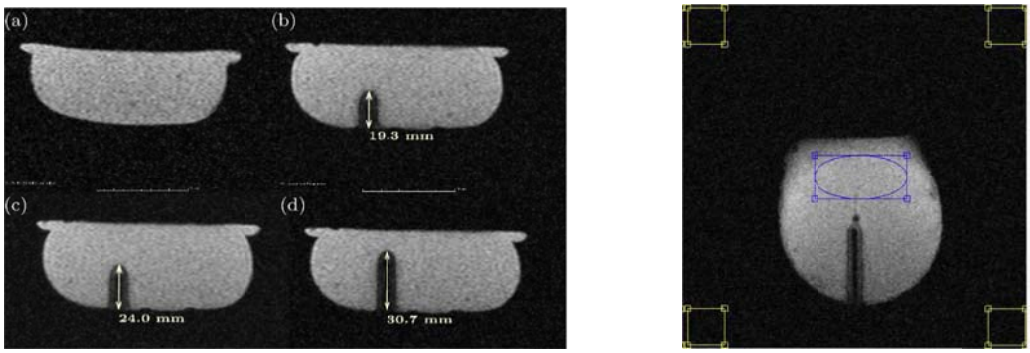

Fig. 6 (left) MRIs of the needle insertion. (right) MRI used for computing SNR of the robot

4. PUBLICATIONS AND AWARDS

[1] D Navarro-Alarcon, S Singh, T Zhang, H Chung, KW Ng, MK Chow, YH Liu. Developing a Compact Robotic Needle Driver for MRI-Guided Breast Biopsy in Tight Environments. IEEE Robotics and Automation Letters (RAL), vol. 2, no. 3, 1648–1655, 2017

[2] T Zhang, D Navarro-Alarcon, KW Ng, MK Chow, YH Liu, H Chung. A novel palm-shape breast deformation robot for MRI-guided biopsy. IEEE Int. Conf. on Robotics and Biomimetics, pp. 527-532, 2016

[3] F Zhong, D Navarro-Alarcon, Z Wang, YH Liu, T Zhang, HM Yip. Adaptive 3D Pose Computation of Suturing Needle Using Constraints from Static Monocular Image Feedback. IEEE/RSJ Int. Conf. Intelligent Robots and Systems (IROS), 5521–5526, 2016

[4] D Navarro-Alarcon and YH Liu. Contour-Based Deformation Servoing: A New Marker-Free Algorithm to Actively Deform Soft Objects into Desired Shapes with Manipulators. IEEE Transactions on Robotics (TRO), under review, 2017 (under review)

[5] KW Ng, MK Chow, D Navarro-Alarcon, S Singh, T Zhang, H Chung, YH Liu. Developing a Compact Robotic Needle Driver for MRI-Guided Breast Biopsy in Tight Environments. IEEE/RSJ Int. Conf. Intelligent Robots and Systems (IROS), 2017 (under review)
[6] S Singh, D Navarro-Alarcon, D Kwok, KW Ng, MK Chow, T Zhang, YH Liu. Towards Developing Benchmarking Indices for MRI-Compatible Robots: An Experimental Quantitative Study. IEEE/RSJ Int. Conf. Intelligent Robots and Systems (IROS), 2017 (under review)
[7] S Singh, D Navarro-Alarcon, MK Chow, KW Ng, T Zhang, YH Liu, H Chung. Can a Tesla Turbine be Utilized as a Pneumatic Actuator for MRI Interventions? Journal of Mechanism and Machine Theory, 2017 (under review)

WORK IN PROGRESS

INTENTION-DRIVEN SHOULDER REHABILITATION FOR TARGETED NEURO-MUSCULAR TRAINING USING AN EXO-MUSCULOSKELETAL ROBOT

Principal Investigator: Professor Darwin Tat Ming LAU
Department of Mechanical and Automation Engineering, CUHK

Co-Investigator (if any):
Prof. Raymond Kai Yu Tong [(2)]

Research Team Members:
Dr. Ghasem Abbesnejad [(1)] (postdoctoral fellow)

[(1)]Dept. of Mechanical and Automation Engineering, CUHK
[(2)]Dept. of Biomedical Engineering, CUHK

Reporting Period: 1 July 2016 – 30 April 2017

ABSTRACT

This project aims to develop an intention-driven rehabilitation robot for muscle-specific training of the human shoulder. By designing a cable-actuated exoskeleton where the cables are arranged to match the wearer's anatomy, the effectiveness of targeted neuromuscular training of the shoulder muscles will be explored through a pilot study involving both healthy human subjects and stroke patients.

Current rehabilitation robots have two noteworthy features. First, such robots provide assistance only in producing gross motion rather than assistance to the individual muscles. Second, an assist-as-needed (AAN) approach is used where more assistance will be provided if the patient is unable to complete a desired task themselves. The proposed device will aim to address the shortcomings resulting from these features. In recent years, a promising alternative to the AAN is intention-driven rehabilitation (IDR), where the assistance provided to the patient is proportional to the strength of their neuromuscular signals in order to train their ability to generate stronger signals. This approach has already been shown to be effective for simpler joints such as the elbow and wrist, but has not yet been studied for more complex joints such as the shoulder.

During the first reporting period of the project, three main tasks were completed: 1) the development of prototype of the exo-muscular robot; 2) integration of EMG sensors into the system to detect user intention; and 3) preliminary testing on healthy human subjects to show the validity of the prototype and methods.

1. OBJECTIVES AND SIGNIFICANCE

1. Develop a prototype of a wearable exo-musculoskeletal rehabilitation robot actuated by cables:
   a) Arrange the robot cables anatomically to actuate in parallel six of the major shoulder muscle groups: *pectoralis major*, *deltoid*, *teres major*, *teres minor*, *infraspinatus* and *supraspinatus*.
   b) Allow the system to be attached to the person's upper arm conveniently, to be worn comfortably and the attachment locations of the cable to be easily rearranged.
   c) Capable of providing assistance to a healthy person to carry an extra load in addition to the weight of their arm.
   d) Implement intention-driven control of the exo-muscles through electromyography (EMG) signals that are attached onto the surface of the arm (non-invasively).
2. Demonstrate the potential of intention-driven muscle-specific training through three pilot studies:
   a) The preliminary pilot study will consist of 10 healthy human subjects, each using the developed system for 10 x 30 minute training sessions to demonstrate the effects of

muscle-specific training by only providing assistance to particular muscles of the system.

b) Compare the effectiveness of intention-driven rehabilitation (IDR) with the assist-as-needed approach (AAN) performed on another group of 10 healthy human subjects.
c) Finally, a pilot study of the system will also be performed on a group of 15 stroke patients.

Shoulder pain and impairment is a severe problem that affects the quality of life of the impaired subject and inhibits the motion of the arm even in performing even simple daily tasks, such as reaching for objects and feeding one self. Causes of such impairments include stroke, muscle weakness and shoulder subluxation (instability of the shoulder). Furthermore, shoulder subluxation is a common cause of pain for post-stroke patients (between 16-72% of stroke patients). The treatment of such impairments places significant burden on the health system. Successful completion of this project is expected to provide a new approach for performing effective shoulder training to patients with shoulder pain and impairment. Effective treatments would not only improve the quality of life of the patient and also decrease the burden on the Hong Kong health system.

2. RESEARCH METHODOLOGY

In the proposed project, an exo-musculoskeletal IDR robot for the shoulder will be developed. The cables will be arranged in parallel to the subject's muscles and will provide assistance to a particular muscle group. Using EMG feedback, an intention-driven scheme will be employed to perform muscle-specific training. The proposed project combines experiences of cable-driven robot development and musculoskeletal analysis skills of the PI with the experiences in intention-driven rehabilitation of the co-I. The research plan will consist of three main tasks: 1) design and prototype of the exo-musculoskeletal robot; 2) intention-driven control using EMG; 3) pilot study on healthy subjects to demonstrate the effectiveness of this method.

I. Design and prototype of the exo-musculoskeletal robot

In this project, the PI proposes to develop a new type of exo-musculoskeletal robot that has cables arranged in an anthropomorphic manner. Six muscle groups identified as the major contributors to shoulder motion and are also situated closer to the surface will be used to design the arrangement of cables for the robot: the *pectoralis major*, *deltoid*, *teres major*, *teres minor*, *infraspinatus* and *supraspinatus*.

The cable actuators that will be used in the proposed prototype are the *Myomuscle* units developed by the Myorobotics project consortium who the PI collaborates with. In the design and development of the system, the robot should: be easy to attach onto the patient and wear, allow for reconfiguration of the pulley locations on the frame such that cables can be arranged to be in parallel with the muscles, and be safe for the subject to use given the high maximum cable force of the myomuscles.

The arrangement of cables in an anthropomorphic manner is one of the keys to allow the system to provide targeted muscle-specific training. By arranging cables in parallel to specific muscles, the force applied to a particular cable can be controlled to promote strengthening of the corresponding muscle. This is a key difference between the proposed system and existing rehabilitation robots that only assist in producing the gross motion.

II. Intention-driven control using electromyography (EMG) signals

After the development of an initial prototype, the intention-driven control system for the exo-musculoskeleton will be implemented and tested. With the co-I's experience in EMG and IDR control, the placement of the EMG electrodes such that signals from the six muscle groups can be obtained will be properly considered. These signals will be used to control the cables through a simple intention-driven scheme, where

$$\mathbf{f}(t) = K_p \mathbf{V}_{EMG}(t) \quad (1)$$

The vector $\mathbf{V}_{EMG}$ contains the EMG readings and $\mathbf{f}$ is the forces that the cables should execute. The gains K_p correspond to the amount of assistance after considering the effort from the subject. As observed in [16], it is anticipated that the IDR approach will promote the subject to improve their neurological signal and muscle training in order to complete the set task, for example, the lifting motion of the arm.

III. Pilot study of the exo-musculoskeletal robot on healthy subjects

To verify the effectiveness of the developed rehabilitation device and intention-driven control system, three studies will be performed. In the first study, a group of 10 healthy human subjects will use the exo-musculoskeletal robot to assess the effects of IDR on the shoulder. Each subject will use the robot for 10 sessions of 30 minutes per session. During these sessions, the subject would be required to perform a designed set of shoulder motion trajectories, ranging from the basic motions such as flexion/extension, adduction/abduction, and internal/external rotation, to more general trajectories. The trajectories will be selected to allow the activation of different muscle groups to be observed. During each of the sessions, the EMG signals, cable forces and kinematic trajectory of the motion will be recorded. This data allows the analysis of whether the IDR approach trains specific muscles when different trajectories are being performed.

In the second study, another group of 10 subjects will use the AAN control approach for the same set of exercises. This study serves to compare the IDR and AAN methodologies on the same robotic rehabilitation system to gain a better understanding on the effectiveness of the two approaches. Such a comparison has not been done within the literature to the best of the team's knowledge.

In the final study, the proposed device will be tested on a group of 15 stroke patients, again for 10 x 30 minute sessions. The selection criteria for the subjects are: first stroke with unilateral lesion in the chronic stage (that is, more than 6 months after stroke). Such patients would already have a stable condition and no significant improvements are normally expected. This would allow the effects of the developed device to be more clearly observable. Note that the subjects for all three studies must be above the age of 18.

3. RESULTS ACHIEVED SO FAR

In the initial phase of the project, progress has been primarily focused on tasks 1 and 2 from the research methodology, and preliminary work in task 3 has also been undergone. The progress will be described in three sections: 1) mechanical prototype; 2) EMG-robot integration; and 3) preliminary human subject experiments.

3.1. Mechanical Prototype Development

In the first 6 months of the project, the prototype of the current exo-muscular robot (Figure 1) was completed. This prototype was reached to after six design iterations and trials. The current prototype possesses three muscle groups, the deltoid anterior, deltoid middle and deltoid posterior (as shown in Figure 1c).

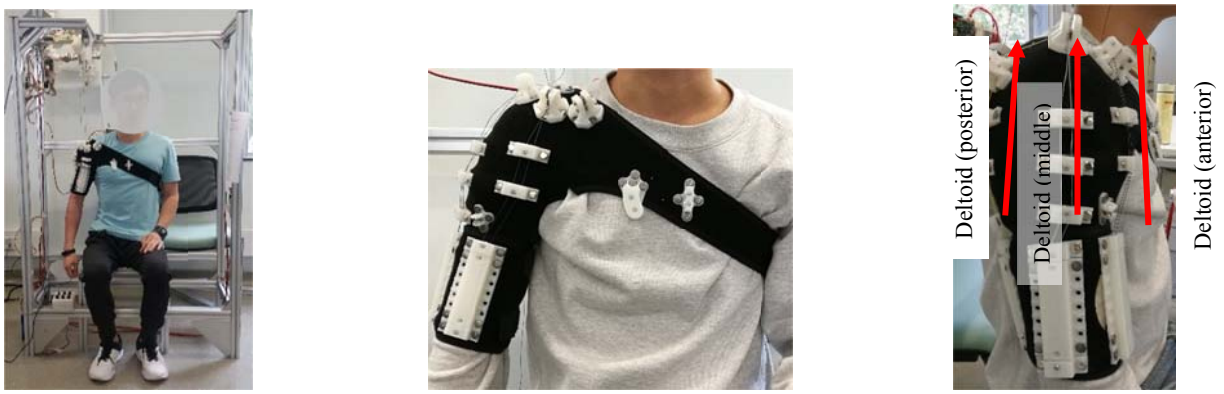

Fig. 1. Exo-muscular robot prototype. Overall view (left), front view (middle) and side view (right).

The three muscles, deltoid anterior, middle and posterior, are involved primary in the shoulder flexion, abduction and extension, respectively. Figure 2 shows the motion produced by the robot on the subject by providing cable force actuation to each of the muscles, demonstrating the capability of the exo-muscle robot to motion that is similar to that of the corresponding muscles they are parallel to. Using the Myomuscle cable actuator units, integration with the ROS cable robot software (ROS-CASPR) developed by the PIs lab is completed in order to command the exo-muscles. In conclusion, during the first report period, the concept and design of the robot has been essentially completed with three muscles demonstrated. The next step is to attach additional exo-muscles to other muscles of the shoulder, such as the pectoralis major and teres major/minor.

Fig. 2. Flexion (left), abduction (middle) and extension (right) motions of the shoulder produced through the robot prototype using the Myomuscle actuator units

3.2. EMG integration with the robot

The robot prototype (presented in the above section) can be controlled in two modes: 1) manual command input; and 2) EMG IDR feedback. The manual command input scheme was achieved through potentiometer dials that command each muscle (Figure 3 (left)). This mode is primarily used for testing and calibration. The main mode to be used within the IDR scheme is the EMG sensor feedback from the corresponding muscles that have exo-muscles attached. The EMG sensors, as shown in Figure 3 (right), record the electrical activity of the muscles and then send this information to the ROS software framework. This is then used to provide the actuation command for the corresponding muscle through the proposed scheme in (2).

Fig. 3. Command mode of robot: 1) potentiometers dials for each muscle (left); 2) EMG on muscles (right)

Within this task, an appropriate calibration methodology for each muscle was developed. This involves the recording and determination of EMG range and calibrate sensors such that there is no over-saturation and that the required operating EMG range can be measured. The successful EMG integration with the robotic system was demonstrated through a teleoperation experiment. In the experiment, one subject wore the EMG sensors while another wore the robot system, and the detected EMG signals are used to actuate the wearer of the robotic system, while the wearer remains relaxed. Results of the experiment showed that EMG detection in muscle and shoulder motion intention was successful and the produced corresponding motion to the wearer of the exo-muscle robot.

3.3. Preliminary Human Subject Experiment

Preliminary human subject experiments were performed in order to demonstrate the working principles and confirm the potential of the proposed approach. These experiments were performed on three healthy subjects. In this experiment, each subject wore both the EMG sensors and robot, in the same manner as would be expected during the rehabilitation, and the subject were asked to perform shoulder flexion, abduction and extension motion while carrying different amount of weights. The EMG signals on the shoulder muscles were then recorded both with and without the exo-muscle robot assistance for a fixed intention-assistance gain. As shown in Figure 4, it can be clearly observed that the robot assistance using the IDR scheme produced lower measured EMG, indicating that lower muscle forces were required. Consequently, this supports the idea that using the same EMG strength, the wearer would be capable of carrying a heavier load. This validation is important later experiments with impaired subjects as it demonstrates that the robot would be capable of providing additional force during their therapy through the IDR scheme. In the remaining time of the project, additional experiments on a wider range of healthy and stroke patient subjects will be aimed to

be performed.

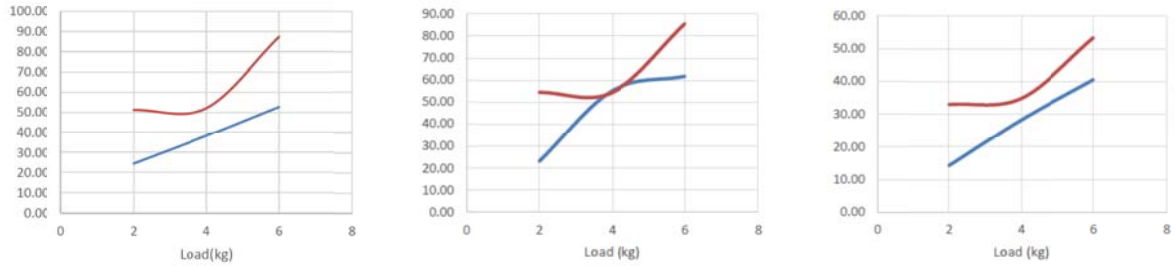

Fig. 4. Summary of human experiments. Load vs EMG reading without robot (red) and with robot (blue). Anterior for flexion motion (left), middle for abduction (middle) and posterior for extension (right).

4. PUBLICATION AND AWARDS

Two final year projects from the MAEG programme and the BME programme were involved in this project. They were primarily involved in the system design and their project was awarded the 1st runner up of the CUHK Charles K. Kao Student Creativity Award for the individual entry. Furthermore, we are now preparing a publication to be submitted to the IEEE Transaction on Robotics (leading journal in robotics).

WORK IN PROGRESS

ENGINEERING ANTIMICROBIAL SURFACES BASED ON MICRO-TOPOGRAPHY USING A NOVEL ULTRASONIC MACHINING METHOD

Principal Investigator: Professor Ping GUO
Department of Mechanical and Automation Engineering, CUHK

Research Team Members:
Yang Yang, PhD student [(1)], Hanheng Du, Research assistant [(1)]
Meiyu Liu, Research assistant [(1)]

[(1)]Dept. of Mechanical and Automation Engineering, CUHK

Reporting Period: 1 July 2016 – 30 April 2017

ABSTRACT

There are great demands of antimicrobial surfaces, which could prevent the adhesion of micro-organisms and the formation of biofilms. Microbial contamination of surfaces, which are directly exposed to human tissues (surgical equipment) and food (utensils), can cause serious infection and the associated disinfection costs. Biomedical implants, such as prosthetic devices and artificial joints, are subjective to adhesion of pathogenic bacteria and biofilms, which not only significantly reduce the lifespan of the implants but also increase the risks of various infections. Biofouling on marine vessels of barnacles and algae is a great concern in shipping industry due to corrosion to the ship hulls and increased fuel and maintenance costs.
The project aims to develop a novel manufacturing process for fast creation of micro-structured surfaces for the antimicrobial surfaces application directly on stainless steel and titanium alloy surfaces which are mostly widely used in the hospitals, food industry, and biomedical market. The outcome from this project will enable the creation of antimicrobial surfaces based on surface micro-topography, which is non-toxic, permanent and chemical free, to be applied to the related applications in hospitals, biomedical implants and devices, food packaging, marine industry, etc.

1. OBJECTIVES AND SIGNIFICANCE

1. The research project, if carried out successful, will enable the technology to create antimicrobial surfaces, which could prevent the adhesion of bacteria and formation of biofilms, in many critical applications, such as surgical equipment, biomedical devices and implants, and food packaging.
2. The project aims to develop a novel manufacturing process for fast creation of micro-structured surfaces for the antimicrobial surfaces application directly on stainless steel and titanium alloy surfaces which are mostly widely used in the hospitals, food industry, and biomedical market.
3. The project aims to systematically study and test the surface micro-topography and its effects on the prevention of microbial adhesion. The surface wettability and an innovative surface roughness engineering index will be utilized as the criteria to categorize different surface micro-features.
4. The project aims to carry out experiments to produce various micro-patterned stainless steel and titanium surfaces according to the optimized results from our model. These antimicrobial surfaces will then be tested to verify their retention ability of different micro-organisms.

2. RESEARCH METHODOLOGY

The research project, if carried out successful, will enable the technology to create antimicrobial surfaces, which could prevent the adhesion of bacteria and formation of biofilms. There are three main research tasks in this project, namely, (1) development of the ultrasonic texturing system for creating micro-structured surfaces; (2) study of the relationship between surface micro-topography and its effects on microbial

retention; (3) to generate various micro-patterned surfaces to test against smooth/polished surfaces.
In order to make the micro-structured surfaces effective against microbial attaching, the feature size must be reduced to be comparable to the size of targeted micro-organisms, which is in the range of 1-5 μm. The previously developed ultrasonic texturing system by our group was used to create features in tens of microns for the friction reduction application. The system will be adapted to control the trajectory of the cutting tool to create more specific surface patterns. The same vibration texturing principle will be utilized but a new non-resonant tool will be designed and adopted to achieve higher precision as shown in Figure 3(c).
While it is commonly accepted that the microbial adhesion responds to the surface topography, the intrinsic mechanisms are yet to be fully understood. Some think surface roughness (Ra) is a key parameter to the effectiveness of microbial retention, but some works suggest otherwise. The surface roughness is good to characterize a surface with random or simple surface features, but it cannot fully describe the complex patterns. In this project we take two parameters to hypothetically characterize the effectiveness of surface topography on microbial retention. One is the wettability or contact angle of surfaces; the other is engineering roughness index proposed by Schumacher et al.
We will design and optimize the surface topography based on the surface wettability, engineering roughness index, and the capability of our texturing system. These patterns will be directly machined on stainless steel and titanium surfaces, which are most widely used in hospitals and biomedical related devices. Experiments of their effectiveness on microbial retention will be tested using different micro-organisms to compare with smooth and untreated surfaces.

3. RESULTS ACHIEVED SO FAR

3.1 Design and manufacturing of anti-fouling surfaces

The settlement of chlorella is mainly influenced by the feature size, geometry, and roughness of the engineered surface. For a more comprehensive description of the relationship between these factors and the adhesion density, engineered roughness index (ERI) is developed.

$$ERI = (r * df) / f_D$$

The ERI consists of three variables associated with the size, geometry, and spatial arrangement of the topographical features: Wenzel's (1936) roughness factor (r), depressed surface fraction (f_D), and the degree of freedom for movement (df). These values are based on the preferential settle tendencies of Ulva spores and the hypothesis that increasing the tortuosity of surface topography will make the surface less favorable for settlement. This formula indicates that an interaction exists between roughness measures and feature spacing that must be considered when designing topographic surface.
Chlorella prefer to squeeze along the recessed area with the surface topography and seldom bridge between the features within the repeat unit. So, the width of recessed area between features is better smaller than the diameter of chlorella (3 – 10 μm).
However, there is still a lower number of chlorella were observed on the protruded features, leaning against the edge of the triangle feature, instead of settling on the flat top surface. So the protruded feature can be in larger size. According to these regulars, we choose two different patterns to carry out the experiments as shown in Figure 1 and Figure 2.

(1) $df = 1$

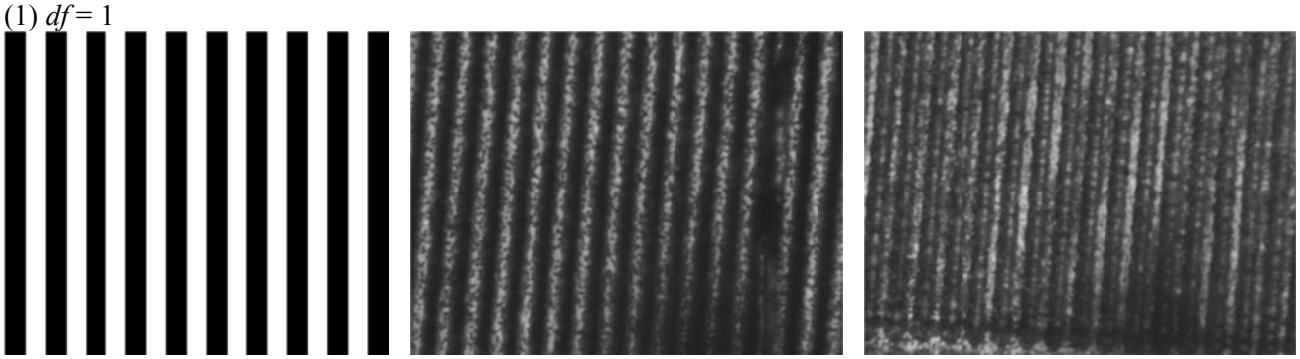

Figure 1. Designed channel patterns with degree of freedom of 1: designed patterns and laser machined patterns.

(2) $df = 2$

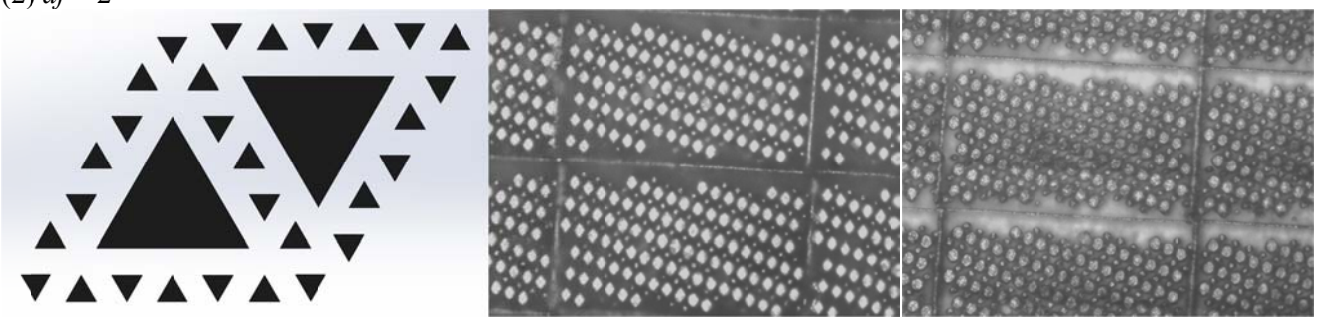

Figure 2. Designed diamond patterns with degree of freedom of 2: designed patterns and laser machined patterns.

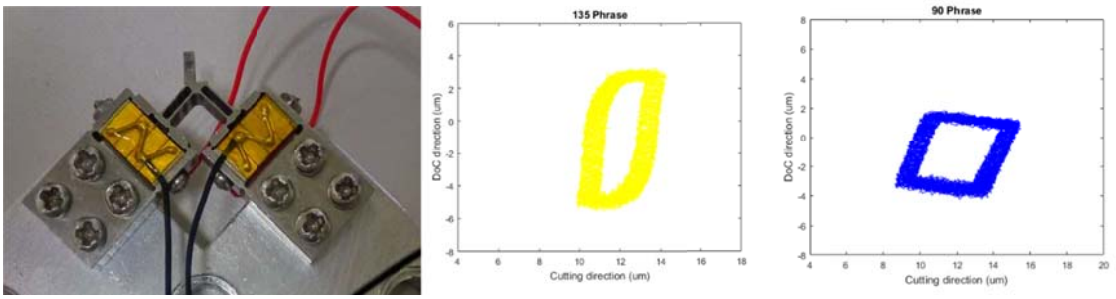

Figure 3. Prototype of non-resonant vibration cutting tool and generated arbitrary tool paths.

3.2 Machining micro patterns using vibration cutting

In our research, we focus on manufacturing micro-patterns with our two dimensional non-resonant tertiary motion generator, which is based on the flextensional structures. The holder of cutting tool is connected to two perpendicularly placed flextensional actuators with flexure hinges which decouple the motion outputs from the two actuators. The prototype has been developed shown in Figure 3.

We plan to manufacture the channel patterns based on the Cardioid line, and the trajectory of tool tip is shown in the following picture with $f = 2500$ Hz and $v = 13$ mm/s, such that

$$x = 2\sin(wt) + vt$$

$$y = 3\sin(wt + \theta) - 2\sin(2wt + \theta)$$

By applying this trajectory, one side of the channel features is nearly vertical as shown in Figure 4, which is more effective to avoid settlement of the micro-organisms.

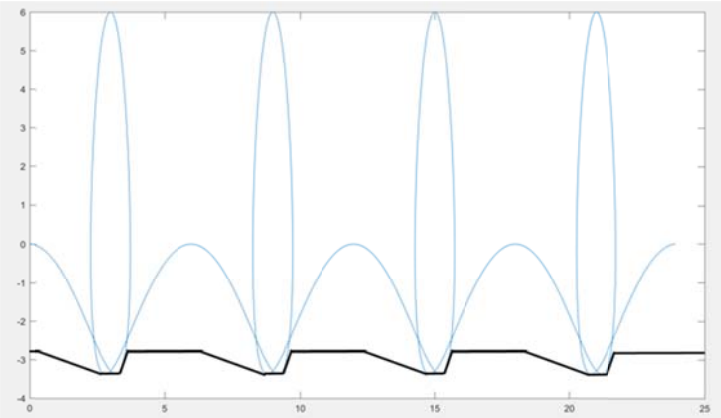

Figure 4. Proposed vibration cutting method for fast generation of micro-patterns.

3.3 Human mesenchymal stem cell (hMSCs) spreading on patterned surfaces

We have also tested the hMSCs spreading on patterned aluminum surfaces. The machined patterned surfaces have hierarchical micro-structures, which have first level of features in the range of several tens of microns and a second-order textures of several microns. The represented surfaces are shown in Figure 5.

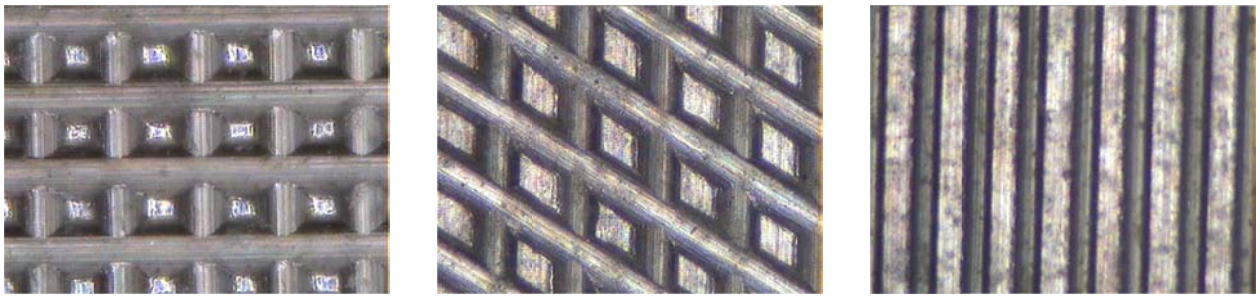

Figure 5. Machined patterned surfaces on aluminum workpieces.

hMSCs are cultured on the sample surfaces to test their effect on the spreading and differentiation of the stem cells. The results are summarized and compared in Figure 6. According to the results, hMSCs tend to attach and spread in the valley of patterns. Few cells are on the top of patterns.

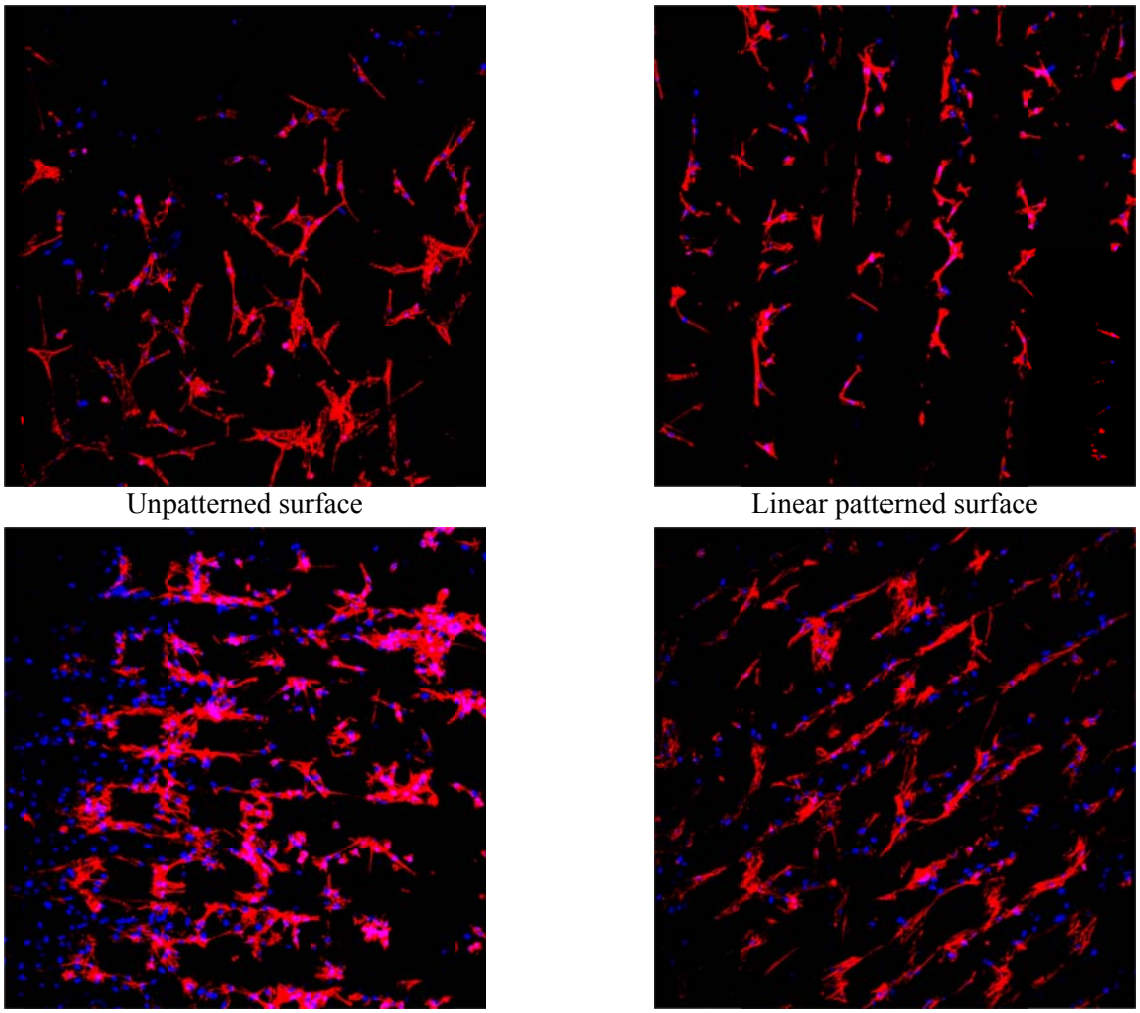

Unpatterned surface | Linear patterned surface

Rectangular patterned surface (high cell density) | Diamond patterned surface (high cell density)

Figure 6. hMSCs spreading and differentiation on unpatterned and patterned surfaces.

COMPLETED

DEVELOPMENT OF A NOVEL FLEXIBLE SURGICAL ROBOT WITH HAPTIC SENSATION

Principal Investigator: Professor Zheng LI
Department of Mechanical and Automation Engineering, CUHK

Co-Investigator (if any):
Joseph J.Y. Sung [(1)], Philip W.Y. Chiu [(1, 2, 3, and 4)] and Ruxu Du [(5)]

Research Team Members:
Hongmin Wang, RA [(1, 2)], Chengzhi Song, Junior RA [(1, 2)]

[(1)] Institute of Digestive Disease, CUHK
[(2)] Chow Yuk Ho Technology Centre for Innovative Medicine
[(3)] Biomedical Engineering, CUHK
[(4)] Dept. of Surgery, CUHK
[(5)] Dept. of Mechanical & Automation Engineering, CUHK

Project Start Date: 1 July 2015
Completion Date: 30 June 2017

ABSTRACT

This project aims to develop a novel tele-operated flexible surgical robot for general minimally invasive surgery (MIS). In the proposed robot, key drawbacks in existing surgical robots will be addressed. The performance of the robot will be evaluated systematically in the CUHK Jockey Club Minimally Invasive Surgical Skills Center and the Chow Yuk Ho Technology Center for Innovative Medicine by ex vivo mockup surgeries and animal (pig) tests.

Robot assisted MIS brings to patient multiple benefits, including shorter hospital stay, less post-operative pain, less blood loss, better cosmesis, etc. In the market, the da Vinci robot is the dominant player in MIS. It is equipped with slender rigid arms and lacks of tactile sensation which is crucial in surgical interventions. The rigid arms pivot about the trocar and lack of dexterity inside the body. Also, the pivoting creates a large sweeping motion, which may cause damages to vital structures. Flexible robot is intrinsically safer. However, their payload capacity is small due to the low stiffness. The sweeping motion generated by the arm bending remains significant. Also, the workspace and dexterity are limited due to the lack of control in either the length or the curvature of the bending section. In this project, a novel constrained tendon-driven serpentine mechanism (CTSM) will be employed to design the proposed flexible surgical robot. In the CTSM both the length and curvature of the bending section are controllable, which gives the robot much improved dexterity and larger workspace. A shape reconstruction based force sensing method will be developed to enable the robot's tactile sensation. What's more, a tension based stiffness control method will be implemented to endow controllable stiffness to the flexible robot. Therefore, the payload capability can be actively adjusted based on the surgical task. As a summary, the developed robot will integrate the following advantages: tactile sensation, much reduced sweeping motion, controllable stiffness, enhanced dexterity, and expanded workspace.

1. OBJECTIVES AND SIGNIFICANCE

Objective: Development of a novel tele-operated flexible surgical robot based on the constrained wire/cable/tendon-driven mechanism. The developed robot is expected to have the following advantages or performances without sacrificing the surgical robot arm's dimensions:

(a) Tactile sensation with a force sensing resolution of finer than 0.1 N.
(b) Controllable stiffness: the robot can work with at least two stiffness options, i.e. stiff-floppy.
(c) Reduced sweeping motion than existing rigid/flexible surgical robot arms at same dimensions.

(d) Improved dexterity than existing rigid/flexible surgical robot arms at same dimensions and same end effector condition.
(e) Larger reachable workspace than existing rigid/flexible surgical robot arms at same base movement.
(f) Tele-operation: the slave flexible robot can be controlled stably with the master input device.

Significance: Every upgrade in surgical tools can bring multitude benefits to patients and surgeons, as shown by the da Vinci robot system. The successful completion of this work will yield a surgical robot much more capable than the existing da Vinci robot, including restored tactile sensation, controllable stiffness, reduced sweeping motion, enhanced dexterity, and expanded workspace inside the body. The tactile sensation is not possessed by the da Vinci robot yet. It gives surgeons an additional sense, therefore more comprehensive intraoperative decisions can be made. The improved dexterity and expanded workspace enable the surgeons fulfilling operations in an easier way and new operations that is less invasive and less time consuming is predictable. The reduced sweeping motion and controllable stiffness enable the robot avoiding damages to vital structures during the operation. Thus, safety can be improved. The controllable stiffness can suits the robot arm to variable surgical tasks. Therefore less surgical tools are needed during the surgery and the cost can be reduced.

2. RESEARCH METHODOLOGY

Based on the CTSM, the PI proposes to develop a flexible surgical robot arm using bio-compatible materials at first. In this robot arm, four tendons will be used to control the omnidirectional bending of the flexible section. The length of the bending section is controlled by the constraint tube and the curvature is controlled by the tendons. This gives the robot arm a wide range of configurations to access the target position (enhanced dexterity). Meanwhile, the sweeping motion can be greatly reduced. Tactile sensation of the robot arm is achieved by the shape reconstruction based force sensing model. The force at the distal end is sensed and is reflected to the operator by a haptic device.

3. RESULTS ACHIEVED

3.1 Design of the CTSM

The constrained tendon-driven serpentine mechanism (CTSM) is based on the conventional tendon-driven mechanism. The working principle is illustrated in Figure 1. In conventional TSM, the bending of the flexible backbone is controlled by a set of wires/cables/tendons (they are referred to as tendons in the later context). In the bending section, all the joints rotate equally. As the number of DOFs is much higher than the number of actuators, the TSM is under-actuated. In the CTSM, a constraint is applied to the TSM. For the constrained section, the bending is limited, while for the distal section it could be bent by the tendons as usual. For details, please refer to 8115049-J[2] and 8115049-C[1].

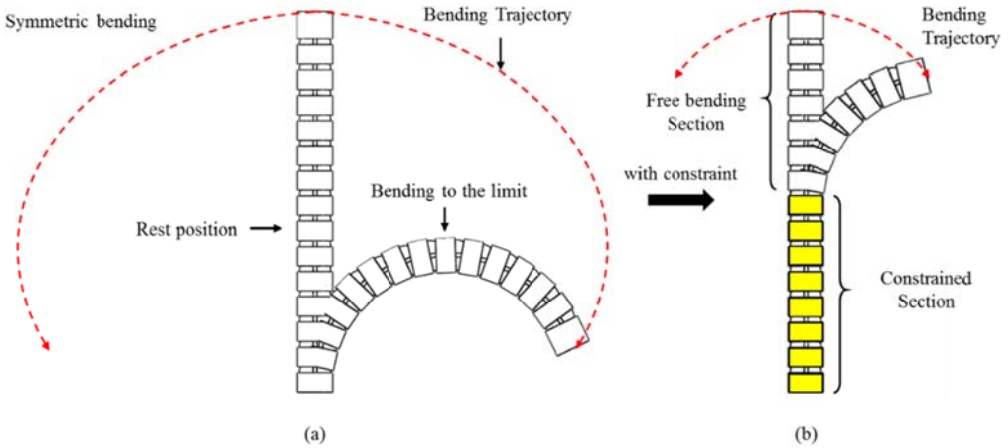

Fig. 1 Work principle of the CTSM: (a) bending of the conventional TSM; (b) in the CTSM the constraint changes the length of the bending section.

3.2 Kinematic modeling of the CTSM

The CTSM distal end is positioned and oriented by the tendons and the constraint tube, which control the curvature and the length of the bending section. Hence, the kinematics model can be divided into two parts as shown in Figure 2. The first part is the mapping between the actuator space and joint space, while the second part is the mapping between the joint space and task space. In the modeling, the constant curvature assumption is used. It is widely adopted in modeling flexible robot and has been proved to be accurate enough for load free or small loading conditions. Details of the kinematic modeling, please refer to 8115049-J[2].

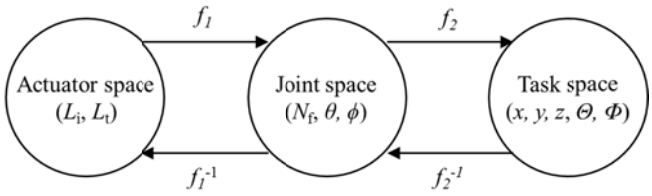

Fig. 2 Kinematics mappings in the CWFM.

3.3 Workspace and Dexterity of the CTSM

3.3.1 Workspace

Figure 3 (a)-(c) show the workspaces of the conventional wire-driven flexible mechanism (WFM), concentric tube mechanism (CTM) and CTSM when the base is fixed, i.e. zb=0. From the results, for WFM and CTM the distal end can only move along a fixed trajectory, while for CTSM there are N+1 trajectories. The workspace of the WFM is a subspace of that of the CTSM. From the result, the workspace is much expanded without considering the base movement. Figure 3 (d)-(f) show the workspace of the WFM, CTM and CTSM with a mobile base which can translate along the Zw axis and the range of translation is [0, 25] mm. The start position (SP) and end positon (EP) of the base are represented by the squares in the figures. By adding a mobile base, the workspace of the WFM, CTM and CTSM all increased and in such condition the workspace of the CTSM remains larger than that of the WFM. The location of the workspaces of the CTM and CTSM are different. From the simulation results, we can also tell that the area of the CTSM workspace is larger. For details, please refer to 8115049-J[2].

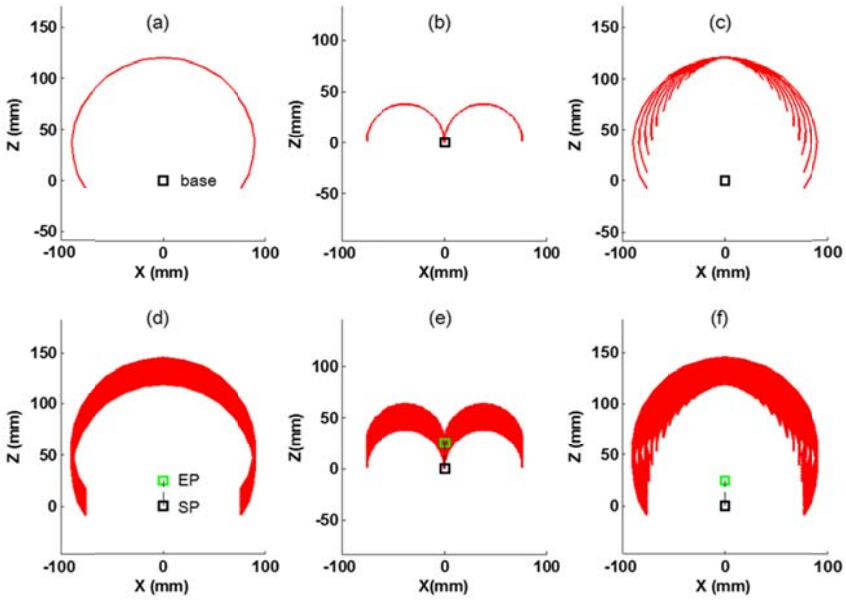

Fig. 3 Comparison of the workspace in the X_wZ_w plane: (a)-(c) workspace of the conventional wire-driven mechanism (WFM), concentric tube mechanism (CTM) and CTSM with a fixed base; (d)-(f) workspace of

the WFM, CTM and CTSM with a mobile base, and the range of base translation along Z_w axis is [0, 25] mm.

3.3.2 Dexterity

The dexterity of a manipulator can be evaluated locally and globally. It can be evaluated by several indexes, such as the condition number of the Jacobian matrix. However, a more intuitive way is to use the kinematic flexibility. It is related to the number of configurations with which the distal end can reach the target position, or the number of solutions in the inverse kinematics. For a particular position, it is measured by the absolute kinematic flexibility. For the entire workspace, it is measured by the relative kinematic flexibility. Assuming the manipulator can reach a point P with fa configurations, the absolute kinematic flexibility of the manipulator at P is fa. The larger the f_a the more dexterous the manipulator is at P. Assuming the volume of the entire workspace is V, and Vi represents the volume of the region in the workspace where fa=i, the relative kinematic flexibility is defined as:

$$f_r = \frac{1}{V}(V_1 + 2V_2 + 3V_3 + \mathrm{L}\ ) \tag{1}$$

For the CTSM (serpentine constrained wire-driven flexible mechanism), the distal end can reach positions in the workspace with finite configurations. The relative kinematic flexibility is suited to evaluate its dexterity. Figure 4 compares the dexterity of a conventional WFM and the CTSM. From the results, it shows that on average the CTSM is about 4.7 more dexterous. For details, please refer to 8115049-J[2].

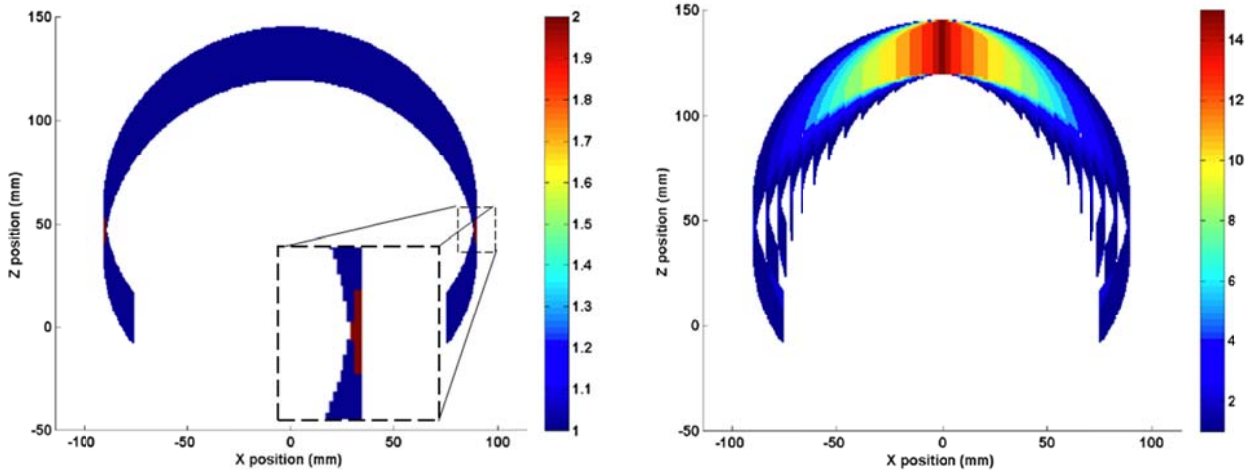

(a) (b)

Fig. 4 Dexterity comparison of the WFM and CTSM: (a) dexterity distribution of the WFM; (b) dexterity distribution of the CTSM.

3.4 Shape sensing of the CTSM

To control the CTSM, including the tip position, orientation and shape of the bending section, a shape sensing method based on electromagnetic (EM) sensor is proposed. In this method, one EM sensor is used to measure the position and orientation of the CTSM distal tip. The deformed shape of the backbone is estimated using the Cubic Biezer curve, as expressed in Eq. (2). The shape of the curve is controlled by the four controlling points P_0, P_1, P_2 and P_3. The two middle control points P_1 and P_2 could be expressed by the orientations at P_0 and P_3 as in Eq. (3), where H_0 is the orientation at P_0 and H_3 is the orientation at P_3, S_1 and S_2 represent the $||P_0P_1||$ and $||P_2P_3||$.

$$\mathbf{B}(t) = (1-t)^3\mathbf{P_0} + 3(1-t)^2 t\mathbf{P_1} + 3(1-t)t^2\mathbf{P_2} + 3t^3\mathbf{P_3} \tag{2}$$

$$\begin{cases} \mathbf{P}_1 = \mathbf{P}_0 + S_1\mathbf{H}_0 \\ \mathbf{P}_2 = \mathbf{P}_3 - S_2\mathbf{H}_3 \end{cases} \tag{3}$$

In the CTSM, the position and orientation of the proximal of the bending section could be obtained from the controller and the information of the distal end could be obtained using EM sensors. Since the length of the CTSM is constant, the length of the estimated curve should be the same. This is the critical information for solving the S1 and S2. The length of the estimated Bezier curve is as in Eq. (4).

$$L_c = \sum_{i=1}^{n} \left\| \mathbf{B}_i - \mathbf{B}_{i-1} \right\| \tag{4}$$

Figure 5 shows some of the simulation results. From the results, this method could well predict the deformed shape of the CTSM at different bending angle and different length of bending section. In the near future, experiments will be carried to validate this shape sensing method. For details, please refer to 8115049-J[1] and 8115049-J[6].

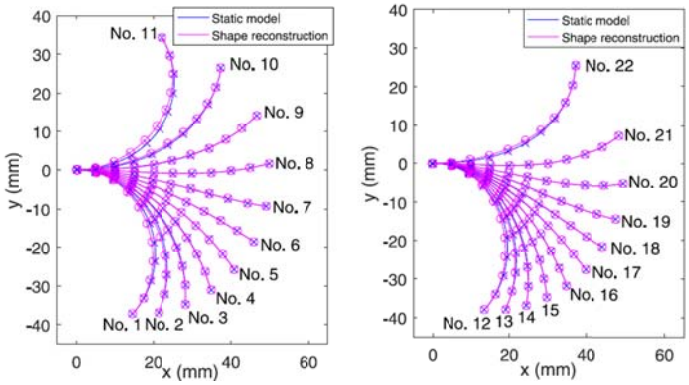

Fig. 5 Shape sensing results compared with shape from static modeling.

3.5 Force sensing of the CTSM

Force sensing model is developed based on the shape sensing and static modeling. Below summarize the results of force sensing algorithm. For the details of the method and validation, please refer to SHIAE8115049-J[6]. Results show that the proposed force sensing model could well predict the external load applied to the flexible manipulator. One example is given in Table 1.

Table 1 Force sensing result of the flexible manipulator with 15g external load.

Applied external load: 15 g

No.	F_{CI}(g)	F_{CII}(g)	F'_{ex}(g)	e(g)	e_p(%)	$F_f(g)$	$\frac{\lvert F_f \rvert}{F_C}$(%)	R_r(g)
23	0	160	12.56	−2.44	16.3	±6.51	4.1	±0.96
24	0	120	14.67	−0.33	2.2	±4.33	3.6	±0.76
25	0	80	15.23	0.23	1.5	±2.51	3.1	±0.40
26	0	40	15.19	0.19	1.2	±1.07	2.7	±0.15
27	0	0	15.41	0.41	2.8	0	0	0
28	40	0	15.37	0.37	2.4	±0.71	1.8	±0.07
29	80	0	14.71	−0.29	1.9	±1.28	1.6	±0.12
30	120	0	15.28	0.28	1.9	±1.85	1.5	±0.16
31	160	0	15.22	0.22	1.4	±2.54	1.6	±0.21
32	200	0	14.79	−0.21	1.4	±3.65	1.8	±0.29

3.6 Robot Prototype

Figure 6 shows one of the robot prototype developed based on the CTSM. In the prototype, the flexible backbone has 25 vertebrae. The vertebrae are fabricated by means of 3D printing, and the material used is plastic. Each joint can rotate up to 7.25° . The total length of the flexible backbone is 100 mm, and the outer diameter is 7.5 mm. A silicon rubber tube serves as the elastic tube. The outer diameter is 3 mm and the inner diameter is 2 mm. Four steel wires with nylon coating are used to control the backbone bending. The

diameter of the steel wire is 0.3 mm. The wires are arranged orthogonally, with opposite wires making a pair. Each wire pair is connected to a drum wheel. The rotation of the drum wheel is controlled by a servo motor. The diameter of the drum wheel is 50 mm. The wires are guided by a Teflon tube, whose outer diameter is 0.9 mm and inner diameter is 0.5 mm. The Teflon tube and the steel wire form a tendon-sheath system, which is similar to the Bowden cable. The constraint is held by a chuck, which is mounted on the linear actuator. The range of the linear actuator is 100 mm. The constraint is replaceable, and two constraints are tested. One is an elastic constraint and the other is a rigid constraint. The outer diameter of the constraint is 1.5 mm. For details, please refer to 8115049-J[2] and 8115049-C[1].

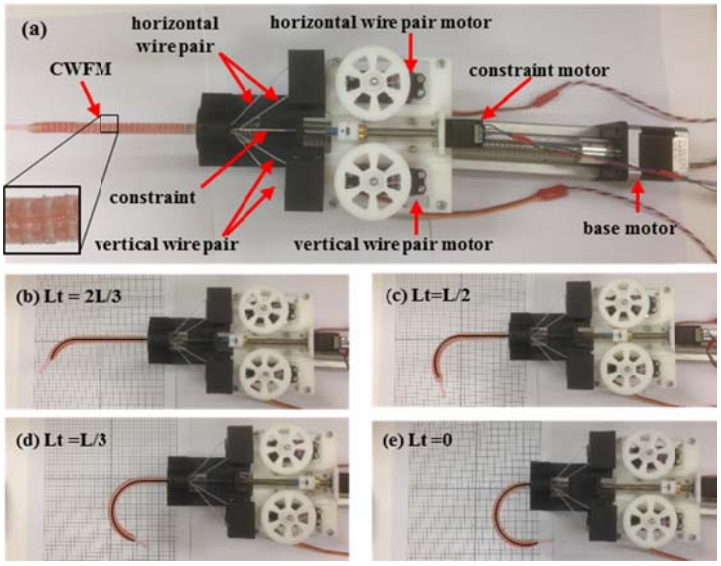

Fig.6 Proof of concept robot prototype based on the CTSM.

4. PUBLICATION AND AWARDS

Journal publications:

J[1] S. Song, **Z. Li**, Q.H. Meng, H.Y. Yu and H.L. Ren, "Real-time shape estimation for wire-driven flexible robots with multiple bending sections based on quadratic Bezier curves", IEEE Sensors Journal, Vol. 15, No. 11, pp. 6326-6334, Nov. 2015

J[2] **Z. Li**, H.L. Ren, W.Y. Chiu, R.X. Du and H.Y. Yu, "A novel constrained wire-driven flexible mechanism and its kinematic analysis", Mechanism and Machine Theory, Vol. 95, pp. 59-75, 2016

J[3] **Z. Li**, M.Z. Oo, V. Nalam, et. al, "Design of a Novel Flexible Endoscope - Cardioscope", Journal of Mechanisms and Robotics, Vol. 8, pp. 051014 1-9, 2016

J[4] **Z. Li** and S.H. Ng, "Future of uniportal video-assisted thoracoscopic surgery – emerging technology", Annals of Cardiothoracic Surgery, Vol. 5, No. 2, pp. 127-132, 2016

J[5] **Z. Li**, L. Wu, H.L. Ren and H.Y. Yu, "Kinematic comparison of surgical tendon-driven manipulators and concentric tube manipulators", Mechanism and Machine Theory, No. 107, pp. 148-165, 2017

J[6] H. Yuan, **W.Y. Chiu** and **Z. Li**, "Shape-reconstruction-based force sensing method for continuum surgical robots with large deformation", IEEE Robotics and Automation Letters, Vol. 2, No. 4, pp. 1972 – 1979, Oct. 2017

J[7] H. Yuan and **Z. Li**, "Workspace analysis of cable-driven continuum manipulators based on static model", Robotics and Computer-Integrated Manufacturing, No. 49, pp. 240-252, 2018

Conference Publications:

C[1] **Z. Li**, H.Y. Yu, H.L. Ren, **W.Y. Chiu** and **R.X. Du**, "A novel constrained tendon-driven serpentine manipulator", Intelligent Robots and Systems (IROS), 2015 IEEE/RSJ International Conference on, Hamburg, Germany, pp. 5966-5971, 28 Sept. -2 Oct. 2015

C[2] **Z. Li**, C.Z. Song and **H.M. Wang**, "Design and prototyping of a concentric wire-driven manipulator", Biomedical Robotics and Biomechatronics (BioRob), 6th IEEE RAS/EMBS International Conference on, UTown, Singapore, pp. 213, Jun. 26-29, 2016

C[3] **Z. Li**, **W.Y. Chiu** and **R.X. Du**, "Design and kinematic modeling of a concentric wire-driven

mechanism targeted for minimally invasive surgery", Intelligent Robots and Systems (IROS), 2016 IEEE/RSJ International Conference on, Daejeon, Korea, pp. 310-316, Oct. 9-14, 2016
C[4] H. Yuan, **Z. Li**, **H.M. Wang** and C.Z. Song, "Static modeling and analysis of continuum surgical robots", Robotics and Biomimetics (Robio), 2016 IEEE International Conference on, Qingdao, China, pp. 265-270, Dec. 3-7, 2016

COMPLETED

DEVELOPMENT OF INJECTABLE SUPRAMOLECULAR HYDROGELS FOR REGENERATIVE MEDICINE

Principal Investigator: Professor BIAN Liming
Department of Department of Biomedical Engineering, CUHK

Co-Investigator (if any): Arthur Mak [(1)]

Research Team Members:
Wei Kongchang. Dr [(1)]

[(1)] Dept. of Biomedical Engineering, CUHK

Project Start Date: 1 July 2015
Completion Date: 30 June 2017

ABSTRACT

Objectives: to develop self-healing, bioadhesive, and mechanically resilient supramolecular gelatin hydrogels for articular cartilage repair.

Motivation: hydrogels are ideal carrier material for the delivery of therapeutic cells (like stem cells) and drugs to enhance the healing and regeneration of damaged biological tissues/organs. However, conventional chemically crosslinked hydrogels have a number of limitations that hinder the clinical translation of these hydrogels. In this project, we aim to develop novel supramolecular hydrogels, which are free of chemical crosslinking and have an array of unique features that are desirable for potential clinical applications.

Methodology: supramolecular hydrogel are generally mechanically weak. We have developed a novel "Host-guest macromer" (HGM) approach to fabricate supramolecular hydrogels with enhanced mechanical properties. Briefly, premixing the free diffusing crosslinkable host molecules with the polymer containing guest motifs significantly enhance the host-guest complexation efficiency due to the low steric hindrance. The subsequent polymerization of the obtained "HGM" produces the supramolecular hydrogels that are highly stretchable and self-healable. Furthermore, the residual hydrophobic cavities of the host molecules in the hydrogels afford the potential for facile modular modifications such as incorporation of hydrophobic drugs and tethering of bioactive molecules.

Impact & benefit: the advantages of the proposed HGM supramolecular hydrogels compared to existing products include mechanical resilience, tissue adhesiveness, self-healing, ease of use, and capability of delivering hydrophobic drugs. These benefits make the proposed hydrogels ideal vehicles for delivering therapeutic cells and drugs to assist treatments of human cartilage defects and a variety of other diseases including spinal cord injury, intervertebral disc herniation, etc.

1. OBJECTIVES AND SIGNIFICANCE

Objectives

Objective 1: To fabricate and characterize the supramolecular gelatin hydrogels
Objective 2: to examine the hMSC chondrogenesis in the physically crosslinked supramolecular hydrogels
Objective 3: To assess the controlled release of hydrophobic chondrogenic small molecules from the supramolecular hydrogels
Objective 4: To evaluate the efficacy of the supramolecular hydrogels as the carrier material of stem cells and drug to repair cartilage defects in an animal model

Significance

The findings from this project will help guide the design and promote the clinical translation of injectable hydrogels for cartilage repair. Hydrogels developed in this study will not only enhance cartilage repair but will also be instrumental to the development of minimal invasive therapies for repairing connective tissues including bone, meniscus and intervertebral disc.

2. RESEARCH METHODOLOGY

Objective 1: To fabricate and characterize the supramolecular gelatin hydrogels

i. Synthesis of mono-functional acrylated host molecule β-cyclodextrins (mono-Ac-β-CD)

Ac-β-CD (or mono Ac-β-CD) will be synthesized as reported previously. Briefly, β-cyclodextrin will be dissolved in 100 mL anhydrous DMF at room temperature followed by the addition of trimethylamine. The mixture will be cooled to 0 °C on ice. Acryloyl chloride will be added slowly. The reaction will be kept at room temperature for 12hr before being dripped into acetone. The precipitate will be washed with acetone and dried in vacuum. The degree of acrylation will be controlled to be around 1.0 and confirmed by ^{1}H NMR.

ii. Hydrogel fabrication, and rheological and mechanical testing

Typically, a mixture of gelatin, Ac-β-CD, photoinitiator (I2959) will be dissolved in PBS and exposed to UV light (10 mW/cm-2, 10min) to form the hydrogels. The effect of additional monomers such as poly (ethylene glycol) acrylate on the hydrogel mechanical properties will also be examined. Dynamic viscoelasticity of the hydrogels will be measured by a rheometer using a plate-plate setup. The mechanical properties of the hydrogels will be measured on a MACH-1 Micromechanical.

Objective 2: to examine the hMSC chondrogenesis in the physically crosslinked supramolecular hydrogels

i. hMSC encapsulation in ECM hydrogels and chondrogenic induction

hMSCs (Lonza) will be expanded to passage 3 in a growth medium consisting of α-MEM with 16.7% FBS (fetal bovine serum). hMSCs (20 million/ml) will be encapsulated in hydrogel constructs (Ø5mm, 2 mm thickness). Constructs will be cultured in chondrogenic media (DMEM, 1% ITS+Premix, 50 µg/ml L-proline, 0.1 µM dexamethasone, 50µg/ml ascorbate) supplemented with transforming growth factor (TGF-β3, 10ng/ml).

ii. Gene expression analysis

RNA will be extracted using Trizol according to the manufacturer's instructions, and the RNA concentration will be determined using a spectrophotometer (Nanodrop). Obtained RNA will be reverse transcribed into cDNA using a reverse transcription kit (Invitrogen). The real time polymerase chain reaction (qPCR) will be performed using Taqman primers and probes specific for GAPDH (housekeeping gene) and other genes of interest (type II collagen, Aggrecan, Sox9). The sequences of the primers and probes are listed in a previous publication [2]. The relative gene expression will be calculated using the ΔΔCT method.

iii. Statistical and power analysis

Statistica (Statsoft) will be used to perform statistical analyses using two-way ANOVA, followed by Tukey's HSD post hoc testing to allow for comparison between groups. Statistical significance will be set at $p < 0.05$. A statistical power analysis indicates that n=8 samples per group should be sufficient for obtaining a study power of 0.85 with significance set at $p<0.05$.

Objective 3: To assess the controlled release of hydrophobic chondrogenic small molecules from the supramolecular hydrogels

i. Incorporation of small molecules and release analysis

The chondrogenic small molecule, kartogenin, will be dissolved in ethanol and mixed with an ac-CD aqueous solution overnight under stirring. The complexation of kartogenin with ac-CD will be verified by an FT-IR spectrometer. The ac-CD solution will then be used for the fabrication of ac-CD-HA hydrogels. The obtained hydrogel will be incubated in PBS. The concentration of kartogenin released from the hydrogels to the PBS will be monitored by UV-vis at selected time points. To evaluate the effect of the carried

kartogenin on chondrogenesis, hMSCs will be encapsulated into hydrogels fabricated with ac-CDs that are loaded with kartogenin. The analysis described in Task 3 will be conducted to assess the chondrogenesis of the hMSCs in the presence of released kartogenin from the surrounding hydrogel scaffold.

Objective 4: To evaluate the efficacy of the supramolecular hydrogels as the carrier material of stem cells and drug to repair cartilage defects in an animal model

i.Implantation in critical-sized focal cartilage defect in rabbits

New Zealand White rabbits (8 weeks) will be used. Surgery will be performed to expose the left knee joints under anesthesia. 3 mm diameter defects will be created in the center of the trochlear groove with a biopsy punch without disrupting the subchondral bone. The hMSCs and kartogenin loaded hydrogels will be injected into the defects. The same procedures will be performed on the right knees without injecting the hydrogels and cells to serve as the control. The knee joints will be closed with sutures. The animals will be followed for 10 weeks.

3. RESULTS ACHIEVED

Objective 1, 2, 3, and 4 are all achieved. Detailed data are presented below.

1. HGM hydrogels maintain the viability of the encapsulated hMSCs

The pre-formed HGM hydrogels can be injected by hand to completely fill up the cartilage defect volume, and the injected HGM hydrogels adhere to the surrounding cartilage and remain in position under mechanical probing by a tweezer (**Fig. 1A**). We injected the pre-formed hMSC-laden gelatin HGM supramolecular hydrogels via a G18 needle, and the viability staining of the injected hydrogels after 3 days of culture shows that majority of the encapsulated cells survive the injection process and remain viable (**Fig. 1B**). We further evaluated the viability of the hMSCs encapsulated in the gelatin HGM hydrogels and the control GelMA hydrogels during extended *in vitro* culture. After 14 days of chondrogenic culture, the majority (>95%) of the hMSCs encapsulated in the GelMA and HGM hydrogels remain viable. Interestingly, the hMSCs encapsulated in the HGM hydrogels show substantial spreading after 14 days of culture, whereas the hMSCs in the GelMA hydrogels remain the initial rounded morphology (**Fig. 2A**). This finding indicates that the cells encapsulated in the HGM hydrogels are able to actively interact with the surrounding hydrogel structures.

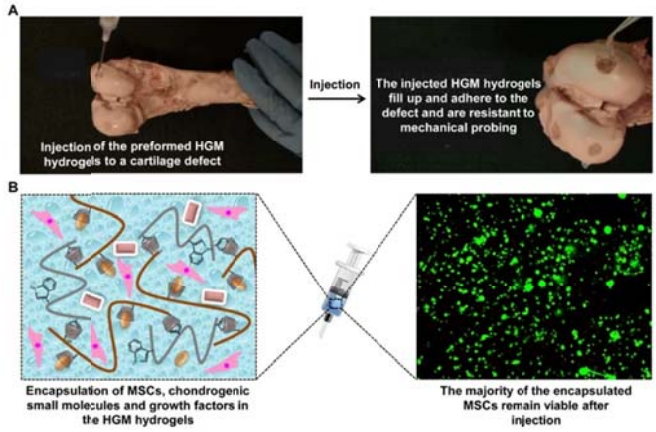

Fig. 1. The injection of HGM gelatin supramolecular hydrogels that are encapsulated with MSCs, chondrogenic small molecules and growth factors for cartilage repair. (A) The injection of pre-formed gelatin HGM supramolecular hydrogels to adhere the cartilage defect. (B) The viability of hMSCs in pre-formed gelatin HGM supramolecular hydrogels after injection via a G18 needle.

2. HGM hydrogels mediate prolonged release of encapsulated hydrophobic drug KGN and a model protein

We further encapsulated a hydrophobic chondrogenic small molecule, kartogenin (KGN), or a model protein, bovine serum albumin (BSA), in the HGM hydrogels to assess the *in vitro* release kinetics. Our finding shows that the release profiles of the cargo molecules from the HGM hydrogel are significantly different from those of the GelMA hydrogels. The HGM hydrogels release the loaded KGN continuously for up to 28 days at an almost constant rate **(Fig. 2B)**. In contrast, almost all the loaded KGN is rapidly released out from the GelMA hydrogels within 7 days. These results indicate that the HGM hydrogels afford enhanced storage and sustained release of the KGN and TGF-β1, which will promote the chondrogenesis of the encapsulated hMSCs. Furthermore, these *in vitro* studies suggest that the HGM hydrogels are more promising than the GelMA hydrogels as the delivery vehicles of chondrogenic agents for cartilage regeneration under the *in vivo*

condition, where a sustained release of an initial bolus dosage of these agents is desired.

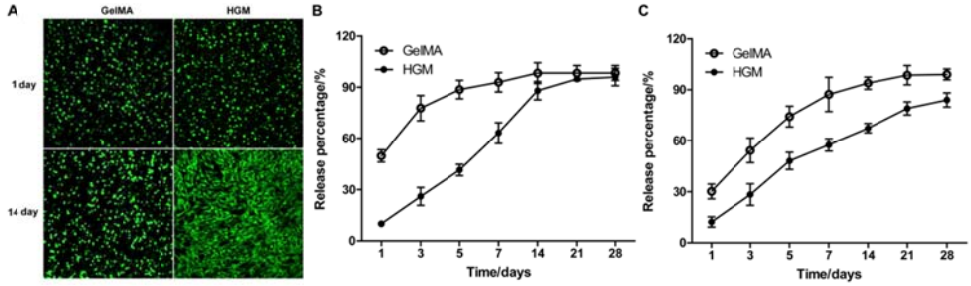

Fig. 2. The property test of the HGM and GelMA hydrogel. (A) Cell viability staining of the hMSC-laden GelMA and HGM hydrogels after 1 day and 14 days of culture. Cumulative release of KGN (B) and BSA (C) encapsulated in the GelMA and HGM hydrogels.

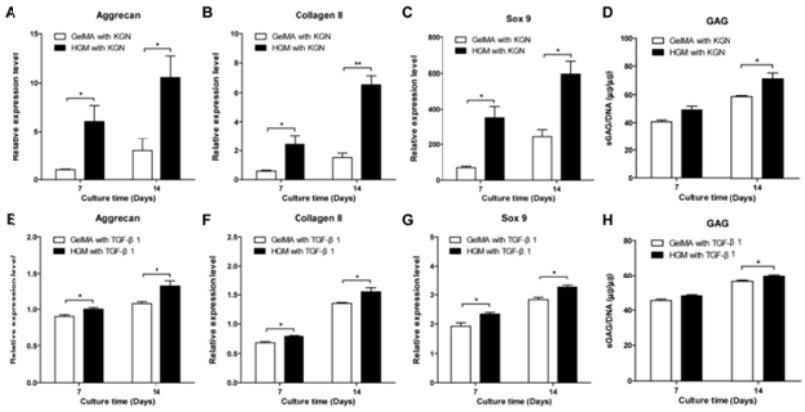

Fig. 3. The chondrogenic differentiation of hMSCs in the HGM hydrogels loading with KGN or TGF-β1 *in vitro*. The mRNA expression of chondrogenic marker genes of hMSCs-laden GelMA and HGM hydrogels constructs with KGN and TGF-β1. Relative gene expression of Aggrecan (A, E), type II Collagen (B, F), and Sox 9 (C, G) by the hMSCs after 7 and 14 days of differentiation is presented. GAG content of hMSCs-laden GelMA and HGM hydrogels constructs with KGN and TGF-β1. Comparison of GAG content in chondrogenic differentiation medium supplemented with KGN (D) and TGF-β1 (H) at 7 days and 14 days. The data are reported as the mean ± SD of the experiments (n = 3). *: $p < 0.05$, **: $p < 0.01$. Scale bar indicates 200 μm.

3. HGM hydrogels enhance the chondrogenic differentiation of encapsulated hMSCs in vitro

We evaluated the chondrogenesis of hMSCs in the KGN (0.5 nmol per hydrogel) or TGF (50 ng per hydrogel) laden HGM and GelMA hydrogels. After 14 days of induction, the hMSCs in the HGM hydrogels exhibits significantly higher expression of chondrogenic markers than those in the GelMA hydrogels groups. For the KGN laden hydrogels, the mRNA expression in the HGM with KGN groups is enhanced by about 253.7 % ± 178.5 %, 332.0 % ± 51.5 %, and 141.4 % ± 69.3 % for Aggrecan, type II Collagen, and Sox 9 compared to that of the GelMA with KGN groups at day 14, respectively (**Fig. 3A-C**). For the TGFladen hydrogels, the mRNA expression in the HGM with TGFgroups is enhanced by about 22.2 % ± 9.4 %, 14.9 % ± 7.8 % and 15.0 % ± 8.2 % for Aggrecan, type II Collagen, and Sox 9 compared to that of the GelMA with TGF groups at day 14, respectively (**Fig. 3E-G**). Consistent with the gene expression results, the quantification of glycosaminoglycans (GAGs), a cartilage-specific matrix component [13], shows that the GAGs content in the HGM group is 21.7 % ± 12.3 % (loaded with KGN) (**Fig. 3D**) and 4.7 % ± 2.1 % (loaded with TGF-β1) (**Fig. 3H**) higher than that in the GelMA group after 14 days of culture *in vitro*.

4. HGM hydrogels enhance the chondrogenic differentiation of encapsulated hMSCs in vivo

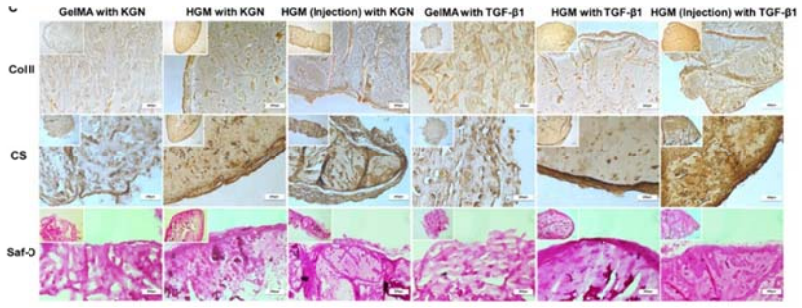

Fig. 4. The Immunohistochemical and histological staining of hMSC-laden hydrogels with KGN and TGF-β1 after 14 days chondrogenic differentiation *in vivo*. Immunohistochemical and histological staining of type II Collagen (col II), Chondroitin sulphate (CS) and Safranin-O (Saf-O) of hMSCs-laden hydrogels,

respectively. The data are reported as the mean ± SD of the experiments (n = 3). *: $p < 0.05$, **: $p < 0.01$. Scale bar indicates 200 μm.

The immunohistochemical staining reveals more intense staining against type II collagen (Col II) and chondroitin sulfate (CS) in the KGN or TGF laden HGM hydrogels than that in the KGN or TGF-β1 laden GelMA hydrogels (**Fig. 4**). The safranin-O (Saf-O) staining of the histological sections also shows more deposition of proteoglycans in the HGM hydrogels than in the GelMA hydrogels (**Fig. 4**). The GAG quantification, immunohistochemical and histological stainings show that the content of the cartilage-specific matrix components in the KGN/TGF-β1 injected HGM hydrogels ("HGM (injection) with KGN/TGF-β1" group) is significantly higher than that in the KGN/TGF-β1 the GelMA hydrogels ("GelMA with KGN/TGF-β1" group) and are similar to that in the directly implanted (non-injected) HGM hydrogels loaded with the same chondrogenic factor ("HGM with KGN/TGF-β1" group) (**Fig. 4**). Therefore, the hMSCs encapsulated in the HGM hydrogels are likely protected from the excessive shear stress of the injection due to the "sol" transition of the surrounding HGM hydrogels [18, 19]. The exellent injectability of the HGM hydrogels makes them an ideal biomaterial carrier of hMSCs for cartilage regeneration by minimally invasive procedures.

5. *HGM hydrogels promote the regeneration of cartilage and subchondral bone in the **animal** osteochondral defect model*

We further assess the efficacy of rMSCs-laden HGM hydrogels loaded with KGN (1 nmol/hydrogel) or TGF(100 ng per hydrogel) for cartilage regeneration in the osteochondral defects in animal knee. GelMA and HGM hydrogels were pressed fit and injected into the cartilage defects, respectively. 6 weeks after the implantation, as shown in **Fig. 5**, macroscopic views of defect area reveal fully regenerated cartilage of white and smooth appearance that is well integrated with the surrounding tissue in all the HGM hydrogels groups, closely resembling the healthy control. In contrast, in the GelMA with KGN/TGF-β1 groups, a partial cartilage defect in the center is still clearly visible, and the circular defect boundary is easily distinguishable at the interface with the surrounding health cartilage. In the non-treated (PBS control) group, the defects were almost empty with little regenerated tissue.

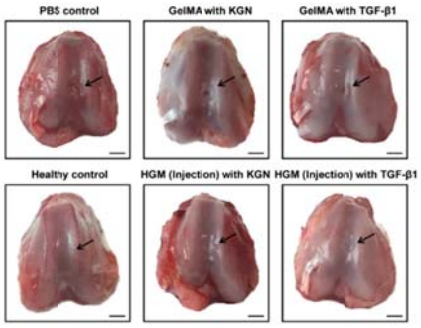

Fig. 5. Macroscopic appearance of the animal knee osteochondral defect either treated with PBS or repaired by using the following hydrogels loaded with chondrogenic agents: GelMA with KGN, HGM (Injection) with KGN, GelMA with TGF-β1, and HGM (Injection) with TGF-β1 at week 6 after surgery. The non-treated (PBS control) left femur (Healthy control) was collected as control. Scale bar: 2 mm.

Histological examination (Safranin-O and H & E staining) reveals the deposition of disorganized fibrous tissue in the osteochondral defects of the non-treatment group (PBS control) with poor integration to the surrounding native cartilage and no regeneration of subchondral bone. In the GelMA with KGN/TGF-β1 groups, the defect is filled with a mixture of fibrous and cartilage-like tissue with little regeneration of the subchondral bone. In clear contrast, the defects in the HGM (Injection) with KGN/TGF-β1 groups show more congruent articular surface, enhanced regeneration of cartilage-like tissue and subchondral bone, and organized osteochondral structure, which is similar to that of the healthy control. The expression of cartilage-specific type II collagen in the defect area is evaluated by immunohistochemical staining (**Fig. 6**). Higher levels of type II collagen expression are found in the HGM (Injection) with KGN/TGF-β1 groups than those of the GelMA with KGN/TGF-β1 groups, and these results are consistent to Safranin-O staining results (**Fig. 6**).

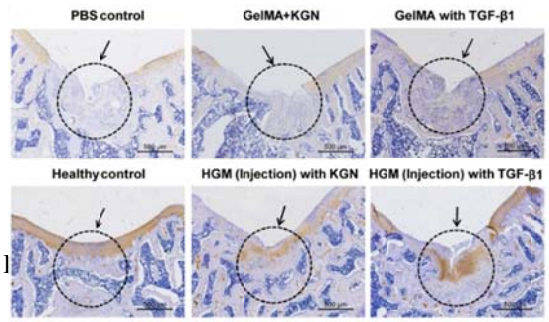

Fig. 6. (A) Safranin-O & fast green staining, (B) H&E staining and (C) immunohistochemical staining against type II collagen of the animal knee osteochondral defects either treated with PBS or repaired by using the following hydrogels loaded with chondrogenic agents: GelMA with KGN, HGM (Injection) with KGN, GelMA with TGF-β1

and HGM (Injection) with TGF-β1 at week 6 after surgery. Arrows heads and dotted circles indicate the location of the articular surface and osteochondral defects, respectively. Scale bar indicates 500 μm.

The quality of the cartilage regeneration is evaluated according to the scoring method described by Wakitani [20, 21]. The average Wakitani score is 9.67 ± 1.86 for GelMA with KGN, 9.50 ± 1.52 for GelMA with TGF-β1, 3.83 ± 1.47 for HGM (Injection) with KGN, and 4.50 ± 1.52 for HGM (Injection) with TGF-β1 groups, respectively, 6 weeks after the implantation (**Fig. 7**). The non-treatment control and healthy control group receives the highest and lowest score, respectively. The HGM (Injection) with KGN/TGF-β1 groups score significantly lower than the GelMA with KGN/TGF-β1 groups, thereby indicating enhanced cartilage regeneration achieved by using the HGM gelatin hydrogels. These results incidate that the HGM gelatin hydrogels promote the chondrogenesis of the encapsulated rMSCs and enhance the neocartilage formation in the animal cartilage defect model. The enhanced regeneration of subchondral bone observed the HGM groups is likely due to that the weak host-guest crosslink in the HGM hydrogels facilitate the infiltration and migration of endogenous osteoblastic cells from surrounding bone tissues as demonstrated in our previous work [3].

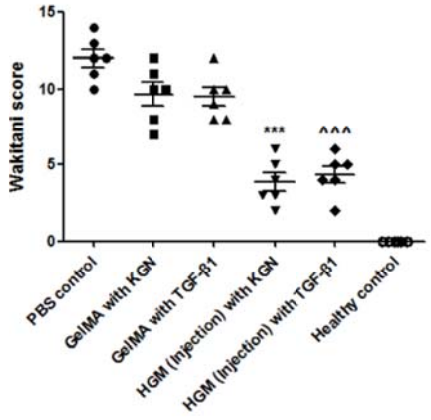

Fig. 7. Cartilage regeneration evaluated by the Wakitani scoring system at week 6 after surgery. $^{***}P<0.001$ vs. (GelMA with KGN); $^{\wedge\wedge\wedge}P<0.001$ vs. (GelMA with TGF-β1).

4. PUBLICATION AND AWARDS

J[1] +Feng, Q.; +Wei, K.; Lin, S.; Xu, Z.; Sun, Y.; Shi, P.; Li, G.; *Bian, L. Mechanically resilient, injectable, and bioadhesive supramolecular gelatin hydrogels crosslinked by weak host-guest interactions assist cell infiltration and in situ tissue regeneration. Biomaterials, 2016 Sept, 101: 217-28.

J[2] Wei, K.; Zhu, M.; Su, Y.; Xu, J.; Feng, Q.; Lin, S.; Wu, T.; Xu, J.; Tian, F.; Xia, J.; Li, G.; *Bian, L. Robust biopolymeric supramolecular "Host-Guest Macromer" hydrogels reinforced by in situ formed multivalent nanoclusters for cartilage regeneration. Macromolecules, 2016 Jan, 49 (3), pp 866–875.

J[3] +Xu, Y.; +Wei, K.; Zhao, P.; Feng, Q.; Choi, C.K. ; *Bian, L. Preserving the adhesion of catechol-conjugated hydrogels by thiourea-quinone coupling. Biomaterials Science, 2016, 4, 1726-1730.

J[4] Huang, H.; Xu, J.; Wei, K.; Xu, Y.; Choi, C. K; *Bian, L. Bioactive nanocomposite poly (ethylene glycol) hydrogels crosslinked by multifunctional layered double hydroxides nano-crosslinkers. Macromolecular Bioscience, 2016; 16 (7): 1019-26.

J[5] +Feng, Q.; +Lin, S..; Zhang, K.; Dong, C., Sun, Y.; Huang, H.; Yan, X.; Zhang, L.; Li, G.; *Bian, L. Sulfated hyaluronic acid hydrogels with retarded degradation and enhanced growth factor retention promote hMSC chondrogenesis and articular cartilage integrity with reduced hypertrophy. Acta Biomaterialia, 2017 Feb.

J[6] Zhang, K.; Feng, Q.; Xu, J.; Xu, X.; Yeung, K.W.K.; *Bian, L. Self-assembled injectable nanocomposite hydrogels stabilized by bisphosphonate-magnesium (Mg2+) coordination regulates the differentiation of encapsulated stem cells via dual crosslinking. Advanced Functional Materials. 2017, June

P[1] Filed US Non-provisional patent: A bioadhesive and injectable hydrogel. Inventors: Feng, Q.; Wei, K.; Lin, S.; Li, G.; Bian, L.

P[2] Filed US Non-provisional patent: A fast, pH-independent, and efficient conjugation method. Inventors: Xu, Y.; Wei, K.; Bian, L.

P[3] Filed US provisional patent: Injectable hydrogels that promote mineralization and afford sustained release of bioactive ions. Inventors: Zhang, K.; Bian, L.

COMPLETED

DEVELOPING OPTOMECHANICALDEVICES BASED ON LAYERED NANOMATERIALS FOR SINGLE-BIOMOLECULE MASS SPECTROMETRY

Principal Investigator: Professor Xiankai SUN
Department of Electronic Engineering, CUHK

Co-Investigator (if any): Prof. Xu, Jianbin [1,2]

Research Team Members:
Ma, Jingwen, Junior Research Assistant [1,2]
Gu, Jiahua, Junior Research Assistant [1,2]
Li, Yuan, Junior Research Assistant [1,2]
Xi, Xiang, Research Postgraduate Student [1]
Yu, Zejie, Research Postgraduate Student [1]
Zhou, Wen, Research Postgraduate Student [1]

[1] Dept. of Electronic Enginnering, CUHK
[2] Shun Hing Institute of Advanced Engineering, CUHK

Project Start Date: 1 July 2015
Completion Date: 30 June 2017

ABSTRACT

The capability of determining the mass of biomolecules with high accuracy and fast speed has been playing a crucial role in proteomics for the development of molecular and cellular biology. Conventional mass spectrometers suffer from high cost, relatively large sample consumption, and low sensitivity. Nanoelectromechanical-system-based mass spectrometers can measure the proteins' mass directly. Landing of analyte (e.g., a protein) onto the device results in a variation of the resonator mass and thus shifts its resonant frequency. By tracking the frequency shift in real time, one can measure the mass variation, so as to determine the analyte species and quantity. However, the large parasitic capacitance and impedance mismatch inherent with the electrical transduction scheme limit the operation bandwidth and detection sensitivity.

Here we develop nanophotonic and nano-optomechanical devices based on a layered nanomaterial (e.g., graphene, MoS_2, or black phosphorus) to obtain the ultimate sensitivity. The mass of the mechanical resonator is greatly reduced from that made in a traditional material, thus enabling a much higher resolution for detecting the analyte mass. By using optical methods for mechanical actuation and detection, we can obtain unlimited operation bandwidth and, more importantly, the ultimate detection sensitivity that is capable for resolving a single biomolecule.

1. OBJECTIVES AND SIGNIFICANCE

Objectives:

1. To design and simulate an optomechanical structure based on a layered nanomaterial that is capable of detecting a single biomolecule for mass spectrometry
2. To establish an on-chip integrated photonics platform that involves simultaneous measurements of photonic, electronic, and mechanical properties

3. To experimentally investigate the schemes of monolithic integration of nanophotonic circuits and nanomechanical resonators with a layered nanomaterial
4. To fabricate an optomechanical device based on a layered nanomaterial and characterize its photonic and mechanical properties

Significance:
Mass spectrometry has been playing a crucial role in proteomics for the development of molecular and cellular biology. Its capability to identify and precisely quantify proteins from complex samples has broad impact on biology and medicine. Conventional mass spectrometers measure electromagnetic properties of ionized biomolecules to determine their mass-to-charge ratios, but this technique suffers from high cost, relatively large sample consumption, and low sensitivity.

Nanoelectromechanical system (NEMS)-based mass spectrometers measure mass of the proteins directly. Such spectrometers serve as an efficient interface between the frontend analyte and the backend outside world with the aid of CMOS integrated electronics. Landing of analyte (e.g., a protein) onto the device results in a variation of the resonator mass and thus shifts its resonant frequency. By tracking the frequency shift in real time, one can measure the analyte mass, so as to determine its species and quantity. However, the large parasitic capacitance and impedance mismatch inherent with NEMS limit the operation bandwidth and detection sensitivity.

To overcome this difficulty, we develop nano-optomechanical devices based on a layered nanomaterial (e.g., graphene, MoS_2, or black phosphorus) aiming to obtain the ultimate detection sensitivity. With a layered nanomaterial being the nanomechanical element, the mass of the mechanical resonator is greatly reduced from that made in a traditional material, thus enabling a much higher resolution for detecting the analyte mass. By using optical methods for mechanical detection, we can obtain unlimited operation bandwidth and, more importantly, the ultimate detection sensitivity that is capable for resolving a single biomolecule. The ability to detect single proteins in real time will eventually lead to the possibility of single-cell proteome profiling, an important milestone in both areas of biology and medicine.

2. RESEARCH METHODOLOGY

2.1. Theory and device design
There are two basic types of nanomechanical resonators: one is a bar-shaped doubly clamped beam resonator with length L, and the other is a circular drum-shaped resonator with diameter D. Their mechanical resonant frequencies can be expressed as

$$f_{\text{beam}} = \frac{1}{2L}\sqrt{\frac{E}{\rho}\varepsilon}, \quad f_{\text{drum}} = \frac{0.766}{D}\sqrt{\frac{E}{\rho}\varepsilon},$$

where E, ρ, and ε are the elastic stiffness, mass density, and strain, respectively. For two-dimensional graphene nanosheets, E = 340 N/m, $\rho = 7.4 \times 10^{-19}$ kg/μm^2, and ε can vary from case to case. Figure 1 shows the calculated resonant frequencies assuming that $\varepsilon = 10^{-6}$.

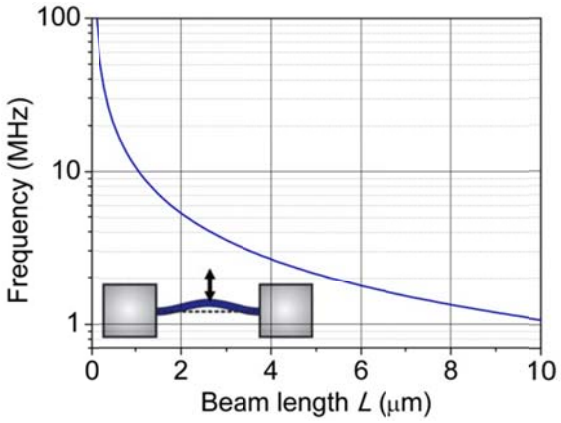

Fig. 1. Theoretical resonant frequency of the fundamental mechanical mode of doubly clamped beam

graphene resonator as a function of the beam length L.

For a beam resonator with length L of 5.5 μm, the fundamental mechanical mode vibrates at a resonant frequency f_0 of ~2 MHz with an effective mass m_0 of 3.5 fg. Variation in the resonator mass can be detected from a corresponding shift of the mechanical resonant frequency. The mass detection resolution δm is proportional to the minimal observable frequency shift δf:

$$\frac{\delta m}{m_0} = 2\frac{\delta f}{f_0} \approx 2 \cdot 10^{-DR/20} \sqrt{\frac{BW}{f_0}\frac{2\pi}{Q}},$$

where DR is the dynamic range in units of dB, BW is the measurement bandwidth, and Q is the quality factor of the mechanical resonator. With reasonable values of DR = 60 dB, BW = 1 kHz, and Q = 100, we estimate a mass detection resolution δm of 39 zeptograms, which is similar to the mass of a typical biomolecule.

2.2. Device description

Figure 2(a) is an illustration of a hybrid integrated graphene/silicon nano-optomechanical device. The photonic elements are realized in a planar silicon photonic circuit while the mechanical element is made of a graphene nanosheet [Fig. 2(b)]. The mechanical motion of the graphene nanosheet is actuated by an a.c. oscillating electrical signal applied onto the electrode. The actuated mechanical motion can be sensitively transduced into the optical domain, due to the strong optomechanical coupling. The optomechanically transduced signal is significantly enhanced by using a ring cavity and setting the detecting light near the cavity resonant wavelength.

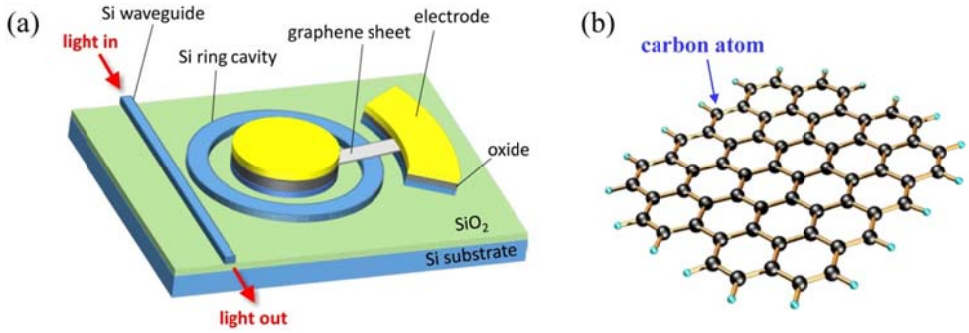

Fig. 2. (a) Optomechanical device based on hybrid integration of a Si ring cavity and a graphene nanomechanical resonator. (b) Atomic arrangement of a graphene nanosheet.

2.3. Device operation principle

Here we elaborate the mechanism of the optomechanical transduction. A cross-sectional view of the device structure is provided in Fig. 3(a). A graphene nanosheet is suspended above a section of the silicon ring cavity. The height of the graphene above the waveguide determines the optical effective index of the waveguide of the ring cavity, which further affects the resonant wavelength of the ring cavity. Figure 3(b) shows the cross-sectional structure of the model set up in Lumerical, a commercial mode solver for photonic structures, where the simulated optical mode profile [Fig. 3(c)] and the corresponding optical effective index were obtained.

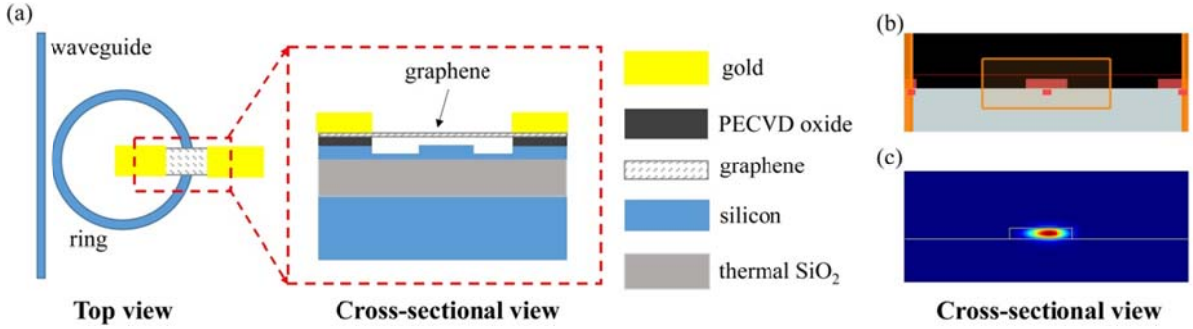

Fig. 3. (a) Top and cross-sectional views of the hybrid integrated graphene/silicon nano-optomechanical resonator. (b) Structure of the model in Lumerical mode solution. (c) Simulated optical mode profile

superimposed on the cross-sectional structure of the ring cavity.

We conducted the simulation for structures with different height of the graphene above the waveguide, with the resulting effective index n_{eff} plotted in Fig. 4(a). We can observe a clear dependence of n_{eff}'s imaginary part on the height of the graphene. The height variation originating from graphene's mechanical vibration leads to a shift in the cavity's resonant wavelength. Figure 4(b) plots the ring cavity's optical transmission spectra assuming the graphene's height varies from 100 nm to 100.02 nm. For an input laser beam with its wavelength fixed near a cavity resonance, its optical transmission will be strongly modulated. The output modulated laser beam carrying the graphene's mechanical vibration signal will be converted by a photodetector into electrical signal and further analyzed in the frequency domain.

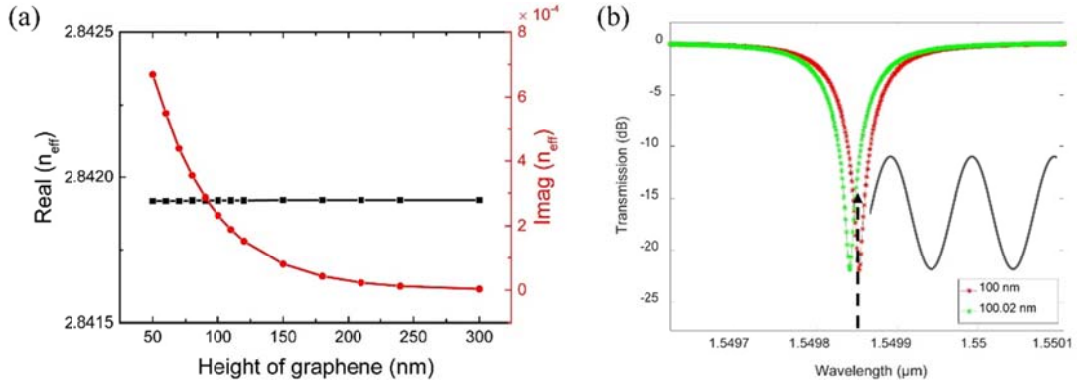

Fig. 4. (a) Real and imaginary parts of the effective index n_{eff} as a function of height of the graphene suspended above the waveguide. (b) Device's optical transmission spectra showing the result of optomechanical transduction of graphene's mechanical motion (height variation) into the optical domain.

3. RESULTS ACHIEVED

3.1. Fabrication of graphene/silicon nano-optomechanical resonators

The devices were fabricated in the CUHK engineering cleanroom (Micro- and Nano-Fabrication Laboratory, ERB G03). With a CMOS-compatible top-down nanofabrication approach, the device fabrication involves 8 major steps as shown in Fig. 5. First, the silicon planar photonic circuits are fabricated on a silicon-on-insulator substrate with electron-beam lithography (EBL) followed by an inductively coupled plasma reactive ion etching (RIE) process. Then, a thin oxide as a sacrificial layer is deposited by plasma-enhanced chemical vapor deposition (PECVD). Next, the graphene sheet is transferred onto the chip, which is further patterned with EBL and oxygen (O_2) plasma etching. After that, gold electrodes are fabricated by electron-beam evaporation followed by a lift-off process. Then, we use wet etching to remove the sacrificial oxide underneath the graphene so that the graphene sheet is released from the substrate. The device fabrication concludes with a step of sample drying in a critical-point dryer.

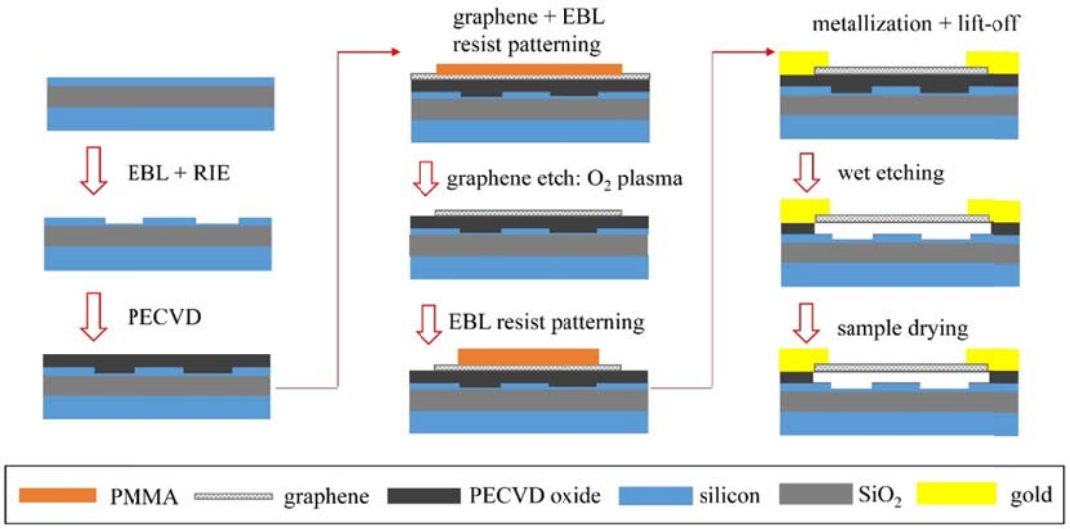

Fig. 5. Flow chart of device fabrication. EBL: electron-beam lithography; RIE: reactive ion etching; PECVD: plasma-enhanced chemical vapor deposition.

The images of a fabricated device are provided in Fig. 6. Figure 6(a) is an image of the fabricated device chip in sample box along with a Hong Kong 50-cent coin as a reference. Figure 6(b) is an optical microscope image of a hybrid integrated graphene/silicon nano-optomechanical device. Figure 6(c) is a scanning electron microscope image zooming in at the graphene nanosheet suspended above the waveguide of the ring cavity.

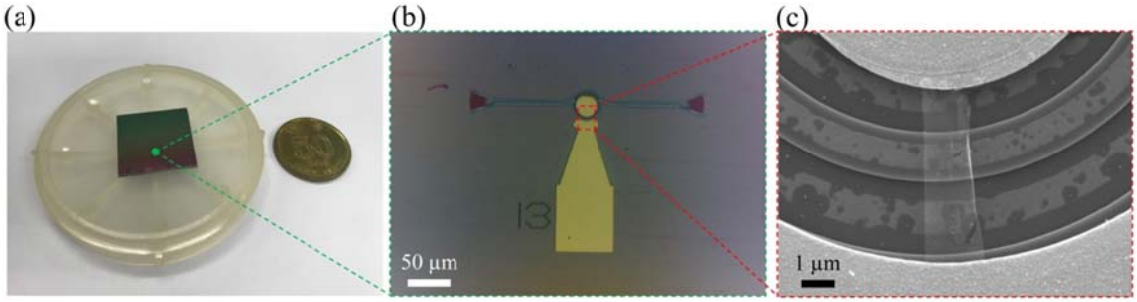

Fig. 6. (a) Device chip in sample box along with a Hong Kong 50-cent coin as a reference. (b) Optical microscope image of a hybrid integrated graphene/silicon nano-optomechanical device. (c) Scanning electron microscope image zooming in at the graphene nanosheet suspended above the waveguide of the ring cavity.

3.2. Characterization of graphene/silicon nano-optomechanical resonators

We characterized our fabricated devices with the most advanced optical and electrical measurement system as shown in Fig. 7, which is capable for detecting mechanical motion with vibration amplitude down to 1 picometer. Light from a tunable semiconductor laser (TSL) passes through a variable optical attenuator (VOA) and a fiber polarization controller (FPC) before coupling into the silicon bus waveguide of the device. The light coupled out of the device is split into two paths. Path 1 (1%) is used for measuring the ring cavity's optical transmission and monitoring the wavelength detuning from the cavity resonance. Path 2 (99%) is amplified by an erbium-doped fiber amplifier (EDFA) before sending to a high-frequency photodetector (PD). A sinusoidal a.c. electrical signal from a vector network analyzer (VNA) is added to a d.c. bias voltage (V_{dc}) before sending to the electrode of the device, which actuates the mechanical motion of the graphene nanomechanical resonator. The device's mechanical response is obtained by amplifying the electrical signal from Path 2 with a radio-frequency amplifier (RFA) and then sending it back to the VNA.

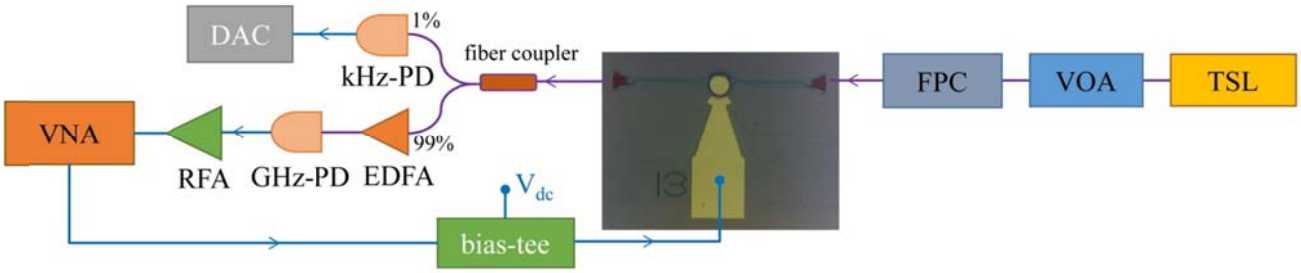

Fig. 7. Device measurement setup. VNA: vector network analyzer; RFA: radio-frequency amplifier; PD: photodetector; EDFA: erbium-doped fiber amplifier; DAC: data acquisition card; FPC: fiber polarization controller; VOA: variable optical attenuator; TSL: tunable semiconductor laser. Purple and blue wires indicate optical and electrical paths, respectively.

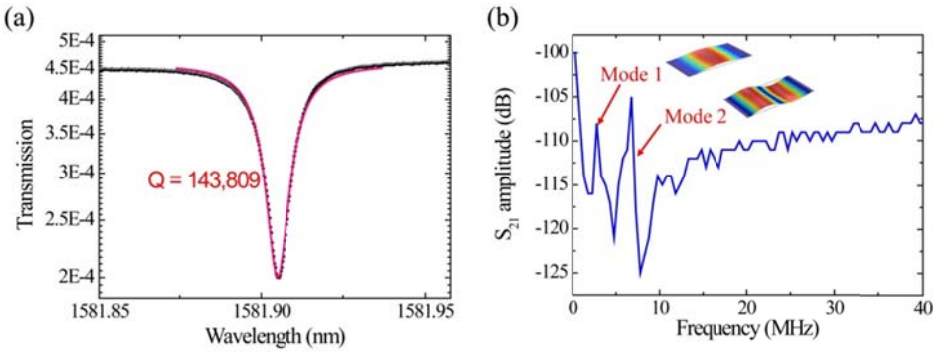

Fig. 8. (a) Optical transmission spectrum of the ring cavity showing the optical quality factor of 1.4×10^5. (b) Spectrum of S_{21} magnitude collected from the vector network analyzer. The identified two peaks correspond to the fundamental (f_1 = 2.5 MHz) and second-order (f_2 = 8.85 MHz) mechanical modes. Their mechanical quality factors are ~10 as measured in ambient air.

The optical quality factor of the ring cavity was obtained by collecting the power transmission of a laser beam through the device with the laser wavelength sweeping across a cavity resonance. Figure 8(a) shows the measured result, with a Lorentzian fitted loaded optical quality factor of 1.4×10^5. The device's mechanical modes were obtained from the spectrum of S_{21} magnitude collected from the vector network analyzer. We have identified two peaks which correspond to the fundamental (f_1 = 2.5 MHz) and second-order (f_2 = 8.85 MHz) flexural modes of the graphene nanomechanical resonator. Their mechanical quality factors are estimated to be ~10 as measured in ambient air.

3.3. Proposal of a graphene-based optical isolator

Optical isolators are a critical component to ensure unidirectional light flow. They are often used in optical systems to prevent reflection of light back into a laser source. In this project we have proposed an integrated version of optical isolator for controlling on-chip light flow based on the same hybrid integration platform. As shown in Fig. 9(a), the structure consists of a photonic bus waveguide and a microring cavity, whose inner top surface is covered by a patterned graphene nanoribbon. When a magnetic field is perpendicularly applied to the device plane, we expect distinct light transmission spectra for the two opposite propagation directions, thus achieving the function of optical isolation. As shown in Fig. 9(c), at 77 K and 8.4 T we can achieve an extinction ratio of ~45 dB with a reasonable insertion loss of ~12 dB for light with a wavelength of 1.552 μm. Such hybrid integrated nonreciprocal devices should find great promise and wide applications in the next-generation on-chip photonic systems. This work was published in *Applied Physics Letters* as a cover article and Editor's Pick. It was selected by *Optics & Photonics News*, The Optical Society's monthly news magazine, as one of the world's 30 most clearly communicated breakthroughs in optics in 2016.

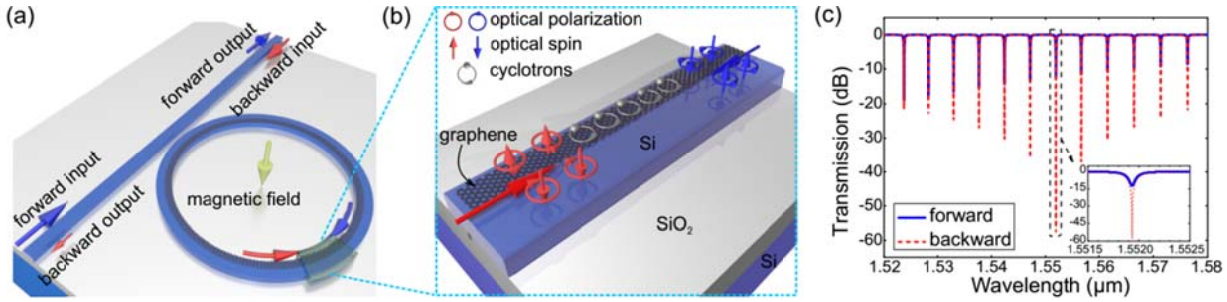

Fig. 9. (a) Schematic of the hybrid graphene/silicon integrated optical isolator. (b) A zoomed section of the isolator showing mechanism of the nonreciprocal optical transmission. (c) Calculated forward and backward light transmission spectra of the proposed device.

4. PUBLICATION AND AWARDS

J[1] Jingwen Ma, Xiang Xi, Zejie Yu, and Xiankai Sun, "Hybrid graphene/silicon integrated optical isolators with photonic spin-orbit interaction," *Applied Physics Letters* 108 (15): 151103, Apr. 2016. [Featured as cover article and selected as Editor's Pick] [Selected as one of the world's 30 most clearly communicated breakthroughs in optics in 2016]

J[2] Wen Zhou, Zejie Yu, Jingwen Ma, Bingqing Zhu, Hon Ki Tsang, and Xiankai Sun, "Ultraviolet optomechanical crystal cavities with ultrasmall modal mass and high optomechanical coupling rate," *Scientific Reports* 6: 37134, Nov. 2016.

J[3] Jiahua Gu, Xiang Xi, Jingwen Ma, Zejie Yu, and Xiankai Sun, "Parity-time-symmetric circular Bragg lasers: a proposal and analysis," *Scientific Reports* 6: 37688, Nov. 2016.

C[1] Jingwen Ma, Xiang Xi, Zejie Yu, and Xiankai Sun, "Spin-orbit interaction of light in photonic nanowaveguides: a proposal of graphene-based optical isolators," *PIERS 2016 in Shanghai*, The Electromagnetics Academy, Shanghai, China, Aug. 2016.

C[2] Jingwen Ma, Xiang Xi, Zejie Yu, and Xiankai Sun, "Hybrid graphene/silicon integrated optical isolators with photonic spin-orbit interaction," *IEEE Photonics Conference 2016*, IEEE, Waikoloa, HI, USA, Oct. 2016.

Multimedia Technologies Track

Research Reports In Multimedia Technologies

Continuing Project (2017 - 2019)	* Achieving Simultaneous Spectral-Spatial Super-Resolution via Reconstruction from Multispectral and Hyperspectral Images

The following reports are enclosed in "Research Highlights" printed in August 2017

Completed Project (2014 - 2016)	* Managing and Analyzing Big Graph Data

The following reports are enclosed in "Research Highlights" printed in June 2015

Completed Project (2012)	* Face Recognition Across Ages Through Binary Tree Learning

The following reports are enclosed in "Research Highlights" printed in June 2014

Completed Projects (2011)	* Semantic Analysis for Image Resizing * Time Critical Applications over a Shared Network * Amplify-and-forward Schemes for Wireless Communications

The following reports are enclosed in "Research Highlights" printed in 2013

Completed Projects	
(2010)	* FADE: Secure Cloud Storage with File Assured Deletion
	* Security and Detection Protocols for P2P-Live Streaming Systems
(2009)	* An Opportunistic Approach to Capacity Enhancement in Wireless Multimedia Networks
	* Computer-Aided Second Language Learning through Speech-based Human-Computer Interaction

The following reports are enclosed in "General Report and Research Highlights 2009-2011" printed in October 2011.

Completed Projects	
(2008)	* Pattern Computation for Compression and Performance Garment
(2007)	* Real-time Transmission of High Definition (HD) 3D Video and HD Audio in Gigabit-LAN
	* High Dynamic Range Image Compression and Display
	* Multimedia Content Distribution over Hybrid Satellite-Terrestrial Communication Networks
(2006)	* Automatic Video Segmentation and Tracking for Real Time Multimedia Services
	* Information Retrieval from Mixed-Language Spoken Documents
	* Wireless Networks and Its Potential for Multimedia Applications

The following reports are enclosed in "Research Highlights 2005-2007" printed in January 2008.

Completed Projects	
(2005)	* Mobile Wireless Multimedia Communication
	* An Automatic Multi-layer Video Content Classification Framework
	* Automatic Multimedia Fission, Categorization and Fusion for Personalized Visualization in Multimedia Information Retrieval

(Funded Year)

WORK IN PROGRESS

ACHIEVING SIMULTANEOUS SPECTRAL-SPATIAL SUPER-RESOLUTION VIA RECONSTRUCTION FROM MULTISPECTRAL AND HYPERSPECTRAL IMAGES

Principal Investigator: Professor Ken MA
Department of Electronic Engineering, CUHK

Research Team Members:
Qiang Li, Dr. [1], Ruiyuan Wu, Mr. [1], Qiong Wu, Ms. [1]

[1] Dept. of Electronic Enginnering, CUHK

Reporting Period: 1 July 2017 – 31 May 2018

INNOVATION AND PRACTICAL SIGNIFICANCE:

This project aims to develop a theoretical framework for hyperspectral resolution, addressing why recovery of a hyperspectral super-resolution image from low resolution images can be possible in theory and further understanding how we can build better systems. While current developments in this context have shown successful results by empirical means, they are practice or intuition-driven and are unable to answer the question of why hyperspectral super-resolution works from a fundamental research viewpoint. The innovative part of this project is that the PI will depart from the standard path of the current research trends (which are somehow bottom-up) and endeavor to tackle much more challenging theoretical problems arising from this relatively new research topic (which is top-down with an emphasis on asking why, and not just how). The impacts are expected to be significant as it will lead to theoretical guidelines on designing provably good hyperspectral super-resolution algorithms and cameras, which is presently unavailable in the literature.

Moreover, the PI should emphasize that hyperspectral super-resolution is currently a rapidly emerging topic with great potential and many possibilities in applications such as computer vision, medical imaging, art conservation, to name a few. The PI sees that now is the great opportunity to investigate this timely topic, seeing the substantial impacts a theoretical framework can reshape the topic and the far-reaching implications in many applications.

ABSTRACT

Please state the abstract of the project in this part. The abstract should appear at the top of the report. All manuscripts must be in English.

Hyperspectral super-resolution (HSR), a recently emerged image processing technique that aims to reconstruct a spectral-spatial super-resolution image from images with either lower spectral resolution or lower spatial resolution, is expected to become a key technology soon. HSR can significantly enhance applications in areas such as computer vision, art conservation, food safety, geoscience and remote sensing, offering an imaging solution that can identify objects that are hard to see by human eyes and with fine resolutions. It holds great potential and we expect the topic will see substantial growth. The goal of this project is to investigate key fundamental problems that arise in this timely topic. Specifically, the PI will study perfect reconstruction conditions of HSR—which is an open theoretical question that none of the

existing literature has been able to answer. Addressing this question satisfactorily will lead to guidelines on how to build provably correct HSR solutions, rather than relying on empirical experience which is currently the case. Furthermore, the PI will study a unified optimization framework for HSR, which is important in establishing a computationally efficient algorithmic toolset in this context.

1. OBJECTIVES AND SIGNIFICANCE

Please state the objective and significance of the project in this part.

1. to analyze conditions under which perfect recovery of a super-resolution image is guaranteed, and to identify good low-rank models and provably correct formulations under such analyses

2. to establish a unified optimization framework for low-rank matrix factorization in HSR

The first objective of this project is particularly innovative. All the current developments in HSR demonstrate feasibility via empirical experiences, and the designs are intuition-driven. A theoretical framework that pins down whether and how super-resolution is possible is still missing—and the PI intends to challenge that piece of uncharted water. The outcomes, if satisfactory, will provide theory-guided designs for HSR, which has much significance from a fundamental research viewpoint and will reshape how practical researchers think when designing an HSR algorithm. The second objective is important in bringing new and computationally efficient tools for practical implementations.

2. RESEARCH METHODOLOGY

Please state the research methodology of the project in this part.

We consider low-rank matrix factorization for HSR---which is a widely adopted approach in the current HSR literature---and investigate two key aspects. First, we aim to answer an open theoretical question, namely, whether and under what conditions low-rank matrix factorization methods can guarantee perfect recovery of the true super-resolution image. Being able to address this question satisfactorily will lead to substantial impacts on developing good algorithms for HSR and on the designs of multispectral and hyperspectral camera. Currently, none of the existing literature is able to show that the low-rank matrix factorization problem can guarantee perfect recovery of the super-resolution image.

Second, we intend to establish a unified optimization framework for low-rank matrix factorization in HSR. The aim is to provide computationally efficient solutions for HSR. The problem size in HSR is large; e.g., a super-resolution image with 200 spectral bands and 1,000x1,000 pixels amounts to 200,000,000 unknowns. Careful designs that exploit problem structures are essential, and the framework should be flexible in being able to accommodate various forms of problem structure-exploiting regularizations. The outcome, if successful, will lead to a powerful computational toolset for practical implementations.

3. RESULTS ACHIEVED SO FAR

Please state the project achievement and highlight (if any) on potential for commercialization and technology transfer in this part.

Achievement 1: Efficient Optimization Schemes for HSR

In C[1], we developed novel optimization schemes for low-rank matrix factorization in HSR. The proposed schemes run many times faster than the state of the art, as our extensive numerical studies showed. We achieve this by considering a hybrid inexact alternating minimization framework. Existing studies often

employ exact alternating minimization, which incurs high computational costs at each iteration. Our idea is to replace the exact updates with inexact proximal gradient or conditional gradient updates, thereby reducing the per-iteration computational costs substantially. The proposed schemes are not just based on engineering intuitions. As a preliminary result at this moment, we showed that these schemes are equipped with theoretical guarantees on convergence.

C[1] achieves Objective 2 very well. As an ongoing work, we are consolidating our findings in C[1]. We are aiming at establishing an optimization framework—which generalizes the current hybrid inexact alternating minimization schemes—that flexibly covers a broad range of low-rank matrix factorization problems in HSR. Under this unified framework, we will provide theoretical analyses that give evidence on why the proposed framework can converge faster than the state-of-the-art. We expect that this will lead to a new standard for low-rank matrix factorization algorithm designs in HSR, and hence this will be one of the key investigations in the second year of this project. The eventual outcome will be submitted as a journal article.

Achievement 2: Guaranteed Perfect Recovery of HSR Images in Polynomial Time

In C[3], and as another signature research output, we were successful in showing a sufficient condition under which we can guarantee perfect reconstruction of the true super-resolution image. Simply speaking, our sufficient condition suggests that if the spectral resolution of the multispectral camera and the spatial resolution of the hyperspectral camera are not too coarse, then HSR perfect reconstruction is possible. This result is significant because it is the first reported result on solving the HSR perfect reconstruction problem in polynomial time—which is surprising as HSR was previously thought to be a computationally intractable (NP-hard) problem. Furthermore, our result suggested that we can, in principle, use very efficient (polynomial-time) algorithms to attain such an HSR perfect reconstruction guarantee.

While preliminary, the theory presented in C[3] is a vital milestone for Objective 1 and beyond. As an ongoing work, we are further analyzing how robust our newly developed theory is under modeling errors. This presents new analysis challenges that are unique to HSR and not seen in the current literature. Also, we are studying what new insights our result shows in terms of algorithm designs. If successful, the aforementioned studies will lead to a major breakthrough in HSR theory.

Achievement 3: A New HSR Formulation by Tensor Factorization

This is a fruitful outcome from international collaboration. The PI and his international collaborators developed a new HSR framework using tensor factorization. The existing works often treat the HSR problem as a (2D) matrix factorization problem, and none considered it as a (3D) tensor problem. Yet, super-resolution images are (3D) tensors by nature. The international collaborators are experts in tensor. The PI shared his insights and experience with the HSR problem, and by tapping on the collaborators' expertise the two sides successfully built a coupled tensor factorization framework for HSR. It is a framework not seen before (neither HSR nor tensor factorization theory), it is equipped with perfect reconstruction guarantees (like that in Achievement 2), and it was empirically found to outperform several existing matrix factorization solutions.

This part of the work leads to two accepted conference papers C[2], C[5] and one submitted journal paper J[1].

Achievement 4: HSR by Convex Optimization

As a variation on the theme of the main research undertaking, we also considered a low-rank HSR formulation using nuclear norm regularization, which led to the research output of C[4]. The idea is different from those of the previously mentioned achievements in that we adopt a convex optimization formulation. It should be noted that all the previous achievements, as well as the existing works, adopt non-convex formulations. The advantage of using a convex formulation is that it does not suffer from local minima, and

more consistent reconstruction performance may be yielded by pursuing such a formulation. Our empirical study indicated that the proposed method is more robust to noise than some state-of-the-art algorithms.

Our latest investigation reveals that the convex HSR formulation mentioned above has several advantages that deserve our further attention. Simply speaking, it works on a more relaxed model compared with the commonly adopted matrix factorization model in HSR. Hence, in practice the former may stand a better chance when the multispectral and hyperspectral images exhibit strong variabilities against the nominal model. We are currently investigating such possibilities.

Before finishing this report, the PI would like to express his gratitude to SHIAE for funding this project. The PI could not have accomplished any of the above reported results—which he believes hold much promise in immediate significance and long-term impacts—without the support of SHIAE.

4. PUBLICATION AND AWARDS

Please list out and number all the publications and/or awards produced under the funded project. All these publications must be directly acknowledged the SHIAE funding support and stated the affiliation with the Institute. The list can be numbered in alphabetic order. When referring to them for the submission in CD, name the file with corresponding reference number in square brackets as "81150xx-J[1].pdf".

C[1] R. Wu, C.-H. Chan, H.-T. Wai, W.-K. Ma, and X. Fu, "Hi, BCD! Hybrid Inexact Block Coordinate Descent for Hyperspectral Super-Resolution," IEEE International Conference on Acoustics, Speech and Signal Processing (ICASSP), IEEE, Calgary, Canada, pp. 2426-2430, April 15-20, 2018.

C[2] C. I. Kanatsoulis, X. Fu, N. D. Sidiropoulos, and W.-K. Ma, "Hyperspectral Super-Resolution via Coupled Tensor Factorization: Identifiability and Algorithms," IEEE International Conference on Acoustics, Speech and Signal Processing (ICASSP), IEEE, Calgary, Canada, pp. 3191-3195, April 15-20, 2018.

C[3] Q. Li, W.-K. Ma and Q. Wu, "Hyperspectral Super-Resolution: Exact Recovery in Polynomial Time," IEEE Statistical Signal Processing Workshop (SSP), IEEE, Freiburg, Germany, June 10-13, 2018.

C[4] R. Wu, Q. Li, X. Fu and W.-K. Ma, "A Convex Low-Rank Regularization Method For Hyperspectral Super-Resolution," IEEE Statistical Signal Processing Workshop (SSP), IEEE, Freiburg, Germany, June 10-13, 2018.

C[5] C. I. Kanatsoulis, X. Fu, N. D. Sidiropoulos, and W.-K. Ma, "Hyperspectral Super-Resolution: Combing Low Rank and Matrix Structure," to appear in IEEE International Conference on Image Processing (ICIP), IEEE, Athens, Greece, October 2018.

J[1] C. I. Kanatsoulis, X. Fu, N. D. Sidiropoulos, and W.-K. Ma, "Hyperspectral Super-Resolution: A Coupled Tensor Factorization Approach," submitted to IEEE Transactions on Signal Processing, April 2018, online available at https://arxiv.org/abs/1804.05307.

Shun Hing Distinguished Lecture Series

To achieve the Institute's mission to promote appreciation of engineering in society through education programs, the Institute has organized a Shun Hing Distinguished Lecture Series. So far, **forty-five** distinguished lectures have been presented by renowned scholars. These lectures all were very well received and we will continue to line up and invite outstanding researchers to visit CUHK and to deliver distinguished lectures for the Institute. Here to show the distinguished lectures between 2017 and June 2018.

A Journey from Surgical Robotics to Virtualizing Healthcare Delivery

by Dr. Yulun Wang

Chairman & Founder, & Chief Innovation Officer
InTouch Health, Inc
USA

Date: 16 April 2018 (Monday)

Abstracts

This talk will cover how the surgical robotics industry began and how it is now evolving. The clinical problems and the technical solutions to these clinical problems will be touched upon. It will also cover how the virtual care industry has been progressing over the past 15 years, and what is likely to happen in the coming years. The challenges that society faces given on-going demographic trends, and the limitations of the existing healthcare delivery system, and how virtual.

Shun Hing Institute of Advanced Engineering (SHIAE)
The Chinese University of Hong Kong
Shatin, N.T., Hong Kong

Office : Room 702, William M.W. Mong Engineering Building
Tel : (852) 3943 4351
Fax : (852) 3943 4354
Email : info@shiae.cuhk.edu.hk
Website : http://www.shiae.cuhk.edu.hk